TECHNISCHE UNIVERSITÄT MÜNCHEN

Lehrstuhl für Humanbiologie

Calcium dependence of metabotropic glutamate receptor-mediated CREB phosphorylation in hippocampal CA1 neurons

Martin Peter Sumser

Vollständiger Abdruck der von der Fakultät Wissenschaftszentrum Weihenstephan für Ernährung, Landnutzung und Umwelt der Technischen Universität München zur Erlangung des akademischen Grades eines

Doktors der Naturwissenschaften

genehmigten Dissertation.

Vorsitzender: Univ.- Prof. Dr. M. Klingenspor

Prüfer der Dissertation:

1. Univ.- Prof. Dr. M. Schemann
2. Univ.- Prof. Dr. A. Konnerth

Die Dissertation wurde am 22.01.08 bei der Technischen Universität München eingereicht und durch die Fakultät Wissenschaftszentrum Weihenstephan für Ernährung, Landnutzung und Umwelt am 29.05.08 angenommen.

Table of contents

Glossary

0Ca	zero calcium ACSF
a.u.	arbitrary unit
AC	adenylylcyclase
ACSF	artificial cerebrospinal fluid
AM	acetoxymethylester
AMPAR	α-amino-3-hydroxy-5-methylisoxazole-4- propionic acid receptor (ionotropic glutamate receptor)
ATF-1	activating transcription factor 1
ATP	adenosine triphosphate
BAPTA	1,2-bis(o-aminophenoxy)ethane -N,N,N',N'-tetraacetic acid
BDNF	brain derived neurotrophic factor
bZIP	basic leucine zipper (family of transcription factors)
CA1	cornus ammonis 1 (subregion of the hippocampus)
CA3	cornus ammonis 3 (see CA1)
Ca^{2+}	calcium ions
CaM	calmodulin
CaMK-IV	Ca^{2+}/calmodulin-dependent protein kinases IV
cAMP	3'-5'-cyclic adenosine monophosphate
CICR	calcium-induced calcium release
CPA	cyclopiazonic acid (inhibitor of the SERCA)
CRE	cAMP responsive element
CREB	cAMP response element binding protein
CREM	cAMP response element modulator
DAG	diacylglycerol
DHPG	S-3,5-Dihydroxyphenylglycine (mGluR group1 agonist)
DMSO	dimethylsulfoxide
DNA	deoxyribonucleic acid
EGTA	ethylene glycol tetraacetic acid
ENO	early network oscillations
ER	endoplasmic reticulum
ERK	extracellular signal regulated kinase (also known as classical MAPK)
Fura-2-AM	acetoxy-methyl ester of Fura-2 (ratiometric calcium indicator)
GABA	γ-amino butyric acid
Glu	L-glutamate
GPCR	G-protein coupled receptor
GTP	guanosine triphosphate
H_2O	water
HAT	histone acetyl transferase
HEPES	4-(2-hydroxyethyl)-1-piperazineethanesulfonic acid
IEG	immediate early gene
iGluR	ionotropic glutamate receptors
IP_3	inositoltriphosphat
K_D	dissociation constant
LTD	long term depression
LTP	long term potentiation
M	molar

MAP5	microtubule associated protein 5 (neuronal marker)
MAPK	mitogen activated protein kinase (see also ERK)
MCPG	α-methyl-4-carboxyphenylglycine (mGluR group1 and 2,3 antagonist)
MEK1/2	MAPK/ERK kinase (a MAPK kinase)
mGluR	metabotropic glutamate receptor
mM	millimolar (10^{-3} mol)
MOPS	3-(N-morpholino)propanesulfonic acid
mosm	milliosmol
n	number of
nA	numerical aperture
nM	nanomolar (10^{-9} mol)
NMDAR	N-methyl-D-aspartate receptor (ionotropic glutamate receptor)
OGB-1	Oregon Green BAPTA-1
p	p-value (probability)
P	postnatal day
pCREB	phospho CREB
PBS	phosphate buffered saline
PFA	paraformaldehyde
PIP_2	phosphatidylinositoldiphoshat (substrate of PLC)
PKA	protein kinase A
PKC	protein kinase C
PLC	phospholipase C
PP1	protein phosphatase 1
PP2A	protein phosphatase 2A
psi	pounds per square inch
ΔR/R	relative fluorescence ratio of Fura-2 (see 2.4.1)
RNA	ribonucleic acid
ROI	region of interest
rpm	rotation per minute
SEM	standard error of mean
ser133	residue of serine 133 of the CREB protein
SERCA	Sarco/endoplasmic reticulum Ca^{2+} ATPase
t-ACPD	trans-(+/-)-1-amino-(1S,3R)-cyclopentane-dicarboxylic acid (mGluR agonist)
TRIS	2-amino-2-hydroxymethyl-1,3-propanediol
Trk	tyrosine receptor kinase
TTX	tetrodotoxin (sodium channel blocker)
µm	micrometer (10^{-6} m)
µM	micromolar
VGCC	voltage gated calcium channels
v/v	volume/volume

1. Introduction

1.1. Aim of the project

Synaptic activity regulates the expression of neuronal gene products (West et al., 2002). An important role in this process plays the transcription factor CREB (cAMP response element binding protein). So far it is thought, that calcium influx through ionotropic glutamate receptors (e.g. NMDARs) (Deisseroth et al., 1996) or voltage-gated calcium channels (VGCCs) (Dolmetsch et al., 2001) is important for the initiation of signaling pathways converging on the activation of CREB (phosphorylation of the residue serine133).

The focus of this project was the analysis of the role of metabotropic glutamate receptor (mGluR)-mediated calcium signals in hippocampal CA1 neurons for the phosphorylation of CREB as a target for the regulation of gene transcription. Specifically, the role of different calcium pools on mGluR-evoked calcium signals in the CA1 area of hippocampal slices of the rat was investigated. Another issue was to determine the level of intracellular calcium concentration necessary to modulate gene transcription via phosphorylation of CREB and to characterize the signal cascade involved in this process. This was carried out on the level of individual cells. Furthermore, activity-dependent CREB phosphorylation on the level of a neuronal network was investigated. During development there is intrinsic activity present in neuronal cells, which is characterized by synchronous calcium oscillations of a large number of cells. These oscillations were termed ENOs (early network oscillations) (Garaschuk et al., 1998) and are thought to drive the development of the brain (Moody and Bosma, 2005). Presently it is not clear how gene expression is regulating these developmental processes, although a role for CREB is postulated (Lonze and Ginty, 2002). Therefore, a question addressed in this study was, whether intrinsic activity in the form of ENOs, is correlated with the phosphorylation of CREB and thereby modulates the developmental profile of gene expression.

1.2. The organization of the hippocampus

This study was carried out on acute hippocampal slices of the rat. The hippocampus is a standard preparation for the study of synaptic transmission in the brain. It is widely held to serve important functions in certain types of memory (Morris, 2006; Morris et al., 2003), ranging from declarative and associative memory (Squire, 1992) to episodic memory (Vargha-Khadem et al., 1997). Metabotropic glutamate receptors were shown to be involved in some of the processes, thought to be associated with the formation of memory in the hippocampus (Bortolotto et al., 1999). The hippocampus exhibits a structural organization, comprised of several distinguishable layers (Lopes da Silva and Arnolds, 1978). This cellular network can be maintained in the acute slice (Figure 1) and makes it possible to study intact cells. The hippocampus is located in the medial temporal lobe of the brain. It forms a part of the limbic system and plays a role in memory formation and spatial navigation. The name derives from its curved shape in coronal or horizontal sections of the brain, which resembles a seahorse (Greek: *hippos* = *horse*, *kampi* = *curve*). The cytoarchitecture (see Figure 1) comprises the densely packed layer of pyramidal cells (stratum pyramidale), which are functionally and histologically separated in four parts namely CA1 to CA3 and a densely packed area of granule cells, the dentate gyrus (Lopes da Silva and Arnolds, 1978). Of special interest is the CA1 area with its important function in memory formation (McHugh et al., 1996; Rampon et al., 2000). The stratum pyramidale consist almost exclusively of pyramidal neurons, which are all oriented in the same way, with their primary dendrites extending into the stratum radiatum, whereas the axons are located in the stratum oriens and exit the hippocampus at the Alveus. The granule cells together with the pyramidal neurons of CA3 and CA1 form the so-called trisynaptic loop (Morris, 2006). The presynaptic origin of the first synapse derives from layer II pyramidal cells of the perirhinal cortex. These pyramidal neurons project via the perforant pathway to the granule cells in the dentate gyrus. The granule cells send their efferent fibers, termed mossy fibers, to the CA3 field of the hippocampus, where they form *en passant* synaptic boutons. The CA3 pyramidal cell efferent fibers, the so-called Schaffer Collaterals, build the third synapse on CA1 pyramidal neurons. The main projections originating from CA1 neurons connect to the subiculum and further to pyramidal cells of layer V of the entorhinal cortex (Morris, 2006). The excitatory neurotransmitter in this trisynaptic circuit is L-

glutamate. Integrated in this circuit of pyramidal and granule cells is a meshwork of inhibitory cells, which are primarily located outside of or adjacent to the stratum pyramidale in the stratum oriens and stratum radiatum (not depicted in Figure 1) (Topolnik et al., 2006).

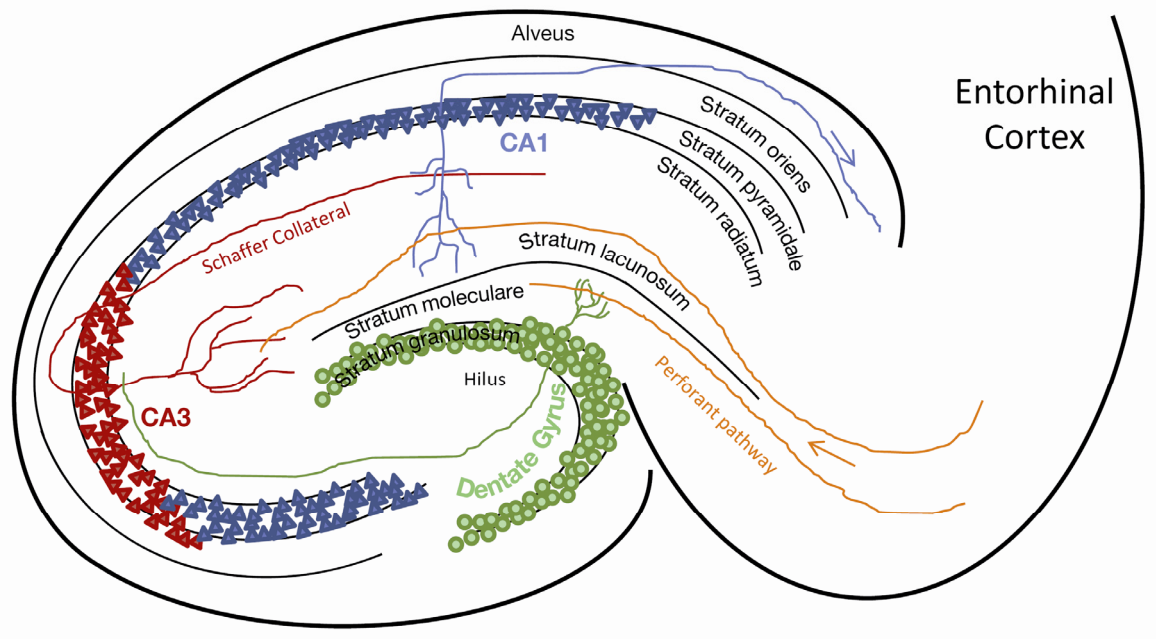

Figure 1: Different cell types and major afferent (orange) and efferent (blue) connections of the hippocampus.

1.3. Metabotropic glutamate receptors

Even though the synaptic connections and especially the CA3-CA1 Schaffer collaterals in the hippocampus are well characterized, there still is controversial data on how mGluRs are involved in the synaptic transmission and plasticity on these synapses (Bortolotto et al., 1999). Until the mid eighties it was believed that glutamate exerts its neurotransmitter actions in the brain exclusively via ionotropic receptors (iGluR), namely NMDAR (N-methyl-D-aspartate receptor), AMPAR (α-amino-3-hydroxy-5-methylisoxazole-4- propionic acid receptor) and kainate receptors (Dingledine et al., 1999). The discovery of glutamate being capable to stimulate the turnover of phosphoinositide (Sugiyama et al., 1987), which is a characteristic feature of G-Protein

coupled receptors (GPCR), lead in the early nineties to the cloning of a receptor now classified as mGluR1a (Masu et al., 1991). Metabotropic glutamate receptors participate in the regulation of diverse forms of neuronal plasticity, especially long-term potentiation (LTP) (Bashir et al., 1993a; Lu et al., 1997; Miura et al., 2002) and long-term depression (LTD) (Bashir et al., 1993b; Bortolotto et al., 1999; Ichise et al., 2000).

Deletion of the different mGluR-genes in mice provide evidence, that these receptors are also involved in neuropathological processes, like epilepsy (Stoop et al., 2003), drug addiction (Chiamulera et al., 2001), schizophrenia (Brody et al., 2003), anxiety (Brodkin et al., 2002) as well as appetite and energy balance (Bradbury et al., 2005).

mGluRs belong to the class C family of GPCRs. Eight different subtypes have been identified so far. They form three groups, according to their homology in amino acid sequence, pharmacological profile and intracellular effectors (Ferraguti and Shigemoto, 2006; Gerber et al., 2007). All mGluRs share common structural motifs. They consist of an extracellular N-terminal region, seven alpha-helical transmembrane domains and a long C-terminal cytoplasmic domain, which is important for the interaction with downstream signaling molecules and positive or negative regulation of the mGluRs (Hermans and Challiss, 2001).

1.3.1. mGluR-mediated signaling cascades

The eight mGluR subtypes are linked via G-proteins to different second messenger systems. Table 1 lists the specific G-proteins, associated with mGluRs and their primary signaling targets.

Group	Receptor	Preferred G-protein	Signaling Mechanism
I	mGluR1 mGluR5	$G\alpha_{q/11}$	PLC activation
II	mGluR2 mGluR3	$G\alpha_{i/o}$	AC inhibition
III	mGluR4 mGluR6 mGluR7 mGluR8	$G\alpha_{i/o}$	AC inhibition

Table 1: Groups of mGlu receptors.

mGluR5 and mGluR1 show the highest expression levels of the mGluRs (mGluR5>mGluR1) in hippocampal CA1 neurons (Lein et al., 2007). Therefore, in this study the effects of the mGluR group I receptors were examined. The group I mGluRs are preferentially coupled to the G-protein $G\alpha_{q/11}$ (Table 1) and were found to be located in postsynaptic somatodendritic domains, whereas group II receptors reside predominantly at the presynaptic membrane (LeBeau et al., 2005). Upon binding of glutamate to mGluRs, G-proteins are targeted to the membrane-bound phospholipase C (PLC), which then cleaves its substrate phosphatidylinositoldiphoshat (PIP_2) to release intracellular freely diffusible inositoltriphosphat (IP_3) and the membrane diffusible diacylglycerol (DAG). IP_3 binds to the IP_3-receptor located in the membrane of the endoplasmic reticulum (ER). This leads to release of calcium from internal stores of the ER, through the calcium permeable IP_3-receptor and an increase in cytosolic calcium concentration. It is hypothesized that downstream of the calcium release, the Ras/MAPK pathway is activated eventually leading to the activation of CREB (see 1.4.1 and Figure 2). DAG in turn can recruit and activate protein kinase C (PKC) at the membrane (Figure 2). PKC in turn is thought to modulate signaling cascades like the Ras/MAPK pathway via phosphorylation of Raf (Figure 2) (Gutkind, 2000; Macdonald et al., 1993) or interact with the calcium/calmodulin-dependent kinase II (CaMKII). This connects PKC with the induction of long-term potentiation (LTP) (Choe and Wang, 2002a; Mayford, 2007).

1.4. Cyclic-AMP response element binding protein (CREB)

CREB is perhaps the best characterized stimulus-induced transcription factor. Based mainly on genetic knockout studies, CREB was shown to be involved in learning and memory formation (Bourtchuladze et al., 1994; Kida et al., 2002), addiction, depression and anxiety (Carlezon et al., 2005). CREB was originally identified as a protein capable to bind to a specific 8 base pair promoter sequence, later termed the cAMP responsive element (CRE). The existence of a CRE-site is necessary to trigger expression of somatostatin, in response to hormonal stimuli, which lead to the production of cAMP (Montminy et al., 1986). Later studies showed that CREB not only is activated through cAMP but through a diverse array of stimuli (Johannessen et al.,

2004). This activation can be attributed to the phosphorylation of CREB at the residue ser133. Although this is not the only it is the crucial step in CREB-dependent gene expression.

There are different splice variants, among CREBα (341 amino acids) and CREBΔ (327 amino acids) are the most prominent ones. They differ in a single exon, a 14 amino acid residue (α-peptide) (Lonze and Ginty, 2002). Both splice variants are ubiquitously expressed throughout the body including all brain cells. It is worth to mention, that two other highly related gene products were discovered, namely ATF-1 (activating transcription factor-1) and CREM (cAMP response element modulator). Together with CREB they form the ATF-subgroup of the so-called bZIP superfamily of transcription factors and show a redundancy in their actions (Mantamadiotis et al., 2002). Other well studied members of this superfamily are c-fos, c-jun or c-myc. bZIP comprises two important functional domains of these proteins (Shaywitz and Greenberg, 1999):

1) The lysine and arginine-rich basic domain, which mediates DNA binding
2) The leucine zipper domain consisting of several leucine repeats, which are necessary for formation of homo- and heterodimers within the bZIP superfamily.

1.4.1. Activity-induced signaling pathways converging on CREB

CREB is a major target for activity-induced alterations in cell behavior (Lonze and Ginty, 2002). A plethora of calcium-dependent and -independent signal cascades have been identified, including protein kinase A (PKA), Ca^{2+}/calmodulin (CaM) kinases and the Ras/MAPK pathway, all converging on the transcription factor CREB (Carlezon et al., 2005; Shaywitz and Greenberg, 1999).

There are three central routes for calcium to enter the cytoplasm, each of which is capable to induce the phosphorylation of CREB. First, synaptic activity triggering calcium influx through ionotropic glutamate receptors like NMDAR or AMPAR is able to trigger the phosphorylation of CREB (Bito et al., 1996; Deisseroth et al., 1996). Second,

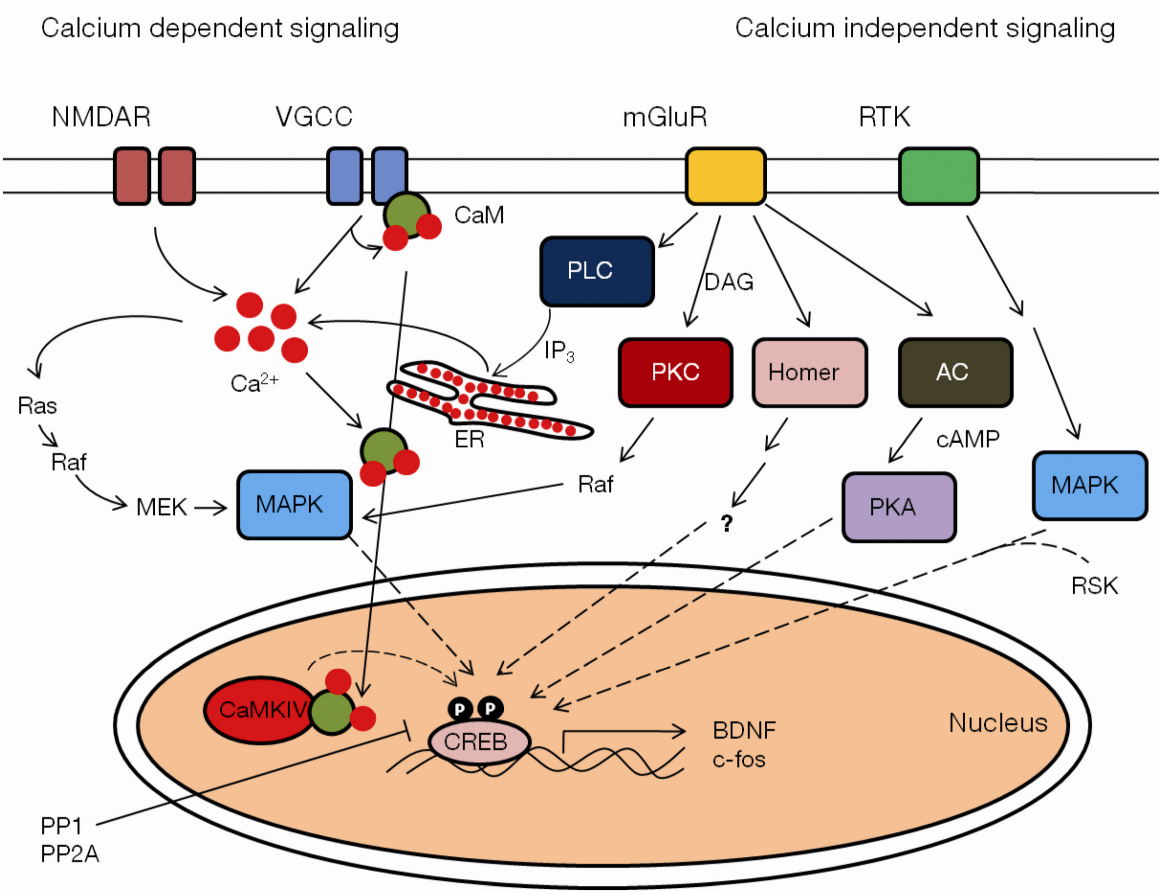

Figure 2: Simplified model of different signaling pathways leading to the phosphorylation of CREB.
The pathways described in this figure represent only a fraction of the steps involved in the regulation of the phosphorylation of CREB. The final step is depicted with a dashed line. (AC: adenylylcyclase; BDNF: brain derived neurotrophic factor; Ca^{2+}: calcium ions; CaM: Calmodulin; CaMKIV: calcium/calmodulin-dependent kinase IV; DAG: diacylglycerol; ER: endoplasmic reticulum; IP_3: inositoltriphosphat; mGluR: metabotropic glutamate receptor; MAPK: mitogen-activated protein kinase; MEK: MAPK/ERK kinase; NMDAR: NMDA receptor; PKA: protein kinase A; PKC: protein kinase C; PLC: phospholipase C; PP1/2A: protein phosphatase 1/2A; RSK: ribosomal protein S6 kinase; RTK: receptor tyrosine kinases; VGCC: voltage gated calcium channel)

calcium entry through voltage-gated calcium channels (VGCC) of the L-type, which are functionally coupled to the calcium binding signaling molecule calmodulin, was shown to be potent to initiate the phosphorylation of CREB (Dolmetsch et al., 2001). Third, calcium release from internal stores leads to the phosphorylation of CREB. This can be triggered by phospholipase C (PLC)-coupled mGluRs (Mao and Wang, 2002a). Other studies claim that nuclear calcium signals derived from calcium release from intracellular stores are crucial to transduce a synaptic signal to the nucleus (Hardingham et al., 2001).

Calcium-independent phosphorylation of CREB can be achieved via activation of growth factor receptors for instance tyrosine receptor kinases (Trk) (Finkbeiner et al., 1997) or GPCRs, which increase the intracellular concentration of cAMP through G-protein-dependent activation of adenylylcyclase (AC) (Gonzalez and Montminy, 1989). Recently, a calcium-independent pathway initiated by mGluR5 was discovered. Crucial for the activation of this pathway is the crosslinking protein Homer (Mao et al., 2005b), which is likely to provide physical linkage between proteins in a signaling complex. Protein phosphatases like protein phosphatase 1, 2A (PP1, PP2A) and calcineurin are also regulated by synaptic signals and are able to shape the phosphorylation status of CREB by dephosphorylation (Bito et al., 1996; Choe et al., 2004; Mao et al., 2005a) and, thereby, to alter CREB-mediated gene regulation.

1.4.2. Activation of CREB-dependent transcription

The activation of transcription of certain genes by CREB is characterized by the binding to a specific palindromic promoter sequence (CRE).

Sequence of CRE:

5´-TGACGTCA-3´

In order to bind to this promoter region CREB has to dimerize. This is established by the formation of homodimers (CREB-CREB) or heterodimers (CREB-ATF1 or CREB-CREM).

The major difference between the different dimers is the half life and therefore most likely the efficiency of transcription. The dimerization itself is promoted by the presence of accessible, meaning demethylated CRE-DNA (Hong et al., 2005) and is independent on the phosphorylation status of CREB (Wu et al., 1998). Because CREB is localized in the nucleus, the binding to the CRE sequence is only limited by the concentration of CREB molecules in the nucleus and the accessibility of the DNA helices.

For proper initiation of transcription the binding of CREB to the DNA is necessary but not sufficient. Furthermore the recruitment of the transcription machinery, namely the RNA polymerase II and some upstream regulatory elements, is crucial for the transcriptional activity of CREB. This recruitment is dependent on a specific adaptor protein called CBP (CREB binding protein). CBP contains a so-called KID interaction domain (KIX), which binds to the phosphorylated serine133 in the kinase inducible domain (KID) of CREB (Chrivia et al., 1993) and features a zinc finger domain, which is thought to be important for the linkage of CREB to the transcriptional machinery (Mayr and Montminy, 2001; Nakajima et al., 1997).

Moreover, CBP possesses an intrinsic histone acetyltransferase (HAT) activity, which is most likely involved in altering the chromatin structure in such a way that the accessibility of the DNA is enhanced (Ogryzko et al., 1996). There are many genes controlled by CREB (Lonze and Ginty, 2002; Mayr and Montminy, 2001), which have a strong heterogeneity in expression levels in different cell types (Cha-Molstad et al., 2004). A recent genomic study revealed that there are about 4000 CRE promoter sites (Zhang et al., 2005) in the human genome, indicating that CREB might be important in modulating the expression level of several thousand genes. Regarding the amount of genes possibly regulated by CREB it is not surprising, that there are also other phosphorylation sites in the CREB protein which have an impact on CREB-dependent gene regulation (Deisseroth and Tsien, 2002; Kornhauser et al., 2002). None the less, most of the genes were not transcribed by simply phosphorylating CREB but rather by recruitment of other coregulatory factors or control of accessibility of the DNA (Hong et al., 2005; Zhang et al., 2005).

1.5. ENOs and the regulation of the phosphorylation of CREB

The activity of CREB is a critical component of developmental processes in the brain (Lonze and Ginty, 2002; Moody and Bosma, 2005). CREB controls the transcription of a plethora of genes. Among them are several genes thought to be important for the regulation of developmental processes such as neurotrophic- (e.g. BDNF) or antiapoptotic factors (e.g. bcl-2) (Mayr and Montminy, 2001). During the period of early postnatal development pyramidal neurons in the rodent hippocampus exhibit large-scale synchronized Ca^{2+}-waves termed early network oscillations (ENOs) representing a form of spontaneous activity. ENOs are most prominent during the first postnatal week (Garaschuk et al., 1998) and are associated with repetitive Ca^{2+} transients in the majority of neurons. ENOs were shown to be dependent on GABAergic synaptic transmission, which exhibits excitatory actions in the developing brain (Ben-Ari et al., 2007). The first postnatal week is also characterized by profound cellular differentiation, strong expression of a variety of genes and growth of neurons and their processes (Uylings et al., 1990). Transcription and expression of many genes during development critically depends upon activation of CREB at Ser133 (Bonni et al., 1999; Walton et al., 1999), therefore the connection between ENOs and the phosphorylation of CREB in rat hippocampal slices was investigated.

2. Materials and Methods

2.1. Chemicals and Solutions

2.1.1. Solutions for patch-clamp recording and calcium imaging

The following solutions were used in this study:

Artificial cerebrospinal fluid (ACSF) contained in mM: NaCl 125, $NaHCO_3$ 26, Glucose 20, KCl 4.5, $CaCl_2$ 2, NaH_2PO_4 1.25, $MgCl_2$ 1. The ACSF was prepared just before usage to avoid any growth of bacteria inside. To set pH at 7.2 and to dissolve enough oxygen in the solution, the ACSF was oxygenated with Carbogen, a gas mixture of 5% CO_2 and 95% O_2 for at least 30 minutes before usage. In 0Calcium-ACSF (0Ca-ACSF) 2mM $CaCl_2$ were replaced by $MgCl_2$ to a final concentration of 3mM and 100µM EGTA was added.

For animals older than postnatal day 12 a special cutting solution was prepared for maximal integrity of the cells in the hippocampus (Bischofberger et al., 2006). This **sucrose based storage/cutting solution** contained in mM: NaCl 87, $NaHCO_3$ 25, Glucose 20, Sucrose 75, KCl 2.5, NaH_2PO_4 1.25, $CaCl_2$ 0.5, $MgCl_2$ 7.

The **intracellular solution** for patching contained in mM: K-gluconate 175, HEPES 12.5, KCl 15, NaCl 5, Mg-ATP 5, Na-GTP 0.5. Before adding ATP/GTP the solution was stirred for 30 minutes at room temperature. The pH was adjusted to a value of 7.3 using 3M KOH and the osmolarity was checked to be 380mosm. The solution was stored at -20°C and melted just before usage. For patch-clamp recording the intracellular solution had to be diluted with H_2O (80:20 Sol/H_2O). Either **Fura-2-5K** (pentapotassium salt of Fura-2) or **Oregon Green BAPTA-1-5K** (OGB-1) fluorescent calcium indicator was added to the intracellular solution to a final concentration of 50µM. To be able to detect the patch-clamped cell in the immunohistological analysis (see Figure 6) **neurobiotin** as an intracellular tracing molecule was added to a final concentration of 0.1% (v/v). The last step in preparation of the intracellular solution was to filter it through a 0.2µm filter device (Millipore, Billerica/USA) to get rid of any aggregates inside the solution, which could interfere with the quality of the patch clamping.

2.1.2. Solutions for immunofluorescence labeling

Phosphate buffered saline (PBS) contained 9.95 g of a premixed powder (Sigma), which was dissolved in 1L H_2O. The pH was adjusted to 7.2 with 1M HCl-solution. The **washing solution** consisted of PBS with 3% Triton X-100. Adding 5% normal goat serum (NGS) to the washing solution produced **blocking solution**, which was freshly prepared and filtered through a 2µm filter device. To fix the slices a **fixation solution** (4% paraformaldehyde in PBS) was prepared. The whole procedure was carried out under the hood to avoid the inhalation of gases evaporating from the PFA-dissolving process. While stirring 200ml H_2O, 10g PFA and 2 drops of 10M NaOH were heated to 60°C. After the solution cleared up, 25ml of 10xPBS was added and the pH was adjusted to 7.35. H_2O was added to result in a final volume of 250ml. After filtering through a paper filter the solution was stored at -20°C. The **immunohistological embedding media** containing 25g H_2O, 6g Mowiol and 6ml of 1M TRIS of pH 8.5 was used to prepare the fluorescence-labeled slices for confocal analysis. This solution was stirred for 10 minutes, heated to 60°C for 20 minutes and then 18.9g of glycerol was added. After stirring for 5 minutes the solution was spun down at 4500rpm and aliquots were stored at -20°C and thawed prior to usage.

A list of the chemicals used in this study and the respective companies, from which they were obtained can be found in the supplemental materials section (see 8.).

2.2. Animals

For all the experiments newborn rats between the age of postnatal day 2 to 14 (P1-P14) were used. Mother Wistar rats (*Rattus norvegicus*) together with their litter were obtained from Charles River Laboratories (Sulzfeld/Germany) and kept with water and food ad libitum.

2.3. Techniques

2.3.1. Slice preparation

Horizontal hippocampal slices were prepared, according to standard procedures (Bischofberger et al., 2006; Edwards et al., 1989). The animals were anesthetized with CO_2 and decapitated at the level of the cervical medulla. In order not to harm the cortical areas, a small incision through the skull superior to the cerebellum was carried out, followed by one saggital cut from caudal to frontal until reaching the olfactory bulb. Using forceps the right and left part of the skull was bent to the side, while carefully cutting the meningeal connections between skull and brain with the forceps. The cerebellum was cut off from the cerebrum. The brain was separated from the skull by cutting the cranial nerves and was immediately transferred to ice-cold carbogen-oxygenated ACSF. In order to obtain horizontal slices of the hippocampus, the brain was cut through the corpus callosum. One hemisphere was placed on the saggital plane on a piece of filter paper and submersed with ice-cold ACSF. Approximately 3mm of the dorsal part of the cortex was cut off with a scalpel in order to produce an even surface. In this way the major connections (Schaffer Collaterals CA3 to CA1) and the dendritic processes of the CA1 region within the hippocampus were left intact. Using cyanoacrylate based superglue (UHU Sekundenkleber, Bühl/Germany) the dorsal plane of the hemisphere was glued on the slicing chamber and submerged in ice-cold oxygenated ACSF. Slices of a thickness of 200 to 400µm were obtained using a vibratome (Leica VT1200S, Wetzlar/Germany) with conventional shaving blades (Gillette, Boston/USA). Vibrations of the blade in the Z-direction were minimized to less than 0.5µm using the built-in Vibrocheck function of the slicer. To remove any remaining grease of the production process, the blade was cleaned with acetone prior to slicing. The blade was advanced from the lateral to the medial side with a speed of 0.15 mm/s. Using a wide-lumen glass pipette the slice was transferred to the maintenance chamber and kept at 34°C in oxygenated ACSF for 30 to 45 minutes. After that the maintenance chamber was kept at room temperature.

For the experiments one slice at a time was transferred to the custom-made recording chamber in such a way that the previous bottom side faced the objective. A platinum frame with nylon threads arranged in a grid like fashion was put on top of the

slice to stably hold the slice in place (Edwards et al., 1989). The slice was then perfused with heated ACSF (32°C).

2.3.2. Patch-clamp recordings

For patch-clamp recordings a setup consisting of an EPC9 amplifier (HEKA, Lambrecht/Germany) connected to a head stage preamplifier was used. Borosilicat glass electrodes with a resistance of about 5 MΩ were pulled with a vertical Narishige puller (Tokyo/Japan). A silver chloride-coated silver electrode, on which the glass electrodes (patch-clamp electrode) were mounted and a reference electrode (Warner Instruments, Hamden/USA), which was placed in the perfusion chamber built the two electrical inputs to the head stage. A micromanipulator (Luigs&Neumann, Ratingen/Germany) was used to move the patch-clamp electrode on a micrometer range. Before entering the bath solution, positive pressure was applied to the patch-clamp electrode to avoid any dirt getting stuck to the opening of the electrode (Numberger and Draguhn, 1996), what would ultimately result in an imperfect patch. Using the Pulse software (Version 8.54, HEKA) a repetitive command voltage pulse (10mV, 4ms) was given to monitor changes in the current while approaching the cell. The offset compensation of the amplifier was set to zero and the patch-clamp electrode was lowered to the cell. The positive pressure applied, resulted in the ejection of solution from the patch-clamp electrode. This ejection created a small dimple on the cell membrane. At this point the pressure on the electrode was removed. Unless a giga seal (increase in resistance to the giga-Ohm range) formed right away, gentle suction was applied to support seal formation. Concurrently, the pipette tip was hyperpolarized to a holding potential of -60mV. The capacitance of the pipette was compensated using the amplifier built-in compensation circuit (C_{fast}) to almost completely delete the current evoked by the test pulse (formation of giga seal). The application of short suction pulses coinciding with zap pulses of -600mV ruptured the cell membrane and access to the intracellular compartment of the cell was established. The series resistance could now be determined from the amplitude of the command pulse-induced current using Ohm´s law (R = U/I) (Numberger and Draguhn, 1996).

In the voltage clamp mode of the amplifier the holding potential was set to -70mV to record currents and if necessary switched to current clamp mode to monitor voltage changes (e.g. action potentials). The data obtained from the recordings were imported in IgorPro (Wavemetrics, Portland/USA) using the “patcher´s power tools” macro (Frank Würriehausen, MPI Göttingen).

2.3.3. Calcium imaging and Fura-2 calibration

The calcium imaging setup consisted of an air-cooled CCD-camera (Till Photonics, Gräfelfing/Germany), a 75W Xenon arc lamp (Ushio, Tokyo/Japan), a monochromator and a control unit for these devices (Till Photonics). The monochromator enables to record fluorescent signals at two excitation wavelengths by switching between the wavelengths in milliseconds. To achieve this, the light of the Xenon arc lamp is split via a prism into a spectrum of wavelengths. The wavelength can be switched by changing the angle of the incoming light to the prism via a fast rotating mirror. The selected wavelength is focused into the glass fiber, which couples the monochromator to the microscope (Zeiss Axioskop, Oberkochen/Germany). The light was then focused on the slice via a dichroic mirror (FT460, incoming light of λ<460nm is reflected, while the mirror is transmissible for light of λ>460nm) and a water immersion objective (60x/nA0.9, 20x/nA0.7 Olympus, Tokyo/Japan; 40x/nA=0.75, Zeiss). The emitted fluorescent signal passed through the dichroic mirror (transmissible for λ>460nm), an emission filter (LP470) and was recorded with the CCD-camera.

Prior to imaging, the slices were perfused with 32°C ACSF. 1.5µl of Fura-2 AM calcium indicator were dissolved in the recording chamber, which was filled with approximately 1ml of ACSF. The chamber was placed in a cell culture incubator (Binder, Tuttlingen/Germany) for 15-20 minutes at 37°C and 5% CO_2. After sufficient uptake of the calcium indicator excess dye was washed out by perfusion with ACSF. For puff application a glass pipette (same as for patch-clamping) filled with the substance to be applied was positioned close to the patch-clamped cell approximately 20µm above the slice. The puff was given with a pressure of 8psi and a duration of 500ms (Parker Hannifin corporation picospritzer, Cleveland/USA). Fluorescence changes were recorded at two excitation wavelengths 355nm and 380nm (see Figure 3;

emission λ=510), with an exposure time of 100ms per wavelength and a cycle time of 250ms (equals a frame rate of 4Hz).

To calculate the ratiometric signals from the dual-wavelength recordings the TillVision software (Till Photonics) was used. First, regions of interest (ROI) around the somata of the neuronal cells were defined. For background subtraction the average pixel value of an image of the cells in the stratum radiatum, taken before the loading of the cells with the calcium indicator was determined. This autofluorescence results from cellular molecules able to absorb the UV excitation light (e.g. NADH) (Neher et al., 2000). The ratio R was calculated as follows:

$$\frac{\mathrm{F355} - \mathrm{Background}}{\mathrm{F380} - \mathrm{Background}} = \mathrm{R}$$

Although the dissociation constant of Fura-2 is known ($K_d \approx 145nM$) it cannot be used to accurately measure intracellular calcium concentrations, because the cytosolic milieu (pH, ionic strength) is influencing its properties dramatically (Neher et al., 2000). A common feature of ratiometric dyes is that depending on the excitation wavelength, their fluorescence emission intensity at one wavelength either increases or decreases upon the same change in calcium concentration (Figure 3). Therefore, the ratio R is relatively independent on changes in excitation intensity or dye concentration (Helmchen et al., 2000). This can be exploited to perform a calibration of the imaging setup for quantitative measurements of changes in cytosolic calcium concentration.

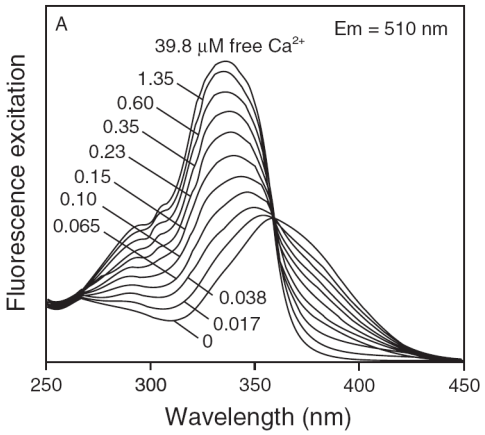

Figure 3: Emission spectrum of Fura-2.
The crossing point of the calcium titration curves is the so-called isosbestic point (approximately at 358 nm). At this wavelength the emission intensity of the dye is calcium concentration independent. (Image taken from Molecular Probes Handbook 2007)

To achieve that, fluorescence measurements of Fura-2 for defined calcium concentrations were carried out. Two solutions from the calibration kit#1 (solution1: EGTA-based zero free calcium (K_2EGTA) and solution2: 39.8µM free calcium buffer (CaEGTA), both containing 100mM KCl and 30mM MOPS pH7.2; Invitrogen, Carlsbad/USA) were mixed together, to produce calibration solutions with different concentrations of free calcium (Table 2). Then Fura-2-5K was added to a final concentration of 50µM (same concentration used for patch clamp recordings, and estimated intracellular concentration after bath loading of Fura-2-AM).To calculate the concentrations of free calcium in the calibration solution, following formula was being used:

$$[Ca^{2+}] = K_d^{EGTA} \times \left[\frac{CaEGTA}{K_2EGTA}\right]$$

The K_dEGTA is strongly pH- and temperature-dependent. Therefore values for the K_dEGTA were taken from Tsien and Pozzan. The pH of the calibration solution was adjusted to 7.25 and the calibration was carried out at room temperature (20°C), resulting in an estimated K_dEGTA of 120nM (Tsien and Pozzan, 1989).

CaEGTA/K_2EGTA ratio	Calculated calcium concentration [nM]
0/1	0
2/1	240
1/0	39800

Table 2: Calcium concentration of the calibration solutions

For the calculation of the K_d of Fura-2 in the solution following formula had to be solved (Grynkiewicz et al., 1985).

$$[Ca^{2+}]_{free} = K_D^{Fura} \times \left[\frac{R - R_{min}}{R_{max} - R}\right] \times \left(\frac{F_{max}^{380}}{F_{min}^{380}}\right)$$

Ca^{2+} calcium concentration in the calibration solution
R_{min} ratio for zero calcium concentration (0/1; Table 2)

R_{max}	ratio for high calcium concentration (1/0; Table 2)
R	measured ratio for intermediate calcium concentration (2/1, Table 2)
F_{max}	fluorescence (380nm) for zero calcium (see Figure 3)
F_{min}	fluorescence (380nm) for high calcium (see Figure 3)
K_d	dissociation constant of Fura-2

To determine the fluorescence ratio for zero free calcium concentration (R_{min}) the cells in the slice were loaded with Fura-2-AM. 0Ca-ACSF was washed in for 20 minutes. Then 100µM Ionomycin a fungal ionophore, which introduces calcium permeable pores into the cell membrane, was puff applied for 10 seconds on the cells. To measure the fluorescence at intermediate and high calcium concentration a cell was patch-clamped, and thereby the intracellular compartment was loaded with the calibration solution (2/1 and high calcium solutions; Table 2). Only patch-clamped cells with a series resistance of <15MΩ and a leak current <30pA were taken, to assure efficient loading of the cell. This is important for the accuracy, with which the intracellular calcium concentration is controlled. Each of the three background corrected values (see 2.3.3) Rmin, Rmax and R were obtained three times and the mean value was taken to calculate the K_D by converting the formula to

$$K_d = [\mathrm{Ca}^{2+}]_{\mathrm{free}} \times \frac{\mathrm{R}_{\mathrm{max}} - \mathrm{R}}{\mathrm{R} - \mathrm{R}_{\mathrm{min}}} \times \frac{\mathrm{F}_{\mathrm{min}}^{380}}{\mathrm{F}_{\mathrm{max}}^{380}}$$

This formula was simplified to

$$K_{eff} = [\mathrm{Ca}^{2+}]_{\mathrm{free}} \times \frac{\mathrm{R}_{\mathrm{max}} - \mathrm{R}}{\mathrm{R} - \mathrm{R}_{\mathrm{min}}}$$

Example measurements for a 2/1 calibration solution (Table 2):

Rmin	= 0.7±0.03 Standard error of mean (SEM)
Rmax	= 4.4±0.12
R	= 1.6±0.08 (ratio for a calcium concentration of 240nM)
Ca_{free}	= 240nM
F_{min}	= 60
F_{max}	= 150
$Kd_{calculated}$	= 298nM
K_{eff}	= 746nM

2.3.4. Immunohistology

Immediately after finishing the calcium imaging experiment the slice was transferred for 30 minutes to 4% PFA fixation solution, then washed for 10 minutes in PBS and blocked with 5% goat serum blocking solution for 1 to 2 hours. The primary antibodies were diluted in blocking solution as followed:

Phospho CREB	(rabbit)	1:200
MAP5	(mouse)	1:200

A drop (30µl) of the antibody solution was pipetted on a piece of parafilm inside a petri dish. Using a small brush the slices were gently transferred into the drop taking care to put the side with the patch-clamped cell facing the surface of the drop. Then the petri dish was tightly sealed with parafilm and incubated in the fridge (4°C) over night. The slices were removed from the drop using a brush, transferred to the washing solution and washed three times for 5 minutes. Then the slices were incubated under light protection for at least 2 hours at room temperature in a small drop (50µl) of secondary antibody solution, containing blocking solution and the antibodies in following dilutions:

Cy3 goat anti rabbit (anti phospho CREB)	1:500
Alexa488 goat anti mouse (MAP5)	1:500
Alexa647 streptavidin (neurobiotin)	1:1000

After the incubation with the secondary antibody the slices were washed twice in washing solution for 10 minutes, 10 minutes in PBS and finally rinsed shortly in H_2O. They were immediately transferred with a brush to a microscope slide, the excess solution was removed using a pipette tip connected to a pump or a piece of filter paper and embedded in 100-200µl Mowiol. After placing a coverslip on top, the slices were kept at least over night at 4°C before imaging on the confocal setup (see 2.3.5). For long time storage the slices were kept at -20°C.

2.3.5. Confocal analysis

For the confocal analysis a Zeiss LSM510 device (Zeiss, Oberkochen/Germany) was used. Slices were scanned either with a 20x (overview images, Z-resolution of 3µm) or a 40x (oil immersion, Z-resolution of 1µm) objective.

The secondary antibodies (see 2.3.4) are labeled with fluorescent dye molecules. To be able to differentiate between the three labels applied to a single brain slice, three different lasers for excitation and respective emission filters were necessary.

Dye	Excitation (wavelength)	Emission Filter
Alexa488	Argon (488nm)	Bandpass 505-550nm
Cy3	Helium/Neon (543nm)	Bandpass 560-615nm
Alexa647	Helium/Neon (633nm)	Longpass 650nm

Table 3:Overview of the dyes, lasers and filters used for confocal imaging.

The scan speed/pixel dwell time was set to 1.6µs (equals a frame rate of 0.6Hz, 1024x1024pixel). A so-called Kalman filter, which calculates the average out of an even number (usually 4) of images of the same stack, was used to reduce the noise in the images. Following parameters were changed for each recording channel to adjust the brightness of the image:

Laser intensity
Photomultiplier voltage
Detector gain
Offset
Pinhole size

Each channel was scanned separately and the scanning parameters were set in such a way that the pixel values of the resulting image were neither saturated (pixel value of 255 for 8-bit or 4095 for 12-bit images) nor zero. For that, a HiLo lookup table (LUT) was used, which shows the zero pixels in blue and the saturated pixels in red, whereas the remaining pixels are shown in a grayscale (Figure 4). Usually the stack size of the different labels differed, due to tissue penetration properties of the antibodies.

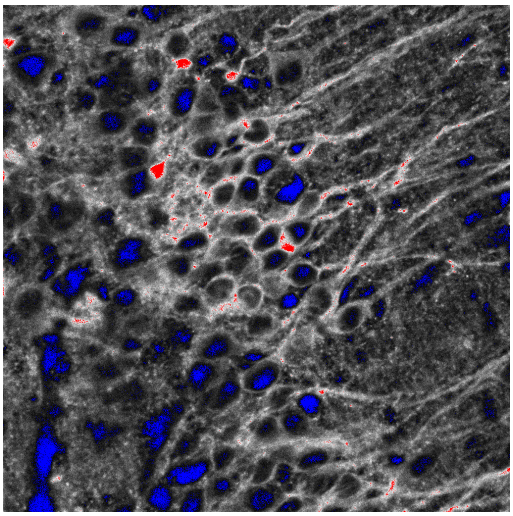

Figure 4: HiLo LookUpTable (LUT)
Display of a confocal image of MAP5 staining in the CA1 area using the HiLo LUT. Blue areas indicate pixels with zero value, whereas red areas represent saturated pixels.

For the MAP5 antibody the first 5-10µm could be scanned, whereas the pCREB antibody diffused 10-20µm into the tissue. The neurobiotin label of the patch-clamped cell could be detected up to 40µm deep in the tissue, because the streptavidin is a much smaller molecule than the secondary antibodies and therefore is able to penetrate the tissue much better.

2.4. Analysis

2.4.1. Calcium transients

The calcium transients were recorded at the soma of the cell which could be identified by the AM-loading of the calcium indicator. To display the calcium transients, either a ΔR/R calculation or the determination of the absolute calcium concentrations was done. For the ΔR/R a custom programmed macro in IgorPro (Wavemetrics, Portland/USA) was used. It divides the relative changes in the ratio of the two wavelength fluorescence intensities ($R_{measured} - R_{Baseline} = \Delta R$) from a defined baseline ($R_{Baseline}$), usually the first 10 frames of the acquisition movie resulting in relative fluorescence ratio changes. The calcium concentrations were calculated using the built-in function of TillVision software, which uses the formula shown on page 18 and

implements a background subtraction before the calculation of the ratios. For background subtraction the autofluorescence of the slice before the staining with the AM-dye was determined (see section 2.3.3). Calcium transients shown in one figure correspond to experiments done at the same day on slices of the same animal.

The experiments in section 3.3 (correlation between ENOs and pCREB) were carried out using the calcium indicator Oregon-Green BAPTA-1 AM. Because this is a single wavelength calcium indicator no calibration was carried out and the calcium signals are displayed as relative fluorescence changes (ΔF/F), as described for the ΔR/R analysis above.

2.4.2. Image processing

Confocal images were processed using ImageJ (NIH, Bethesda/USA) and Photoshop CS2 software (Adobe, San Jose/USA). Fluorescence movies were if necessary corrected for bleaching of the calcium dye using the built-in bleach correction function of ImageJ (for details, see McMaster Biophotonics facility ImageJ homepage). To indicate changes in the relative fluorescence of a certain pixel of an image stack a ΔR/R movie was generated. Therefore a ratio movie was calculated by dividing the movie taken at 355nm and the movie taken at 380nm. Using a built-in function of the TillVision software this ratio movie was then converted into a ΔR/R movie (see 2.4.1). A maximum intensity projection of the movie was carried out to result in relative changes in fluorescence intensity.

To be able to locate the cells in the Fura-2 fluorescence image and later in the immunohistological staining, Photoshop CS2 and custom written macros in ImageJ were used. First the absolute size of the images taken at the calcium imaging setup was calibrated using a micrometer scale bar. Images taken at the LSM510 confocal setup are scaled in µm according to calculations of the Zeiss software. Second, an overlay of the two images was made (Figure 5). With the patch-clamped cell as a reference point, all the other cells from which calcium transients were recorded could be identified. Therefore it was possible to correlate the recorded calcium transients to the pCREB staining in individual cells. pCREB negative cells could be detected using the MAP5 label (see Figure 5, e.g. cell 11).

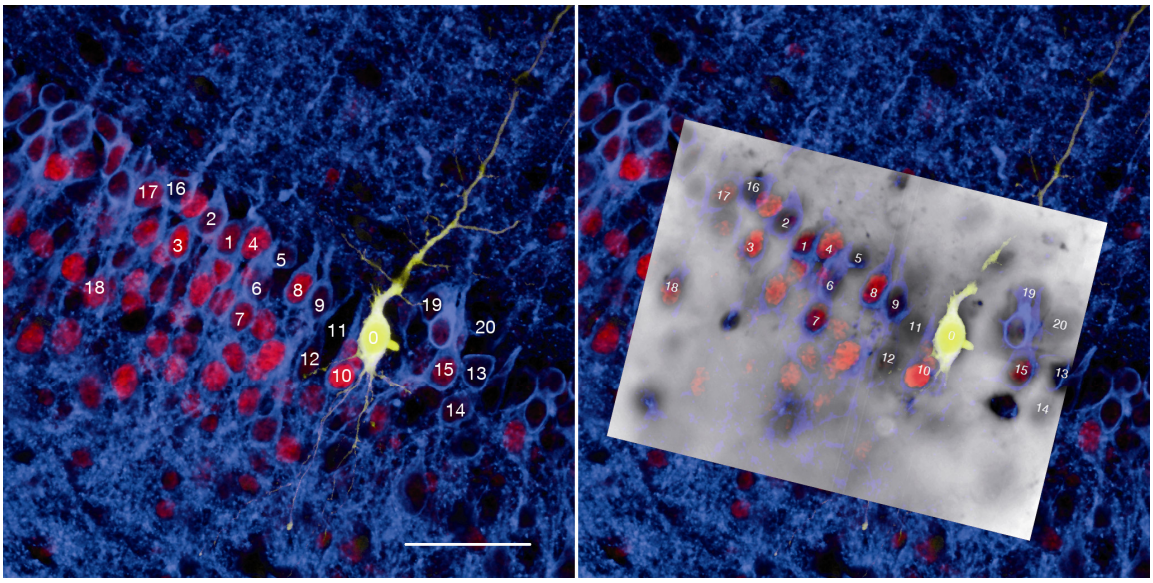

Figure 5: Single cell correlation between calcium signal and pCREB label.
Numbers indicate regions of interest (ROI) defined for the calcium imaging. White rectangle shows Fura-2 fluorescence image projected onto the immune-stained image, with the patch-clamped cell (yellow label) as a reference. pCREB negative cells appear dark (see roi 11; scale bar = 50µm).

2.4.3. Phospho-CREB quantification

Using ImageJ (NIH, Bethesda/USA) and Photoshop CS2 (Adobe, San Jose/USA) software, three different approaches were applied to quantify the intensity of the phospho-CREB staining.

1.) Number of pCREB positive cells per area (150x50µm rectangle around the patch-clamped cell):

A maximum intensity projection of the pCREB image stack was carried out. By utilizing an ImageJ macro implementing several built-in algorithms (e.g.: watershed, median filter, analyze particles) this projection was transformed into a threshold black and white image. The single pCREB positive nuclei were detected according to their size and circularity. Structures with a non-circular shape were occluded. The result was displayed as total number of pCREB positive cells in this rectangle (see Figure 14B).

2.) Correlation of pCREB to the measured calcium signal on a single cell:

The imaged cells were identified using an overlay of the fluorescence image of the calcium measurement and the image showing the immunostaining (Figure 5). To be able to compare the intensities between different experiments the pCREB background intensity of each slice had to be subtracted. For the background subtraction an area in the stratum pyramidale was chosen, which was located outside of the area affected by the puff application. And therefore represents background pCREB immunoreactivity. The relative pCREB immunoreactivity was calculated in arbitrary units (a.u.). Three different ways of displaying the correlation were applied.

First, the relative pCREB immunoreactivity was plotted against the peak calcium concentration of a single experiment (Figure 21). Second, to compare individual experiments, the cells imaged in each experiment were pooled according to their peak calcium concentration (groups of 100-200nM; 200-300nM; 300-400nM; >400nM; Figure 22A and B). Then the mean value of the pCREB immunoreactivity of one particular group was calculated. From all the means of the defined groups of different experiments an average was formed and plotted against the peak calcium concentration (Figure 22A). Third, all cells in the experiments were compared. Therefore the mean pCREB immunoreactivity of all cells from all experiments of a single calcium concentration group (see above) was determined and plotted against the calcium concentration (Figure 22B).

3.) Number of pCREB positive cells in whole frame of the confocal image (analysis of ENO-driven CREB phosphorylation)

The number of neurons was detected using the MAP5 staining and a custom written ImageJ macro (similar to the one described in 1.). In this case all the pCREB positive cells in the image were detected as well as all neuronal cells, as detected by the MAP5 staining. The ratio of pCREB positive cells to the number of MAP5 positive cells was calculated and displayed as percentage of pCREB positive cells (see Figure 27B).

2.4.4. Statistical analysis

For comparison of mean peak calcium concentrations and relative pCREB immunoreactivity the student´s t-test was applied. If not indicated otherwise Excel 2007 (Microsoft, Redmaon/USA) was used to perform an unpaired homoscedastic t-test. Applications of pharmacological substances (for example CPA, BAPTA etc.) were always compared to applications in control conditions (usually ACSF including 500nM of TTX). Variations in results on particular experiments were given as the standard error of mean (SEM), either of the mean peak calcium concentration or the number of pCREB positive cells.

2.5. Simplified chart of the experimental procedure

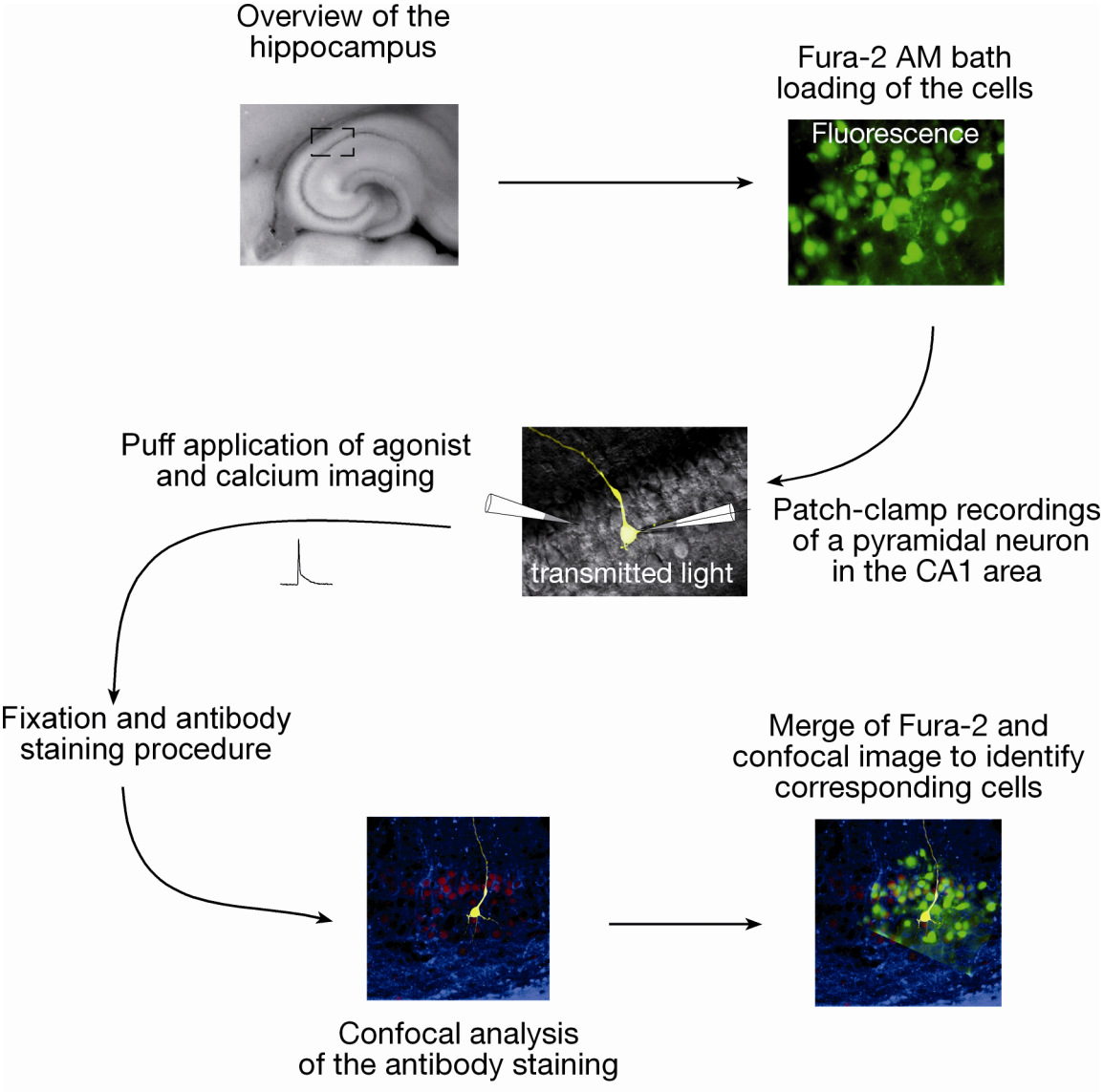

Figure 6: Schematic overview of the experimental procedure
The experiment was carried out in the CA1 area of hippocampal slices (rectangle). Unless indicated otherwise the slices were perfused with ACSF+500nM TTX, to block background pCREB immunoreactivity. The slices were loaded with Fura-2 AM followed by patch-clamp recording of a neuron. Changes in the fluorescence of the calcium indicator evoked by puff application of the agonist were recorded. The slices were fixed and prepared for antibody staining. The fluorescent antibodies were detected using a confocal microscope and later merged with the fluorescent image of the calcium signals to be able to correlate the two examinations on the same the cell.

3. Results

3.1. Pulse-like application of the mGluR agonist DHPG evoke rapid calcium transients

Most studies of mGluR-mediated electrical or calcium signals and especially the induction of CREB phosphorylation via these signals have been performed by bath application of an agonist for at least 30 seconds and up to several minutes (Bianchi et al., 1999; Gee et al., 2003; Mao and Wang, 2002a). In this study, physiologically more relevant pulse-like applications (≤500ms) of agonist that mimic more accurately synaptic activation of receptors were used.

One single puff application of the metabotropic agonist DHPG (500ms; 500µM) was sufficient to trigger a slow depolarization in CA1 neurons, which eventually lead to the initiation of action potentials (Figure 7B). The calcium signal (relative change in fluorescence ΔF/F, see 2.4.1) associated with this slow depolarization showed a fast increase in intracellular calcium concentration at the soma (Figure 7B, lower panel) right after the application of DHPG. The increase in calcium concentration clearly preceded the initiation of action potentials. The calcium dynamics after the initial peak were shaped by the action potentials (Figure 7B, lower panel) and the intracellular calcium concentration returned to resting levels only after the action potential firing had stopped. Blocking the action potentials by bath application of 500nM TTX left the initial calcium peak unaffected (Figure 7C, lower panel). Nevertheless a small depolarization was still present (Figure 7C). The onset and rising phase of the evoked calcium transient in the TTX-containing ACSF showed kinetics comparable to the initial calcium peak in normal ACSF conditions. Therefore 500nM TTX was routinely applied to the bath in all experiments to omit any effects of action potential triggered calcium influx on the DHPG-induced calcium transients.

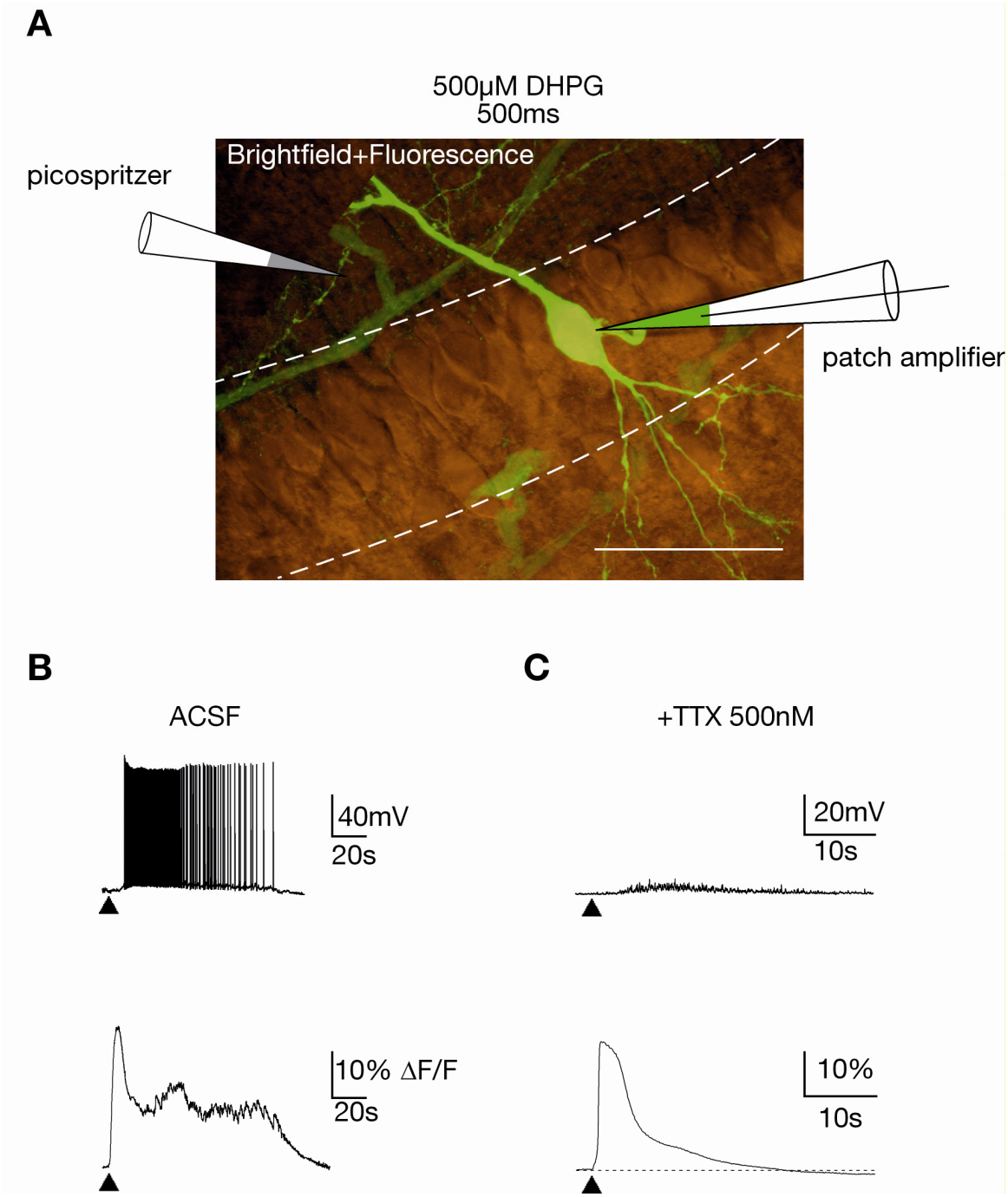

Figure 7: Short puff application of DHPG induces an intracellular calcium elevation and a depolarization of the cell.
(A) Setup of the experiment. Patch pipette was filled with intracellular solution containing OGB-1 (50µM) and 0.1% neurobiotin. The patch-clamped cell is located in the CA1 stratum pyramidale (dashed white lines; scale bar = 20µm. (B) Short puff application of DHPG (500µM for 500ms) induces a depolarization leading to action potential firing and a biphasic calcium transient (B), which initial peak precedes the induction of action potentials. After perfusion of the slice with TTX (500nM) DHPG application lead to a small depolarization (C) but the initial, action potential-independent calcium rise is unaffected (note the different scaling for B and C).

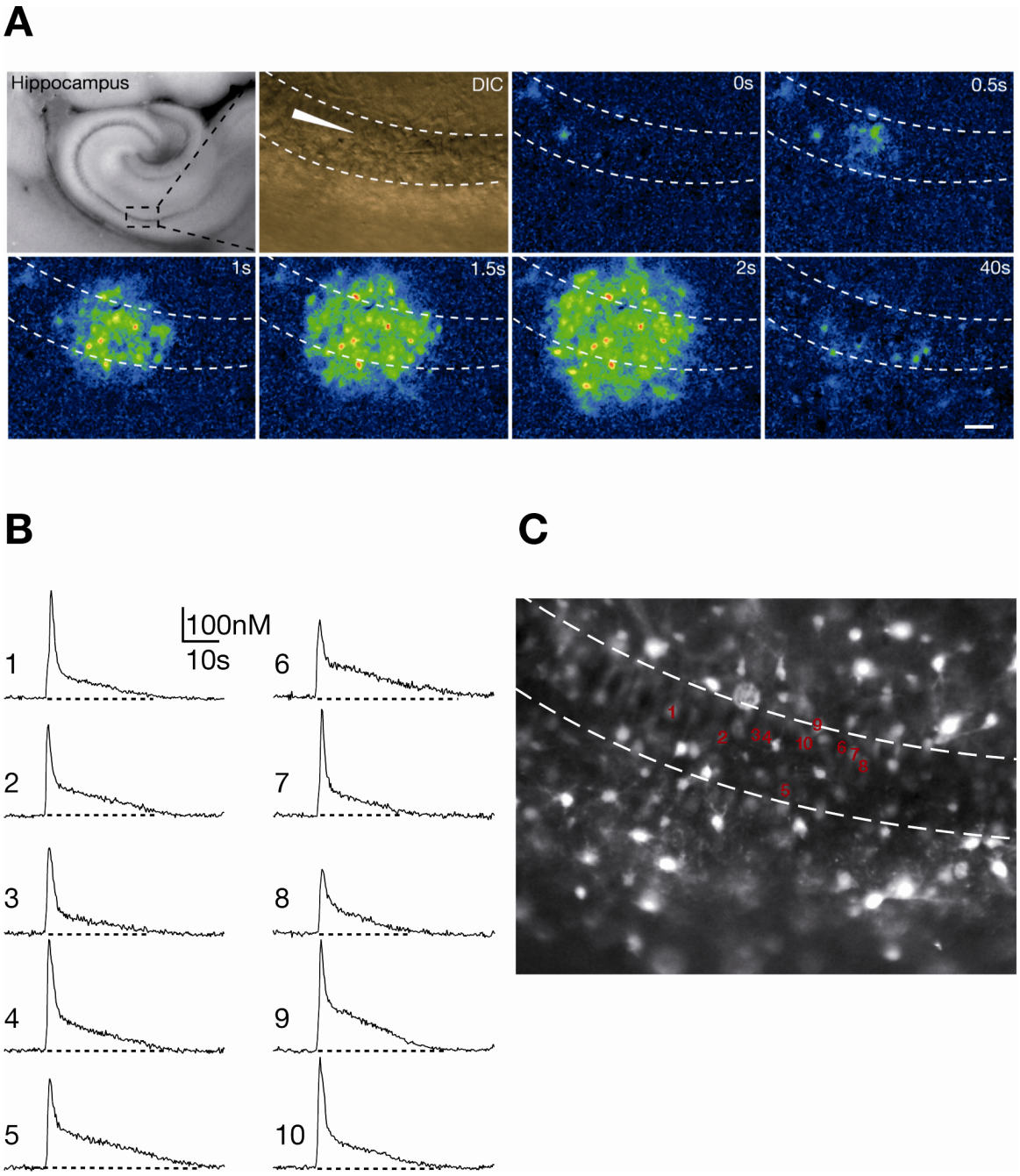

Figure 8: Spatial and temporal features of DHPG evoked calcium transients.
(A) Time course of the DHPG-evoked calcium signal in neurons of the stratum pyramidale in CA1 (dashed white lines).The first image shows the area of the hippocampus in which the recording was performed (indicated by the dashed black line). Location of the puff pipette is indicated by the white triangle. The Fura-2 calcium signal is shown as pseudocolour images, reflecting the relative change in fluorescence ratio (scale bar = 50µm). (B) Calcium transients from individual cells indicated in (C).

In Figure 8, recordings of Fura-2 fluorescence changes at a low magnification (20x objective) were made to investigate the size of the area affected by the puff application of DHPG. Application of DHPG for 500ms induced calcium elevations in an area of about 200µm surrounding the application point (Figure 8A). Already after 2s the largest expansion of the signal could be detected and after 40s all cells returned to resting calcium levels. The neuronal somata in the stratum pyramidale as well as the dendrites and the non-neuronal cells located in the stratum radiatum showed calcium elevations.

Single cell transients from cells located in the stratum pyramidale (Figure 8B) showed a fast initial calcium peak followed by a biphasic decay. The DHPG-evoked calcium transients could be blocked by perfusing the slices with the specific group I/II mGluR antagonist MCPG. 2mM of MCPG were sufficient to block (96% of block; n=4) DHPG-evoked intracellular changes in calcium concentration (Figure 9B). 500ms application of 500µM DHPG in the experiment shown in Figure 9A resulted in peak calcium concentrations of up to 450nM (Figure 9D; black dots representing single cells recorded in one experiment), whereas the perfusion with 2mM MCPG reduced the mean peak amplitude to about 88nM, what equals the basal intracellular calcium concentration.

Puff application of DHPG resulted in mean intracellular peak calcium concentration of 313±12nM SEM (Figure 10B; n=18; SEM: for statistical analysis see section 2.4.4; n represents the number of individual experiments). Additionally, puff applying 500µM trans-ACPD, a less specific mGluR group I and II,III agonist, resulted in similar mean peak amplitude (Figure 10a; 310±24nM; n=4). Bath application of MCPG left the peak amplitude almost unaffected (109±8nM; n=4). ACSF was puff applied to exclude the possibility of activating mechanosensitive channels and to test whether the calcium transients could be evoked by the application itself. In this case no calcium elevation could be detected (97±3nM; n=4; note that the basal calcium level was around 100nM). Statistical analysis showed that the mean peak calcium concentration of DHPG and t-ACPD compared to MCPG/DHPG and ACSF application was highly significant ($p<0.0001$).

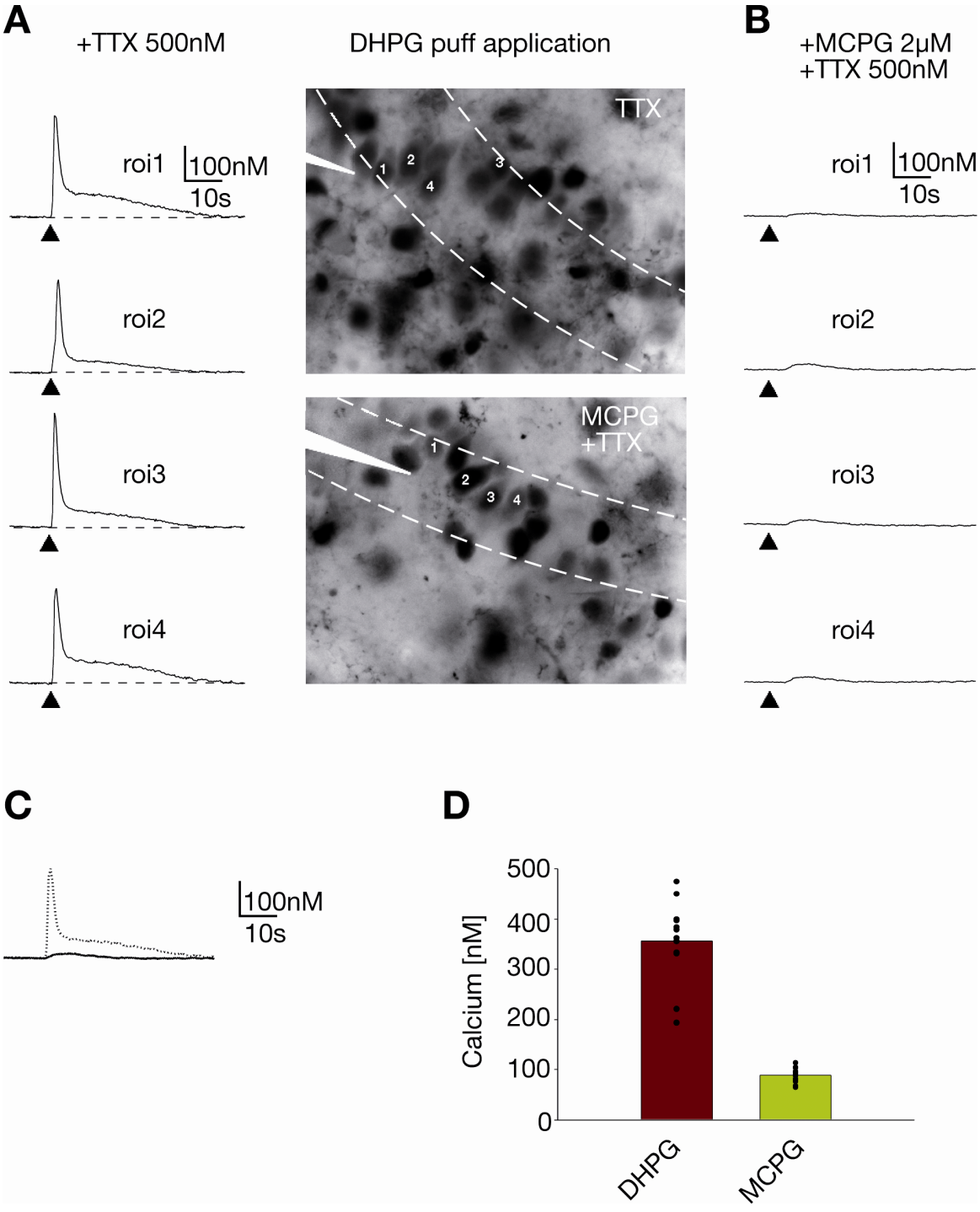

Figure 9: The metabotropic antagonist MCPG blocks DHPG-induced calcium transients.
(A) Single cell changes in calcium concentration evoked by puff application of DHPG (black triangle) of the cells depicted in the Fura-2 fluorescence image (TTX). (B) MCPG blocks DHPG-induced calcium transients. (C) Average transients of 10 cells of the single experiment depicted in (A). (D) Mean peak calcium concentration of DHPG-evoked transients of the experiment in (A). Dots represent single cells.

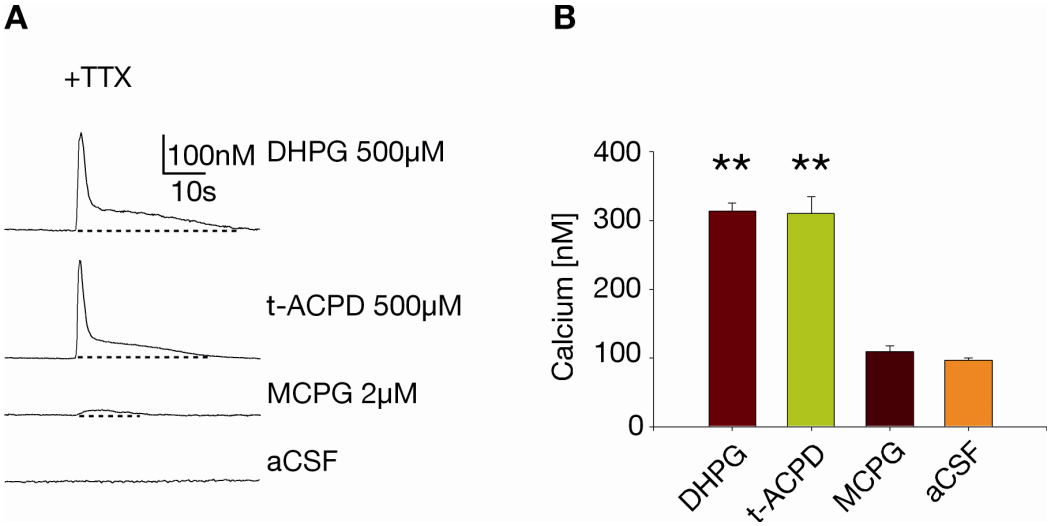

Figure 10: Summary of metabotropic agonist-evoked calcium signals.
(A) Average transients of 5-8 cells recorded in one single experiment. (B) Mean peak calcium concentration of the calcium signal from all experiments (DHPG n=18; t-ACPD n=4; MCPG n=4; ACSF n=4; $p<0.0001$). Note that basal calcium levels were around 100nM.

3.2. Activation of mGluR leads to phosphorylation of CREB at Ser133

Mao et al. showed that prolonged bath application of DHPG is able to induce CREB phosphorylation in striatal neurons (Mao and Wang, 2002a). To test whether the short pulse-like applications of DHPG are sufficient to induce the phosphorylation of CREB, calcium measurements were combined with an immunohistological fluorescent analysis of the phosphorylation status of CREB.

After DHPG-evoked changes in intracellular calcium concentration were recorded acute hippocampal slices were fixed and antibody labeled for phospho-CREB positive nuclei (red; Figure 11). The MAP5 staining serves as a neuronal marker, which labels the dendrites and the somata (blue; Figure 11) but not the nucleus and therefore could be used as a counterstain to the pCREB-label, which is located in the nucleus. The patch-clamped cell was filled with neurobiotin-containing intracellular solution and could be detected in the confocal analysis (yellow; Figure 11, see 2.3.5).

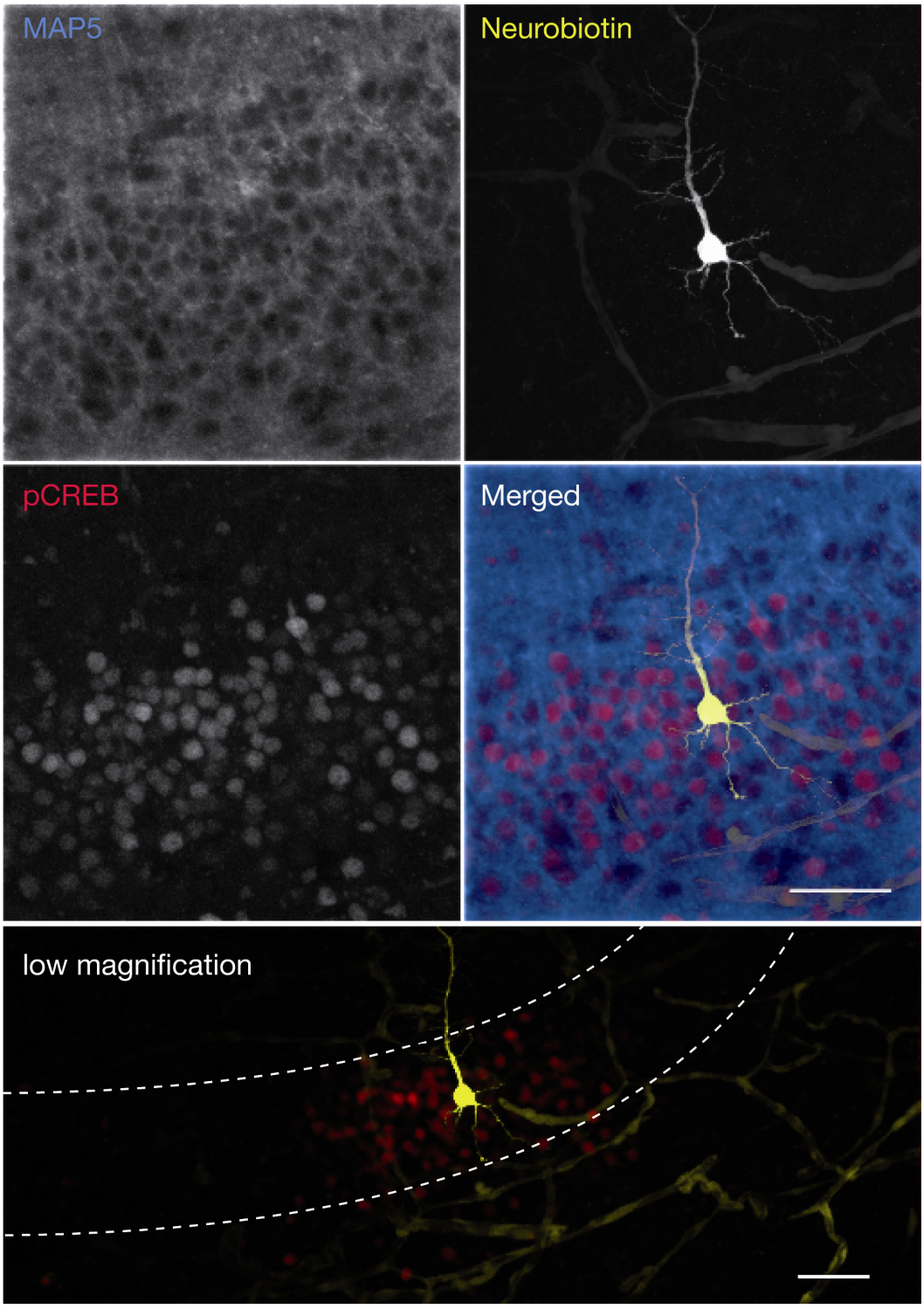

Figure 11: DHPG-evoked CREB phosphorylation
Antibody labeling for MAP5 (neuronal marker), Neurobiotin (patch-clamped cell), and pCREB. Low magnification shows the defined region of pCREB positive cells surrounding the site of application in the stratum pyramidale (dashed line; scale bars = 50µm).

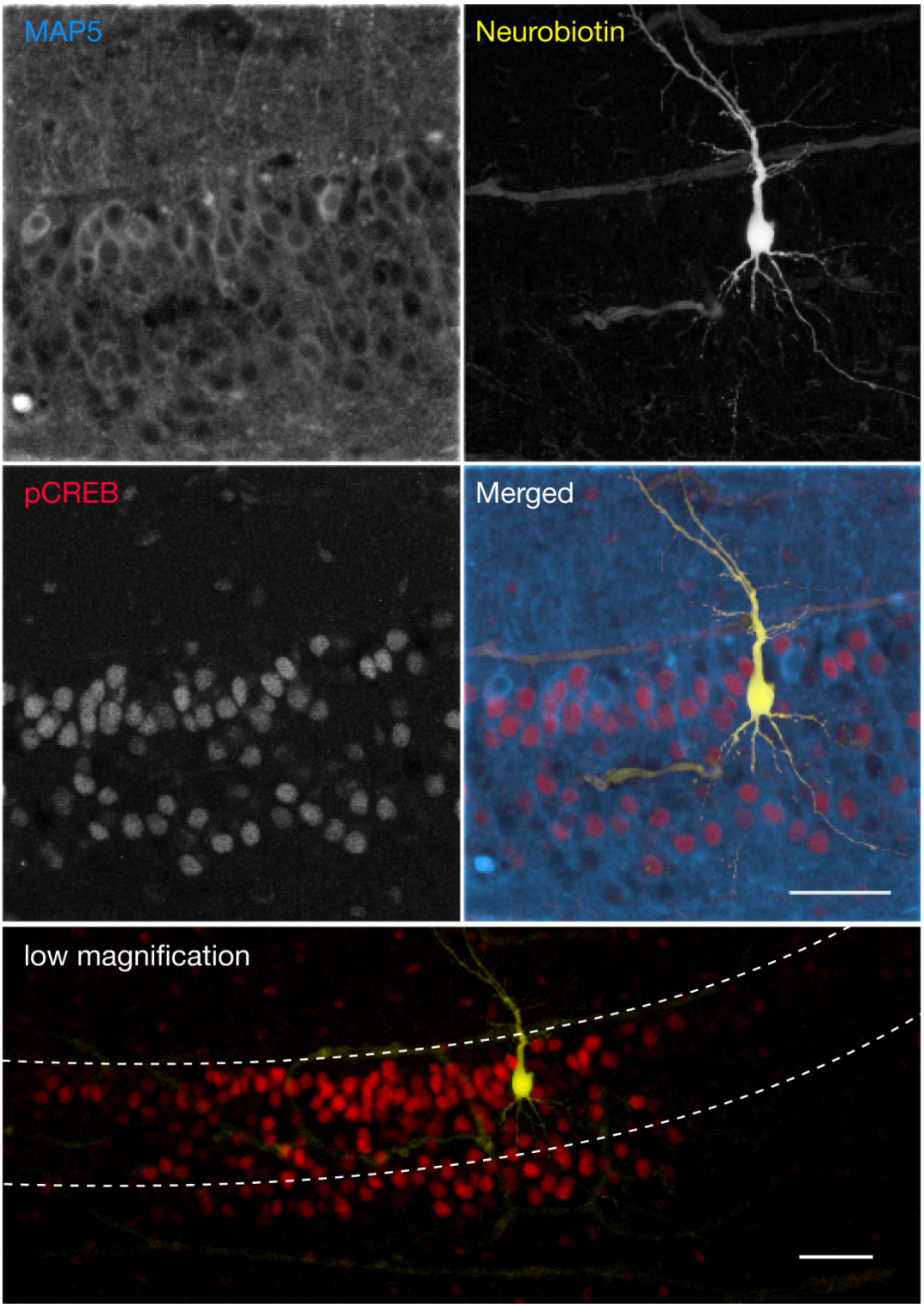

Figure 12: t-ACPD-evoked CREB phosphorylation
Antibody labeling for MAP5 (neuronal marker), Neurobiotin (patch-clamped cell), and pCREB. Low magnification shows the defined region of pCREB positive cells surrounding the site of application in the stratum pyramidale (dashed line; scale bars = 50µm).

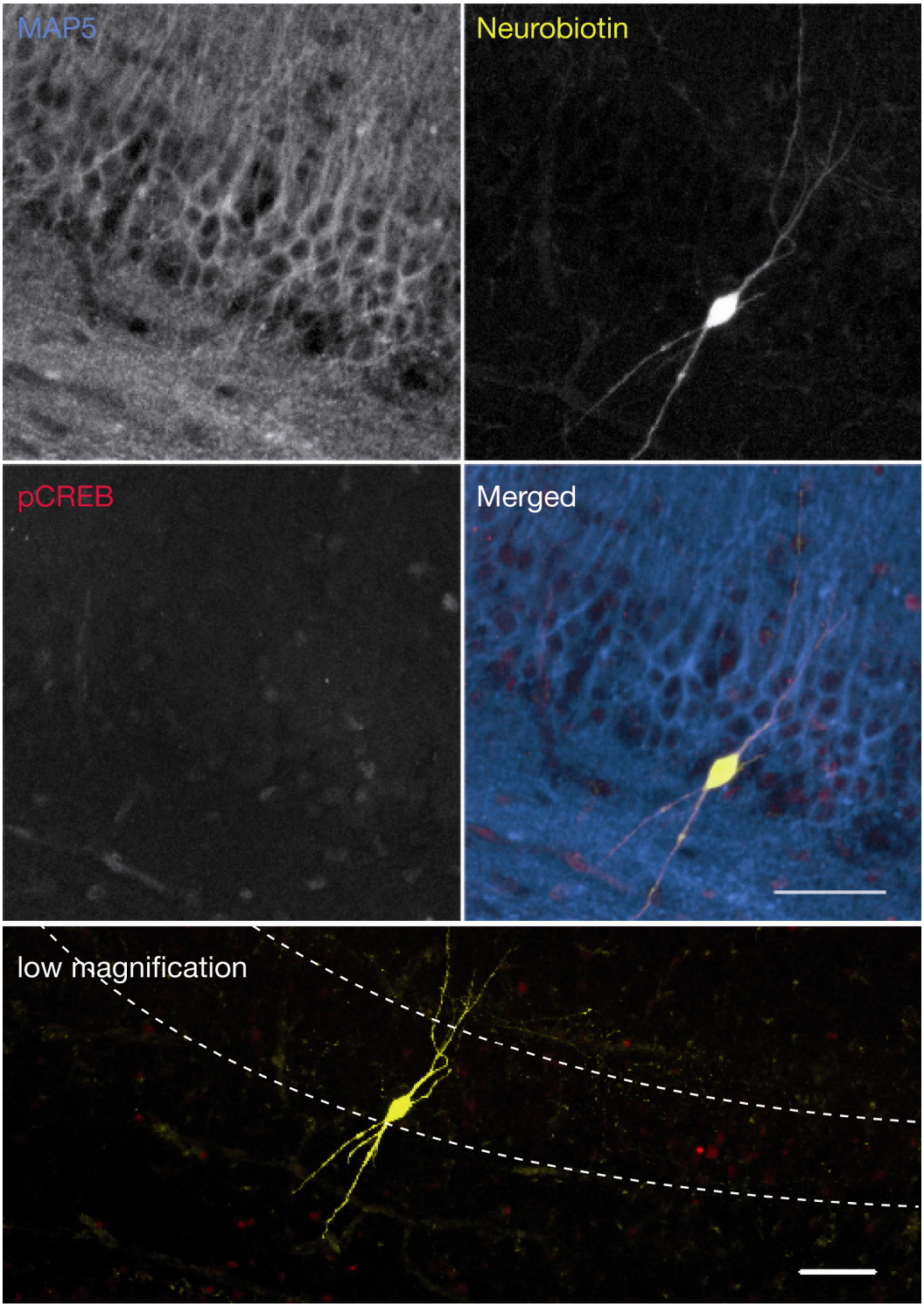

Figure 13: ACSF puff application has no effect on CREB phosphorylation
Antibody labeling for MAP5 (neuronal marker), Neurobiotin (patch-clamped cell), and pCREB. Low magnification shows no pCREB positive cells surrounding the site of application in the stratum pyramidale (dashed line; scale bar = 50µm).

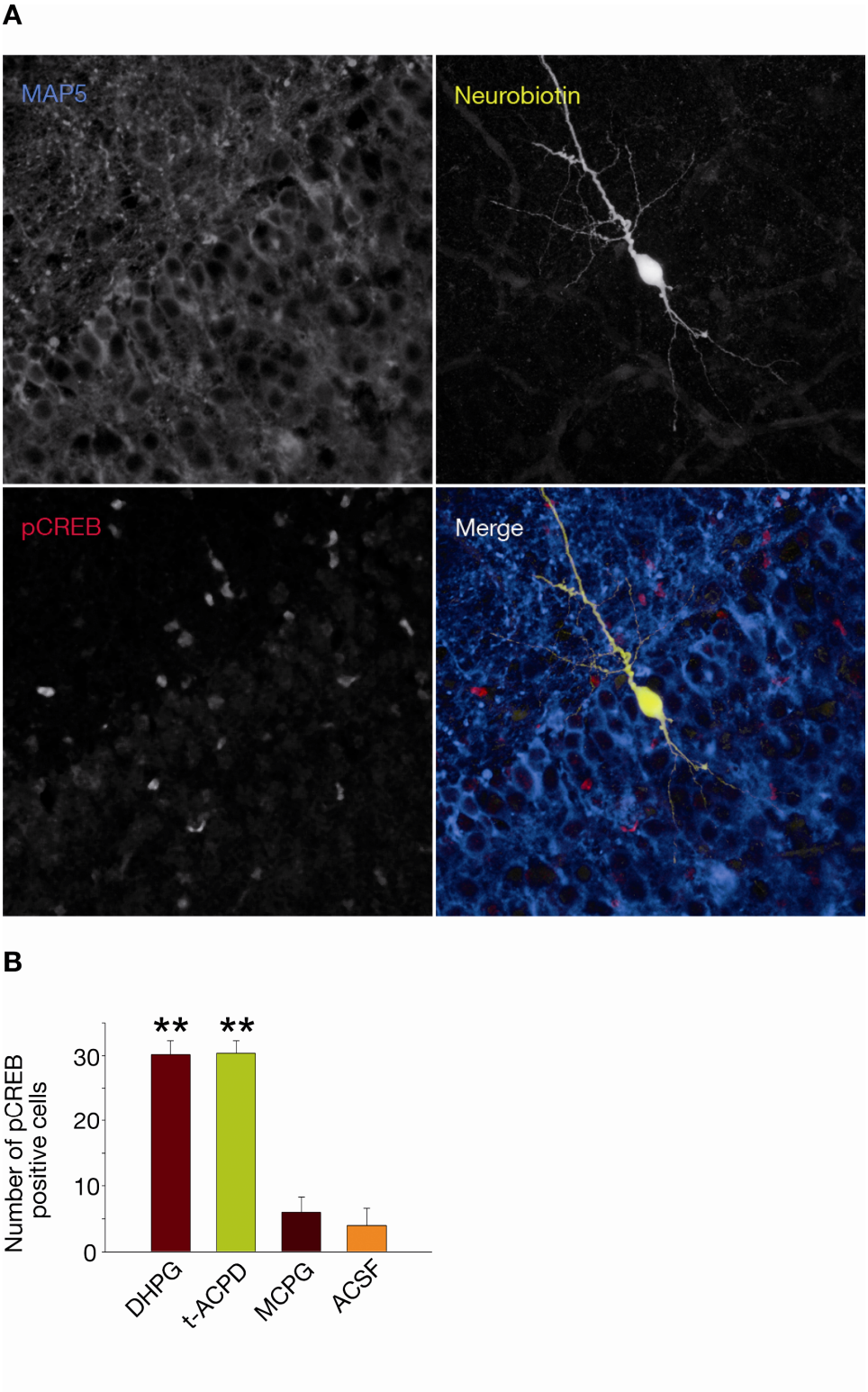

Figure 14: MCPG blocks DHPG-induced CREB phosphorylation
A) Antibody labeling for MAP5 (neuronal marker), Neurobiotin (patch-clamped cell), and pCREB in the stratum pyramidale in close proximity to the patch-clamped cell (dashed line; scale bar = 50µm). B) Statistical analysis of the number of pCREB positive cells in a defined area surrounding the patch-clamped cell (DHPG n=48; t-ACPD n=19; MCPG n=4; ACSF n=4; $p<0.0001$).

Background staining in the yellow channel resulted from neurobiotin, expelled through pressure applied on the patch-clamp electrode while approaching the cell (see 2.3.2). Obviously, neurobiotin had a high affinity to blood vessels, since only locally around the patch-clamped cells small vessels were stained (Figure 11; neurobiotin).

A single short puff application of metabotropic agonists is sufficient to trigger the phosphorylation of CREB (Figure 11 and Figure 12). The number of pCREB positive cell nuclei refers to cells surrounding the patch-clamped cell in a rectangle of 150µm x 50µm (see section 2.4.3). DHPG and t-ACPD were equally efficient to trigger the phosphorylation of CREB upon puff application (Figure 14; DHPG: 30±2 pCREB positive cells; n=48; t-ACPD: 30±2 pCREB positive cells; n=19). MCPG blocks DHPG-induced phosphorylation of CREB (Figure 14A; 6±2 pCREB positive cells; n=4). Application of ACSF has no effect on the phosphorylation status of CREB (Figure 13 and Figure 14B; 4±2 pCREB positive cells; n=4). The statistical analysis showed, that the capability of DHPG- and t-ACPD-induced CREB phosphorylation compared to MCPG/DHPG and ACSF application is highly significant ($p<0.0001$).

To examine the role of extracellular calcium in DHPG-induced calcium transients and CREB phosphorylation the hippocampal slices were perfused with 0calcium-ACSF (0Ca) containing additionally 100µM of the calcium chelator EGTA. After approximately 10 minutes of perfusion with 0Ca the internal calcium stores start getting depleted. The activation of mGluR causes IP_3-mediated release of calcium from internal stores (see 1.3.1), which would therefore be affected by 0Ca. Depolarizing pulses were given to the patch-clamped cell via current injection (Figure 15; arrows) to test whether there is still extracellular calcium influx through voltage-gated calcium channels (VGCCs). As soon as there was no significant change in intracellular calcium concentration (5 to 9 minutes after wash-in) DHPG was applied. At this point the evoked calcium transient resulted almost exclusively from calcium release from internal stores. It showed only a modest yet significant reduction in mean peak calcium concentration (Figure 15C; 241±9nM; n=4) compared to the control application (313±12nM; n=18; $p<0.001$). The effect on the phosphorylation status of CREB showed a decrease in mean number of pCREB positive cells (Figure 16; DHPG 30±2 pCREB positive cells; n=48; 0Ca short 20±5 pCREB positive cells; n=4), but this difference was not statistically significant ($p>0.05$).

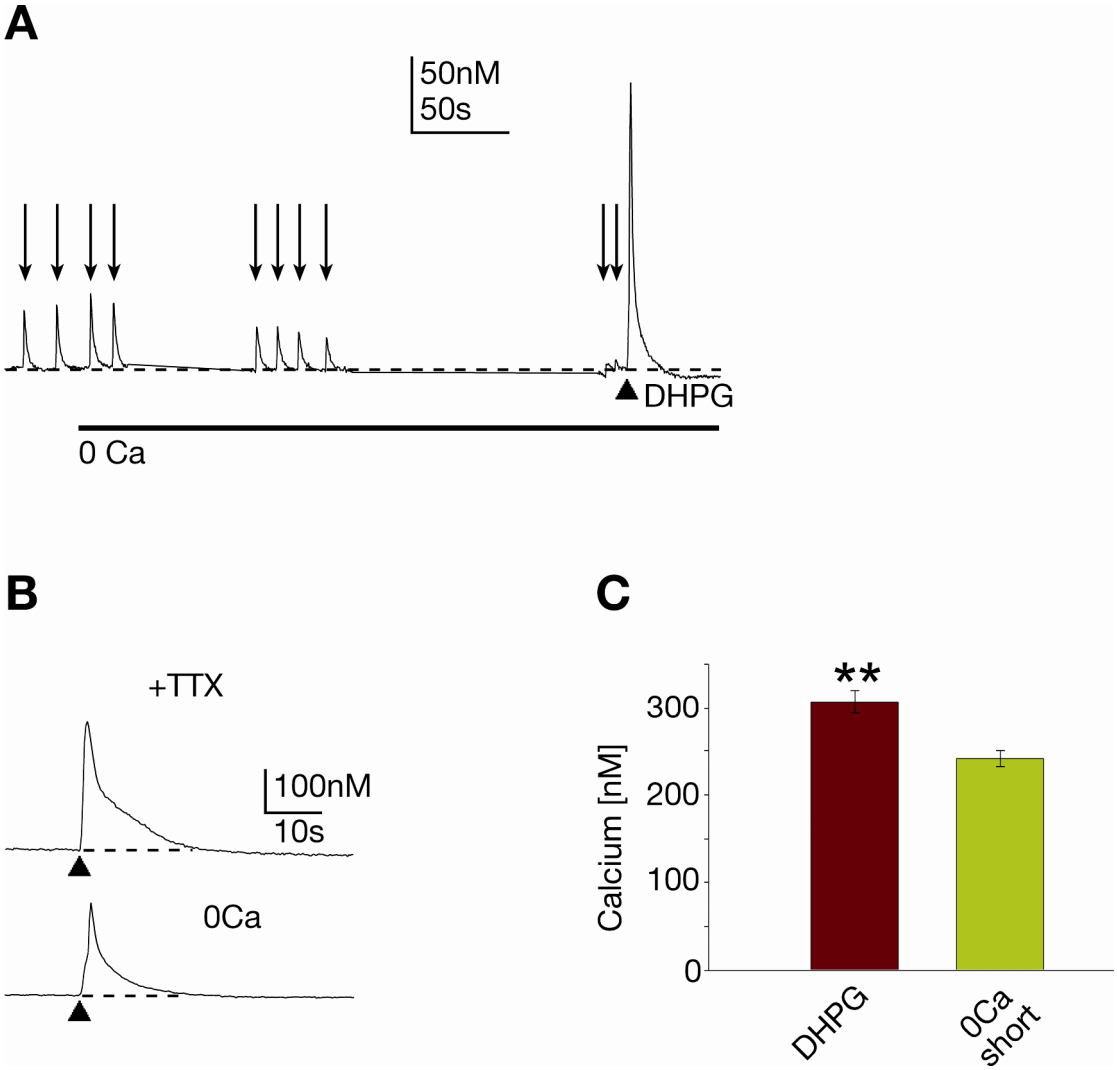

Figure 15: Effects of removal of extracellular calcium on DHPG-induced calcium transients.
(A) Arrows indicate depolarizing pulses, which induce small calcium transients driven by extracellular calcium entering the cell through voltage gated calcium channels. After establishing that there is no calcium influx from extracellular space (last two depolarizing pulses, show almost no intracellular calcium change) DHPG was puff applied, resulting in a calcium signal derived from calcium release from internal stores. (B) Average transients of 6-8 cells of one single experiment showing DHPG-induced calcium transients. (C) Statistical analysis of the mean peak calcium concentration (DHPG n=18; 0Ca short n=4; $p<0.001$).

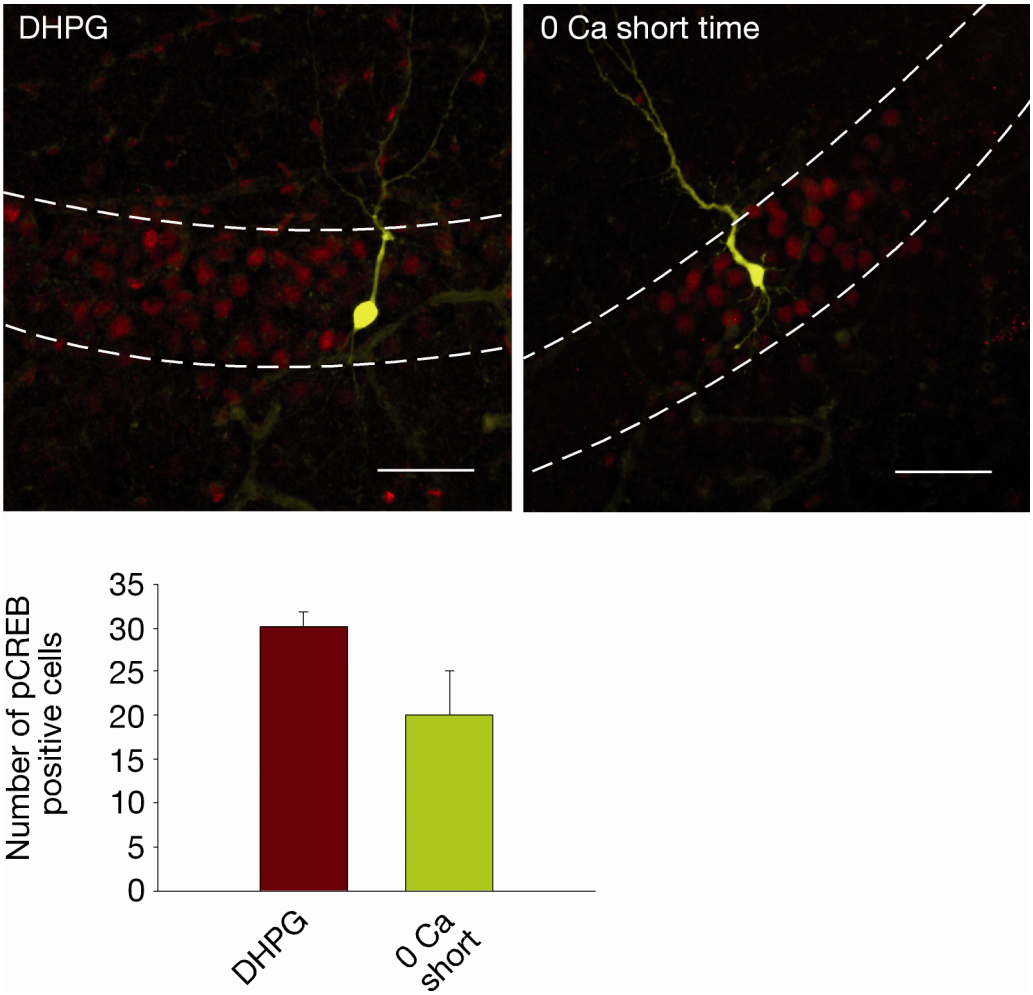

Figure 16: Removal of extracellular calcium for a short time has little effect on DHPG-induced CREB phosphorylation
pCREB immunoreactivity in CA1 pyramidal neurons (stratum pyramidale dashed line; scale bar=50µm) after the application of DHPG in ACSF or zero calcium ACSF. Statistical analysis of the number of pCREB positive cells in a defined area surrounding the patch-clamped cell (DHPG n=48; 0Ca short n=4; $p>0.05$).

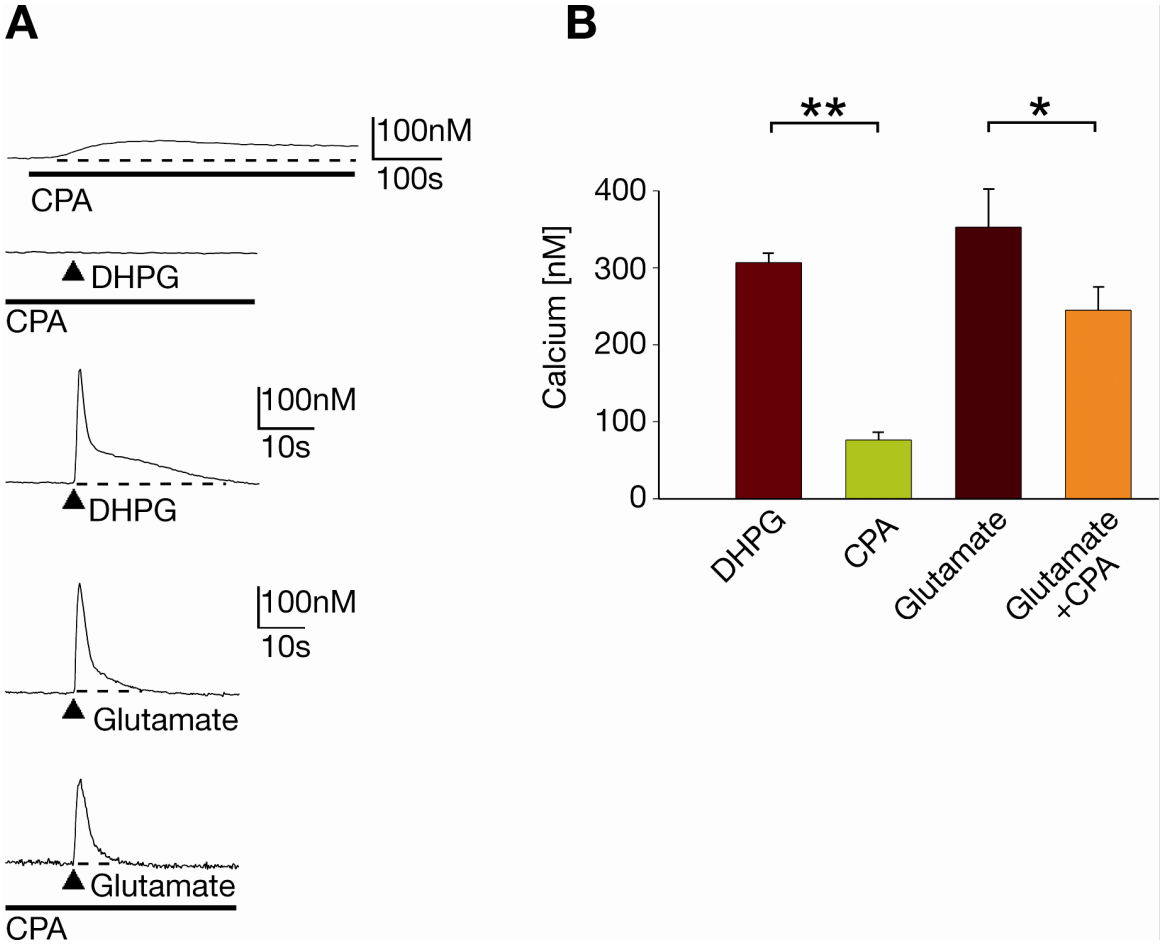

Figure 17: CPA blocks DHPG-evoked calcium transients but has little effect on glutamate-evoked calcium signals
A) Evoked calcium transients in individual cells. Bars underneath the recordings indicate the perfusion with the depicted substance (CPA). B) Statistical analysis of the mean peak calcium concentration. (DHPG n=18; CPA n=4; Glutamate n=4; Glu+CPA n=4; ** $p<0.001$; * $p<0.05$)

To test the significance of calcium release for DHPG-evoked calcium transients cyclopiazonic acid (CPA) a selective inhibitor of the sarco/endoplasmic reticulum Ca^{2+}-ATPase (SERCA), which regulates the uptake of calcium into the endoplasmic reticulum was applied. Bath application of 30µM CPA slowly increased the intracellular calcium concentration to about 130nM (Figure 17A). 20 minutes after wash-in the calcium stores were depleted and the calcium transients evoked by puff application of DHPG were completely abolished (Figure 17B; CPA: 77±10nM; n=4; $p<0.0001$; note the drop in basal intracellular calcium concentration compared to Figure 10).

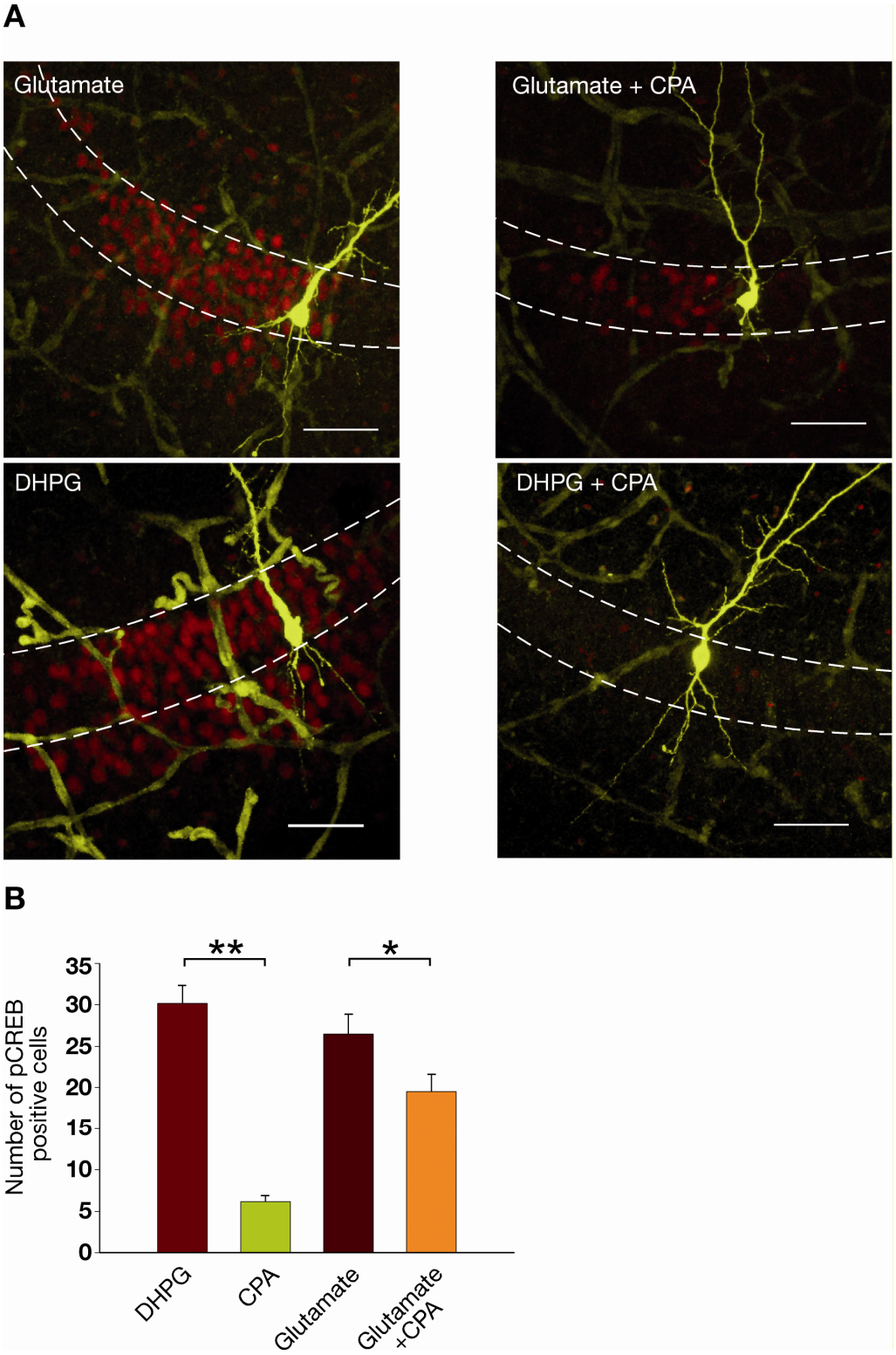

Figure 18: Effects of CPA on DHPG and glutamate-induced CREB phosphorylation.
A) DHPG and glutamate-evoked pCREB immunoreactivity in pyramidal CA1 neurons in the stratum radiatum (dashed line). B) Quantitative statistical analysis of number of pCREB positive cells surrounding the patch-clamped cell (DHPG n=48; CPA n=6; glutamate n=7; Glu+CPA n=4; **$p<0.0001$; $p<0.05$; scale bar=50µm).

The role of intracellular calcium release in glutamate-evoked calcium transients and CREB phosphorylation was examined. Brief puffs of Glutamate (200µM, 500ms) elicited calcium transients similar to DHPG application (Figure 17; Glutamate: 353±50nM; n=4). In contrast to DHPG, glutamate was still capable to induce intracellular calcium elevations in the presence of CPA but with a statistical significant reduction in mean peak amplitude (Figure 17A and B; Glutamate+CPA: 245±30nM; n=4; $p<0.05$). CPA not only blocked the DHPG-evoked calcium transients but also the DHPG-induced phosphorylation of CREB (Figure 18A and B: CPA: 6±1pCREB positive cells; n=6; $p<0.0001$ compared to control application). In contrast, glutamate application in the presence of CPA was still able to induce CREB phosphorylation. On average a decreased number of pCREB positive cells could be detected (Figure 18A and B; Glutamate: 26±2cells; n=7; Glutamate+CPA: 19±2 cells; n=4; $p<0.05$).

To disrupt normal calcium signaling in CA1 neurons, the cells were loaded with the calcium chelator BAPTA. Therefore 50µM of the membrane permeable form BAPTA-AM was bath applied. DHPG application induced a small increase in intracellular calcium concentration (Figure 19A and B; 79±5nM; n=5; $p<0.0001$ compared to control application), because the calcium released from internal stores is buffered by the BAPTA inside of the cell. Interestingly, although the peak calcium concentration was strongly reduced the second phase of the biphasic decay seemed almost unaffected (Figure 19A). The reduction in mean peak calcium concentration resulted in a decrease in number of pCREB positive cells (Figure 19C; BAPTA-AM 9±3cells; n=6; $p<0.001$).

Removal of extracellular calcium by perfusion for at least 20 minutes with 0Ca ACSF including 100µM EGTA completely blocked DHPG-induced calcium transients (Figure 19A and B; 56±6nM; n=3; $p<0.0001$ compared to control application). In comparison to the short perfusion (Figure 15 and Figure 16; 6 to 9 minutes) this treatment also empties internal calcium stores and therefore abolishes DHPG-induced calcium signaling and the phosphorylation of CREB (Figure 19C; 2±1cells; n=4; $p<0.0001$).

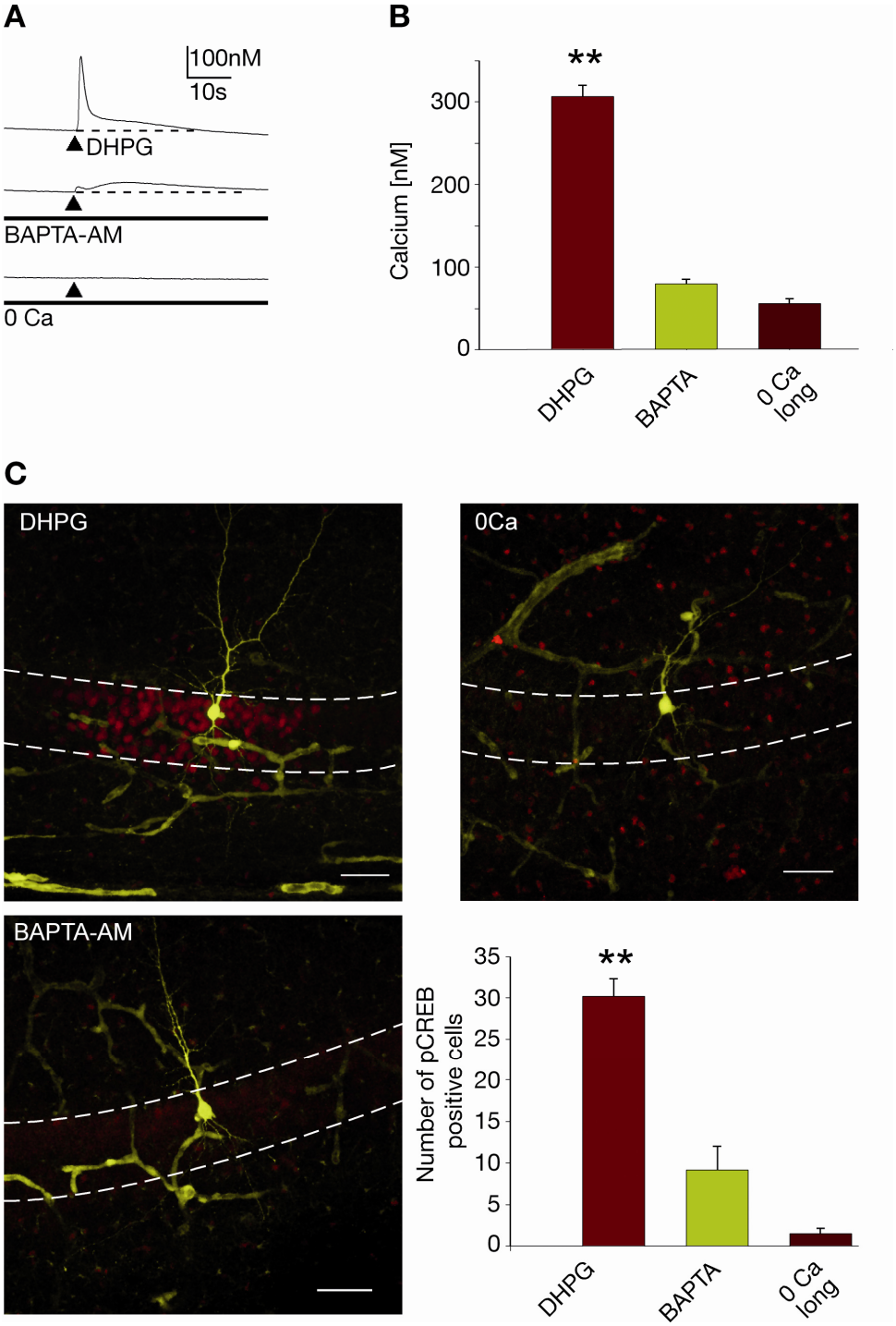

Figure 19: Calcium dependence of DHPG-evoked CREB phosphorylation
A) Effect of DHPG application on changes in intracellular calcium concentration in ACSF, BAPTA-AM (50µM) and 0Ca ACSF. Bars below the transients indicates perfusion with the respective substances. B) Statistical analysis of the mean peak calcium concentration (note the reduced basal calcium concentration; **p<0.0001 compared to control application). C) Quantitative statistical analysis of number of pCREB positive cells (**p<0.0001 compared to control application) surrounding the patch-clamped neuron in the stratum pyramidale (dashed line, scale bar=50µm).

One goal of this study was to show a direct correlation between the DHPG-evoked calcium changes and the pCREB immunoreactivity in one individual cell. The experimental design of this study made it possible to identify cells in the immunohistological staining, which were imaged for calcium changes before and therefore correlate intracellular calcium changes directly with pCREB immunoreactivity.

Figure 20 shows a representative experiment for the single cell correlation. The calcium transients in Figure 20B correspond to the cells labeled in the images in Figure 20A. Pyramidal neurons in the proximity of the patch-clamped cell, which showed a high peak calcium concentration were pCREB positive (cells 1-3 and 5-11), whereas cells with lower peak calcium concentration were pCREB negative (cell 4 and 12). Basal calcium concentrations were around 90±3.2nM (n=14). Cells with intracellular calcium concentrations above 500nM (Figure 20A, color-coded calcium signals, yellow and red) were located outside or adjacent to the stratum pyramidale. Because of their location size and shape these cells represent most likely glial cells and therefore were not included in the analysis,

By plotting the calcium concentration against background-subtracted pCREB immunoreactivity it was possible to make a correlation between the two parameters (Figure 21). Each triangle represents a single cell in this particular experiment (for details see 2.4.3-2). Cells which showed an increase in intracellular calcium concentration to about 300nM showed robust pCREB immunoreactivity depicted in arbitrary units (a.u.). Below 300nM the cells in this experiment were negative for pCREB immunoreactivity.

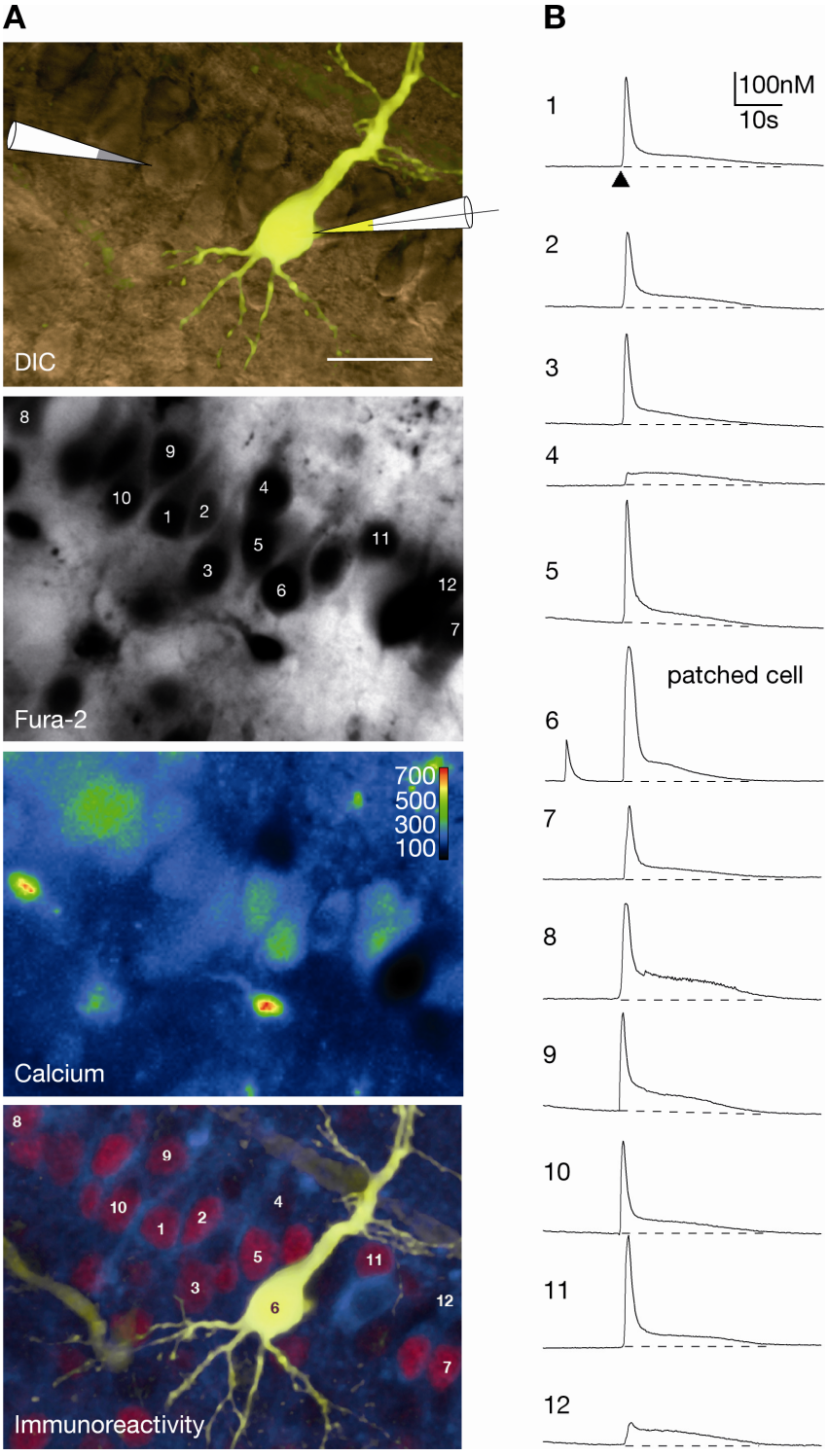

Figure 20: Detecting Fura-2 imaged cells in the immunofluorescence
A) DIC image illustrating the location of the patch-clamped cell (yellow) and the puff pipette (scale bar=20µm). Single wavelength (380nm) Fura-2 staining of cells in the CA1 area. Color-coded peak calcium concentration (in nM). Immunoreactivity of the cells imaged with the Fura-2 dye. B) Calcium transients of the cells shown in A.

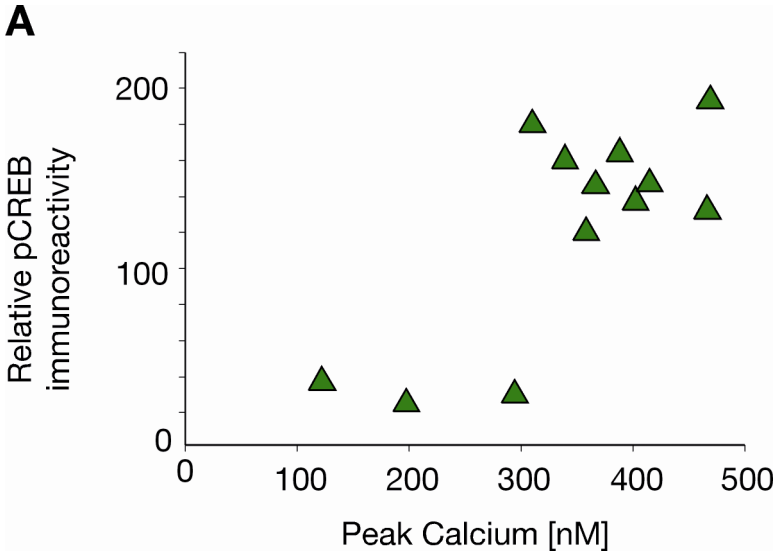

Figure 21: Correlation between calcium concentration and pCREB immunoreactivity
Plot of single cells (triangle) of one experiment according to their relationship between (see Figure 20) DHPG-evoked calcium transients [nM] and measured pCREB immunoreactivity [arbitrary units].

Figure 22 shows the increase in pCREB positive cells according to their peak calcium concentration. For all experiments the mean peak calcium concentrations were split into groups of 100nM. For each experiment the mean pCREB immunoreactivity of the particular calcium concentration group was determined. The mean pCREB immunoreactivity of each experiment for each calcium concentration group was pooled (for details see 2.4.3-2). The cells which responded only with a small calcium elevation showed low pCREB immunoreactivity (Figure 22A; 29±6 a.u. of pCREB intensity; n=10). Cells with a calcium peak between 200 and 300nM already showed a marked increase in pCREB immunoreactivity (66±16 a.u.; n=14). Nevertheless the increase compared to the first group was not significant ($p>0.05$). The two groups of cells which had peak calcium concentrations above 300nM showed no statistically distinguishable pCREB immunoreactivity (117±19 a.u.; n=15 and 132±26 a.u.; n=12; $p>0.6$). Nevertheless, comparing the two groups with smaller calcium changes to the 300-400nM group resulted in significant differences (Figure 22A; $^{**}p<0.001$; $^{*}p<0.05$). In Figure 22B single

cells were grouped according to their calcium peak and plotted against their pCREB immunoreactivity. So in contrast to Figure 22A not the mean values of a single experiment but the mean value of single cells of all experiments was plotted. This plot shows a positive correlation between the peak calcium concentration of a particular cell to its pCREB immunoreactivity.

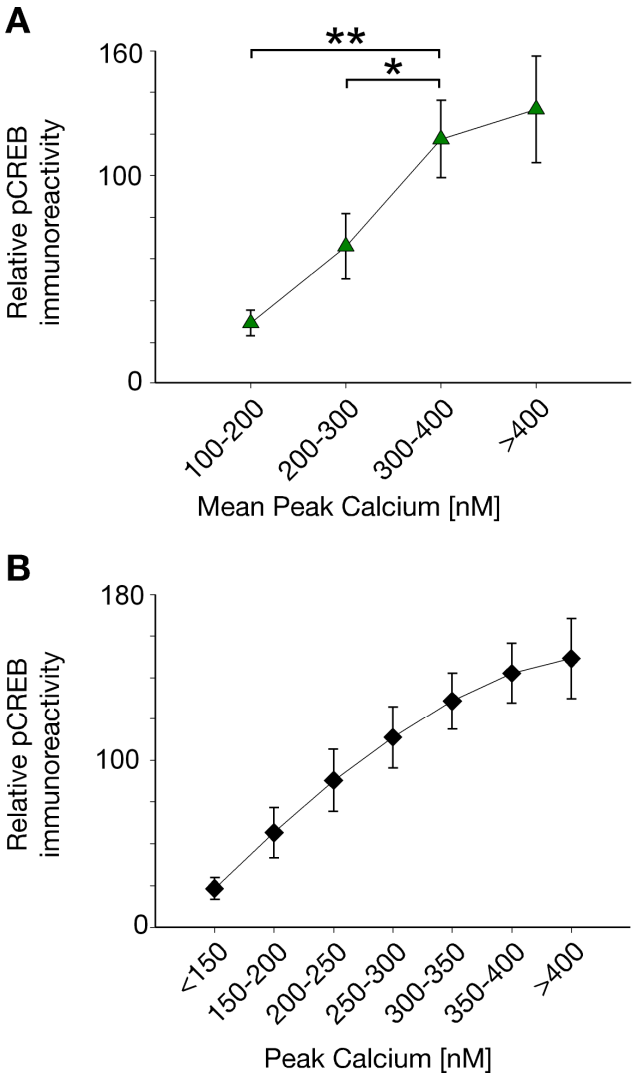

Figure 22: Statistical correlation between calcium concentration and pCREB after DHPG application

A) The mean pCREB intensities of each experiment for each calcium concentration group were pooled and plotted according to the calcium concentration (Error bars represent SEM; paired t-test; **p<0.001; *p<0.05). B) All recorded cells were pooled according to their calcium concentration and plotted against the mean pCREB immunoreactivity of each group (for details see 2.4.3-2).

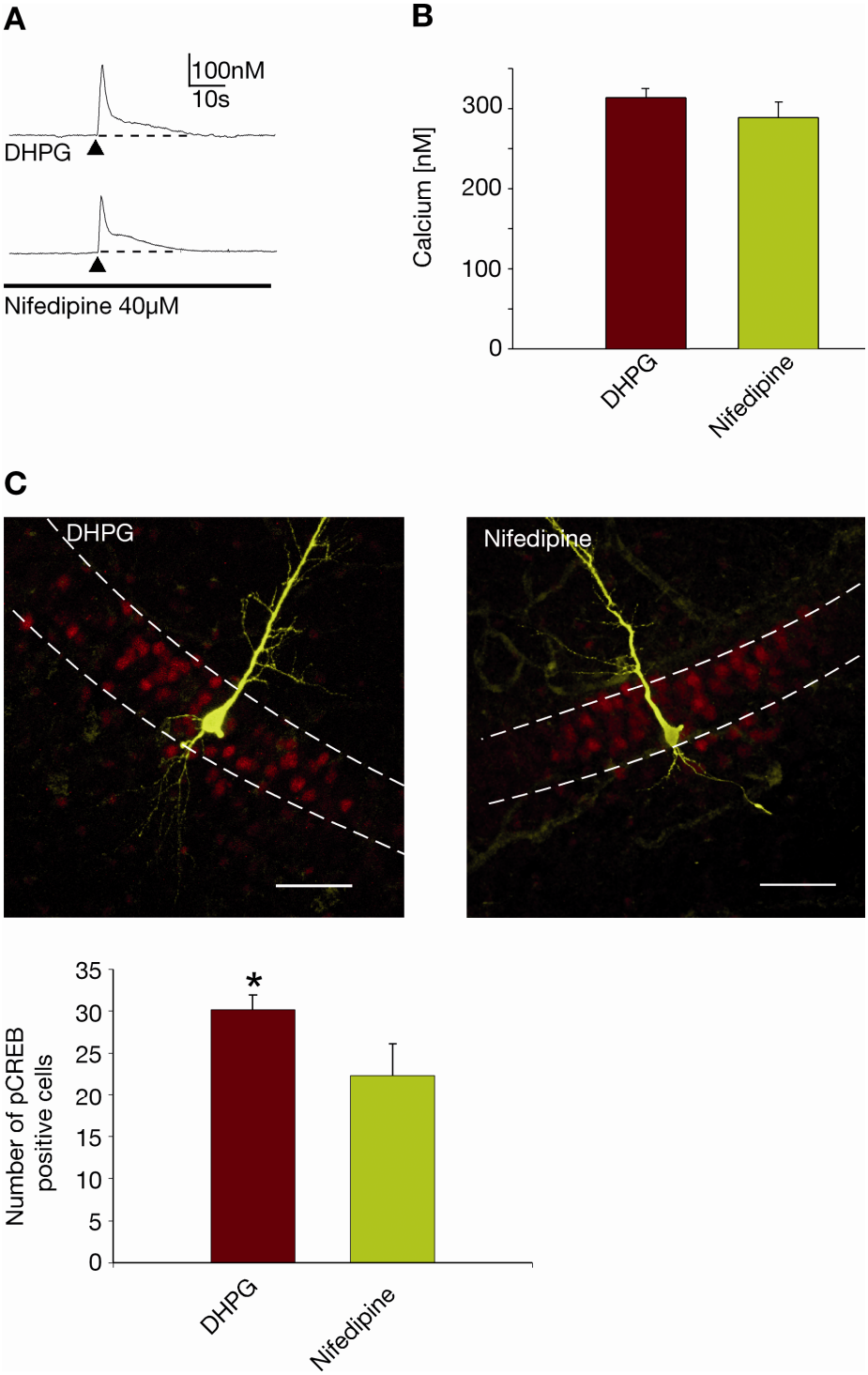

Figure 23: Role of voltage gated calcium channels in DHPG-induced calcium transients and CREB phosphorylation

A) DHPG-evoked calcium transients. The bar below the transients indicates the perfusion with the specified substance. B) Statistical analysis of mean peak calcium concentration (DHPG n=18; Nifedipine n=10; $p>0.2$). C) DHPG-dependent pCREB immunoreactivity in CA1 pyramidal neurons (DHPG n=48; Nifedipine n=19; $p<0.02$; scale bar=50µm).

It was shown (Mao and Wang, 2003) that DHPG-mediated CREB phosphorylation is dependent on calcium entry through L-type voltage gated calcium channels (VGCC). In order to determine the role of L-type VGCCs in the regulation of metabotropic glutamate receptor induced CREB phosphorylation, the dihydropyridine Nifedipine, which is an L-type VGCC antagonist was applied. Perfusion of the slice with 40µM Nifedipine had only little effect on the peak calcium concentration evoked by puff application of DHPG (Figure 23A; 288±20nM; n=10, $p>0.2$). Also the time course of the calcium transients was similar, with a fast increase and a biphasic decay. Nevertheless, a weak but significant reduction in the number of pCREB positive cells could be observed (Figure 23C; 22±4cells; n=19; $p<0.02$).

To interfere with the mGluR-mediated signaling cascade specific inhibitors of putative signal transducing targets in the pathway leading to the phosphorylation of CREB were used. Because release of calcium from internal stores is necessary for mGluR-mediated CREB phosphorylation (see Figure 18), the specific PLC inihibitor U73122 was applied to block the PLC-mediated production of IP_3 and its action on release of calcium from internal stores. The application of U73122 at a concentration of 40µM reduced the calcium amplitude (Figure 24A and B; 190±20nM; n=4; $p<0.002$ compared to control) and also blocked the phosphorylation of CREB (Figure 24C; 9±3cells; n=4; $p<0.005$ compared to control). To probe the pathway after the release of calcium U0126 was bath applied. U0126 is a specific inihibitor of the MEK1/2 kinase, which is thought to transduce the signal to the nucleus. Bath application of 20µM U0126 to the perfusion reduced the calcium amplitude to a small extent (Figure 24A and B; 255±29nM; n=4; $p<0.05$ compared to control) but completely blocked the phosphorylation of CREB (Figure 24C; 4±2cells; n=4; $p<0.0001$ compared to control).

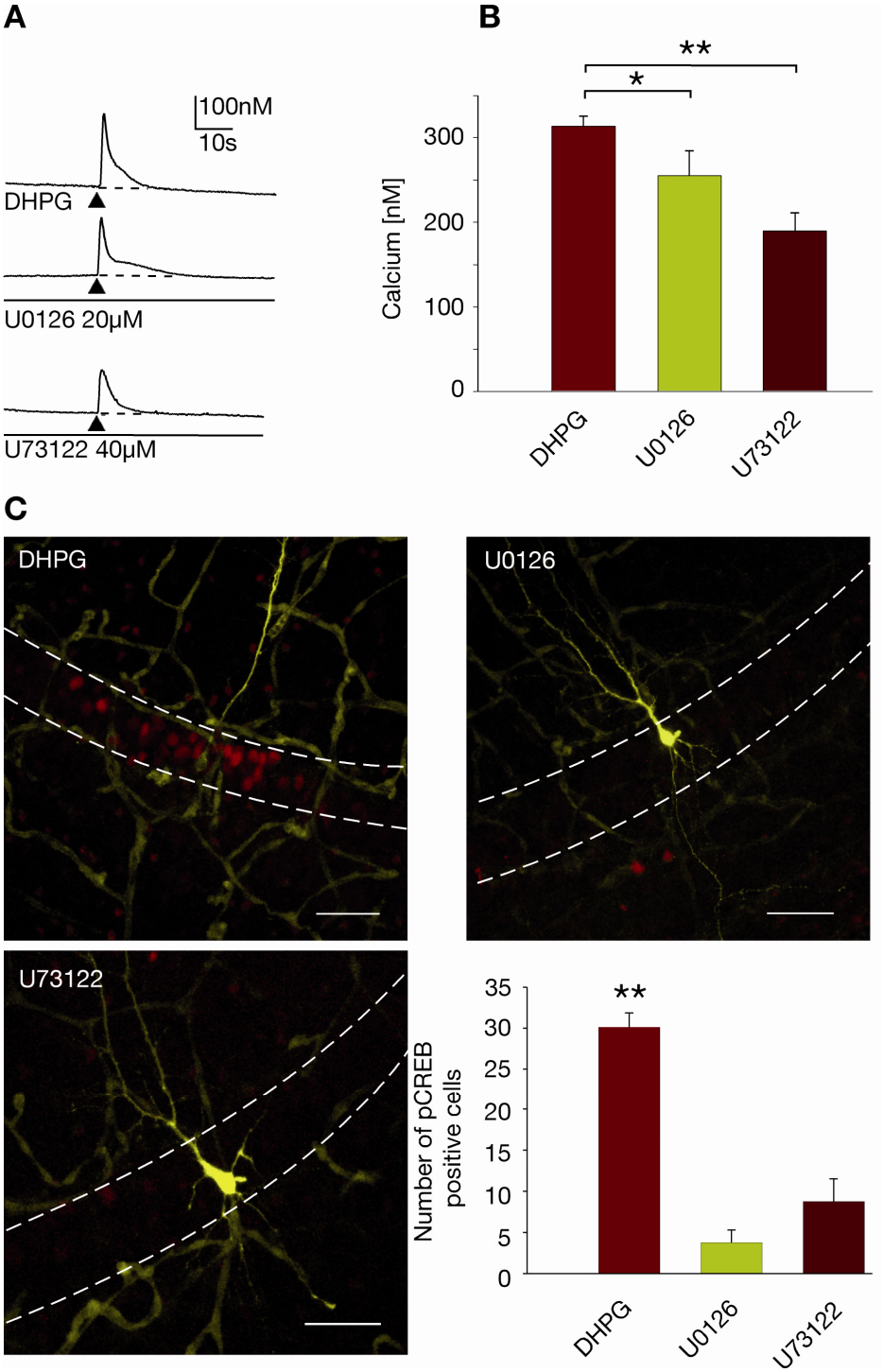

Figure 24: Signaling pathway dissection of DHPG-induced CREB phosphorylation and the effects on evoked calcium transients

A) DHPG-evoked calcium transients of individual cells. Bars below the transients indicate the application of the specified substances. B) Statistical analysis of the mean peak calcium concentration (DHPG n=18; U0126 n=4; U73122 n=4; **p<0.01;*p<0.05). C) DHPG-dependent pCREB immunoreactivity in CA1 pyramidal neurons (DHPG n=48; U0126 n=4; U73122 n=4; **p<0.0001 and p<0.005; scale bar=50µm).

Figure 25 is a schematic drawing of the potential steps in the mGluR-mediated signaling cascade that can be concluded by the application of several distinct inhibitors during this study. The inhibition of PLC by the application of U73122 (Figure 24) leads to reduced mobilization of IP_3 and a decreased release of calcium from internal stores. This release could also be blocked by the application of CPA (Figure 17 and Figure 18), which slowly empties calcium from the endoplasmic reticulum and thereby abolishes internal calcium release. Further downstream in the signaling cascade the activation of the MEK1/2 kinase is a crucial step, since inhibition by U0126 (Figure 24) completely blocked mGluR-mediated CREB phosphorylation.

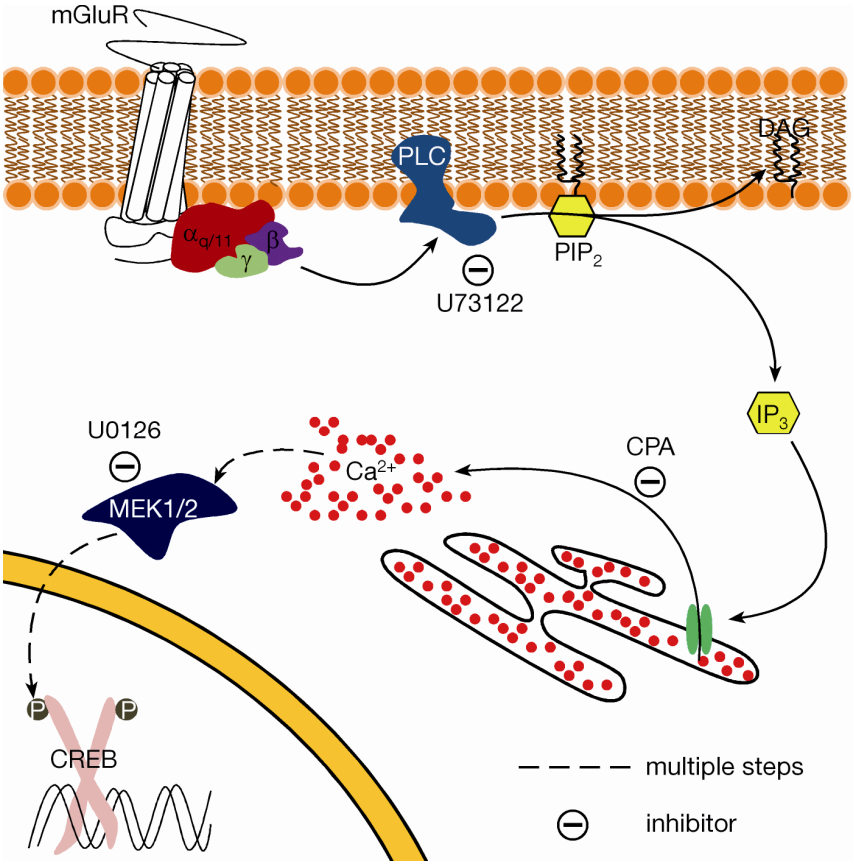

Figure 25: Model of the mGluR-mediated signaling cascade
Initiated by the binding of the native ligand glutamate to the mGluR the signaling cascade is started by the release of the G_α-protein from the G-protein complex, which then activates PLC. This membrane bound enzyme catalyzes the cleavage of PIP_2 to DAG and IP_3, which diffuses to its receptors located on the ER. The binding of IP_3 to the IP_3-receptor opens its intrinsic calcium channel and thereby releasing calcium from internal stores. This leads via several intermediate steps (dashed arrows) to the phosphorylation of MEK1/2 and finally to the phosphorylation of CREB, which is accomplished by MEK1/2 activated kinases (ERK1/2).

3.3. Contribution of early network oscillations for developmental persistence of CREB phosphorylation in young rats

Hippocampal slices from newborn rats of the first postnatal week showed increased background levels of pCREB immunoreactivity. It was unclear what the cellular and molecular determinants of this pCREB immunoreactivity were. Because CREB was shown to act as an activity-dependent transcription factor (Shaywitz and Greenberg, 1999; West et al., 2002), the effects of spontaneous activity, which is present in slices of newborn rats (Garaschuk et al., 1998), on the phosphorylation status of CREB were investigated.

Figure 26 shows that pCREB positive cells in rat hippocampal slices at postnatal day 5 (P5) exhibit ENO-induced calcium changes at high frequencies (Figure 26: Oscillating cells are phospho-CREB positive Figure 26; 12waves/min). The calcium concentration changed synchronously throughout all imaged cells, which is typical for ENOs and makes them clearly distinguishable from other spontaneous but asynchronous events.

Furthermore, in line with the disappearance of ENOs in the second postnatal week (Figure 27A) no pCREB positive cells could be detected at that time of development (Figure 27B). The frequency of the ENOs dropped from 7.9±0.5 waves/min (n=7) in the first 4 postnatal days to 5.5±1.8 waves/min (n=5) between day P5 and P6 (Figure 27A). Beyond the second postnatal week, there were no ENOs detectable (0 waves/min; n=12; $p<0.001$). The same is true for the phosphorylation status of CREB (Figure 27B), which showed no significant change between P2 (77.4±2.8% pCREB positive cells in imaged area; n=7; for details on pCREB immunoreactivity analysis see 2.4.3-3) and P6 (77.6±7.6%; n=5) but declined to 5±2.4% of positive cells at P12 (n=12; $p<0.001$).

To further elucidate the requirement of ENOs for persistent CREB phosphorylation several pharmacological treatments were applied to probe the importance of different inputs for ENO initiation. Removal of extracellular calcium lead to the blockage of ENOs and CREB phosphorylation (Figure 28B). At the low magnification image in Figure 28A and B one can clearly see the even distribution of pCREB positive cell nuclei along the pyramidal layer and the dentate gyrus (Figure 28 dashed line) of the hippocampus and the complete disappearance of pCREB positive cells by perfusion of the slice with 0Ca-ACSF.

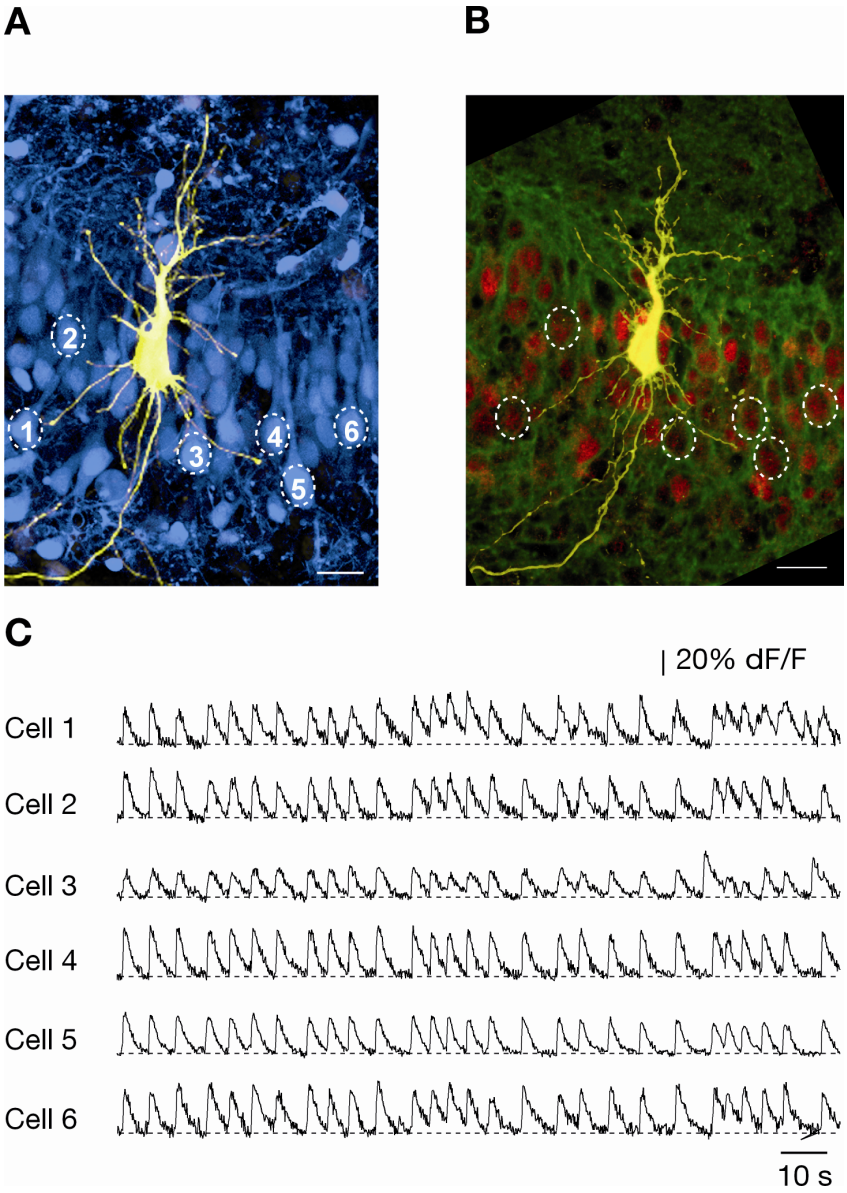

Figure 26: Oscillating cells are phospho-CREB positive
A) Fura-2 AM loaded cells (blue) in the CA1 area of the hippocampus (postnatal day 5). B) Same cells (dashed circles) show pCREB immunoreactivity (scale bar = 20µm). C) Corresponding ENO-like calcium transients of the cells labeled in A.

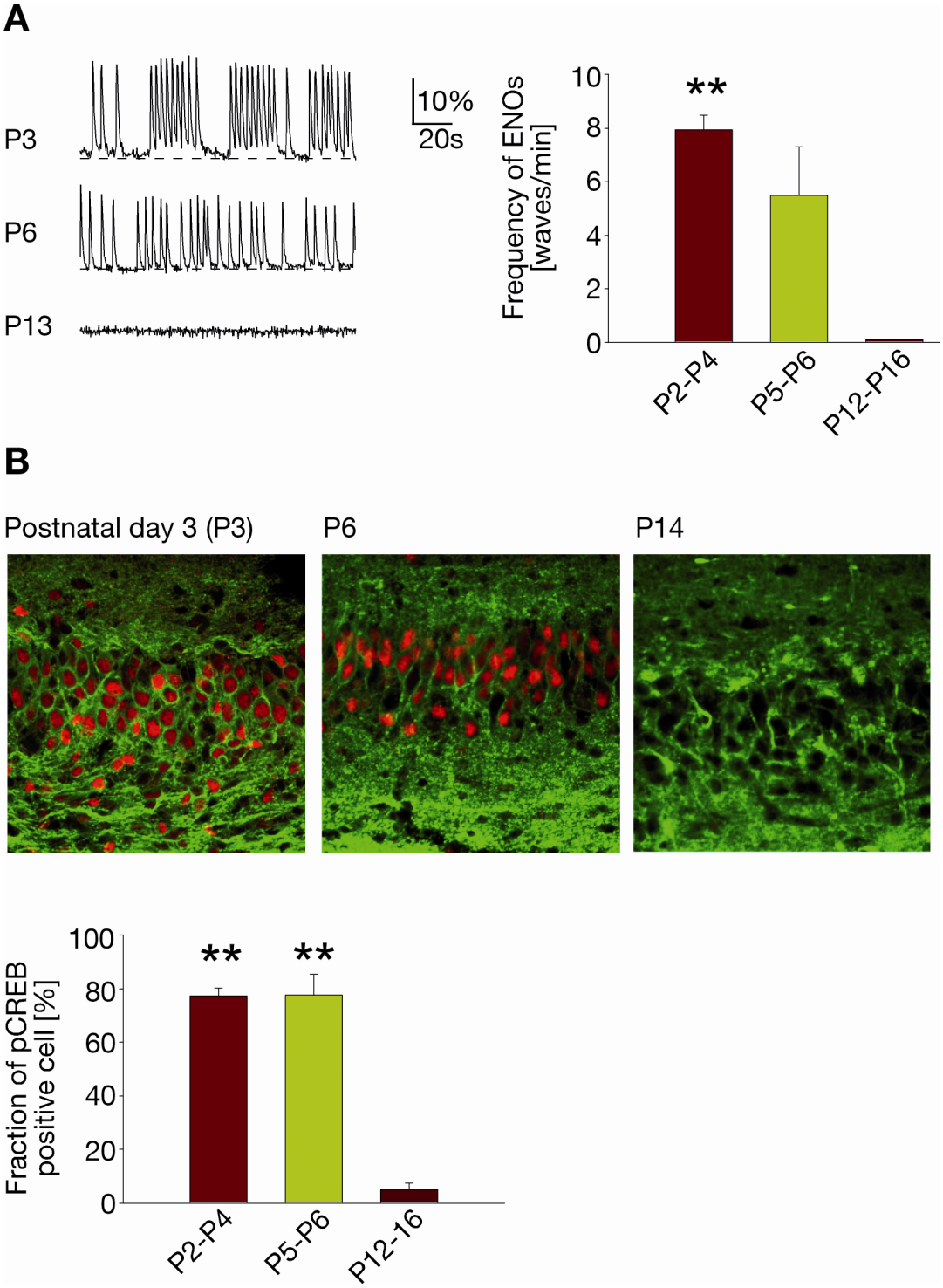

Figure 27: Developmental switch in ENO calcium signaling and basal CREB phosphorylation

A) ENO-evoked calcium transients (relative changes in fluorescence; ΔF/F) at different developmental stages. The right panel shows a statistical analysis of wave frequency plotted against the age of the animal (P2-P4 n=7; P5-P6 n=5; P12-P16 n=12; **p<0.001). B) pCREB immunoreactivity decreases after the first postnatal weak (**p<0.001).

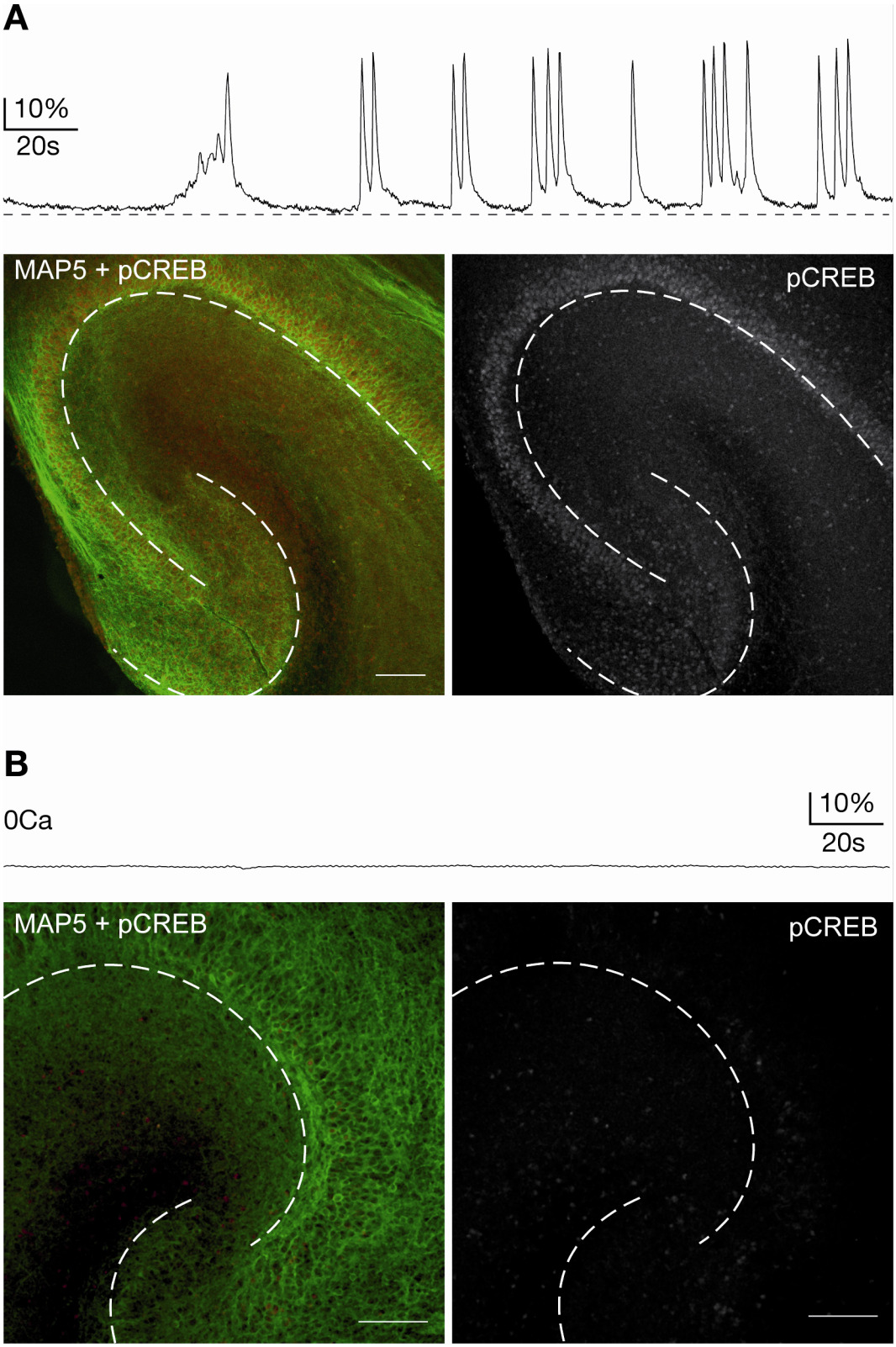

Figure 28: Removal of extracellular calcium blocks the phosphorylation of CREB
A) ENOs (relative changes in fluorescence; ΔF/F) lead to persistent CREB phosphorylation in the hippocampus. B) Perfusion with 0Ca-ACSF blocks ENOs and the phosphorylation of CREB. (scale bar = 100µm)

To investigate the synaptic events involved in the generation of ENOs, several pharmacological blockers of different calcium sources and synaptic transmission were applied. Perfusion with 500nM TTX (Figure 29A), which is an inhibitor of sodium channels and thereby disrupts the initiation and propagation of action potentials and action potential-controlled synaptic activity, clearly reduced wave frequency as well as the number of pCREB positive cells (0 waves/min; 5±0.9% pCREB positive cells; n=5). Picrotoxin a blocker of $GABA_A$-receptor had similar effects on the frequency of ENOs (Figure 29A; 0 waves/min; n=5) and the phosphorylation status of CREB (Figure 29B; 3.7±0.9%; n=5). Urethane a general anesthetic known to block ENOs *in vivo* (Adelsberger et al., 2005) had similar effects in slices when applied at a concentration of 100mM (Figure 29A; 0 waves/min; n=6) and suppressed the phosphorylation of CREB (Figure 29B; 1.7±0.6%; n=6). Both ENO-associated Ca^{2+}-transients and CREB phosphorylation required Ca^{2+}-entry through voltage-gated calcium channels. This was examined by the application of the VGCC blocker Ni^{2+} at a concentration of 1mM. Ni^{2+} blocked ENOs (Figure 29A; 0 waves/min) as well as persistent CREB phosphorylation (Figure 29B; 9±3.3%; n=6). The pharmacological analysis of ENO-evoked signals showed that synaptic activity especially of GABAergic nature is required (Figure 29) and (Garaschuk et al., 1998).

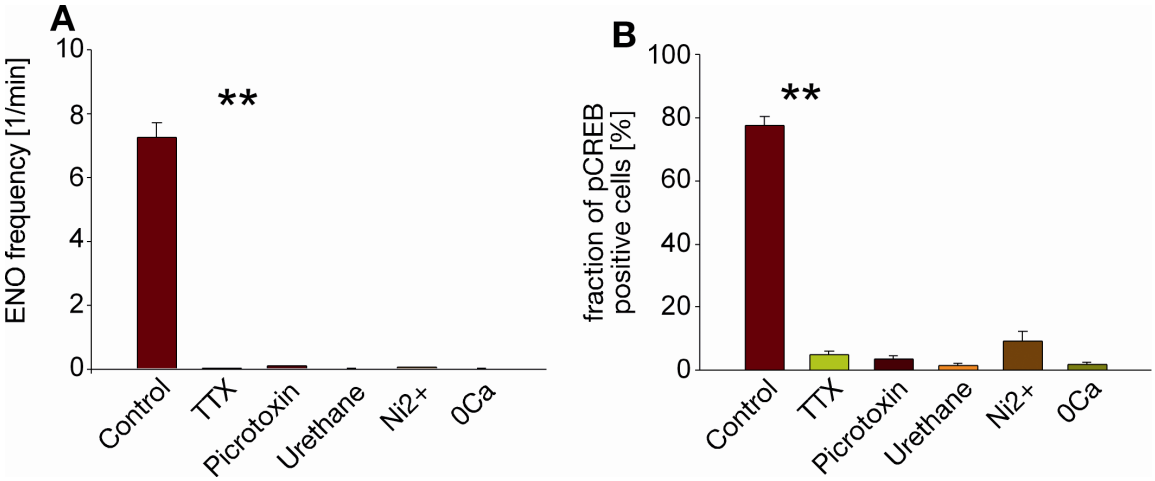

Figure 29: Pharmacological profile of ENOs and ENO-induced CREB phosphorylation
A) and B) Influence of different pharmacological substances on the frequency of ENOs and the number pCREB positive cells (DHPG 500µM, n=12; TTX 500nM, n=5; Picrotoxin 100µM, n=5; Urethane 100mM, n=6; Ni2+ 1mM, n=6; 0Ca, n=5; **p<0.001).

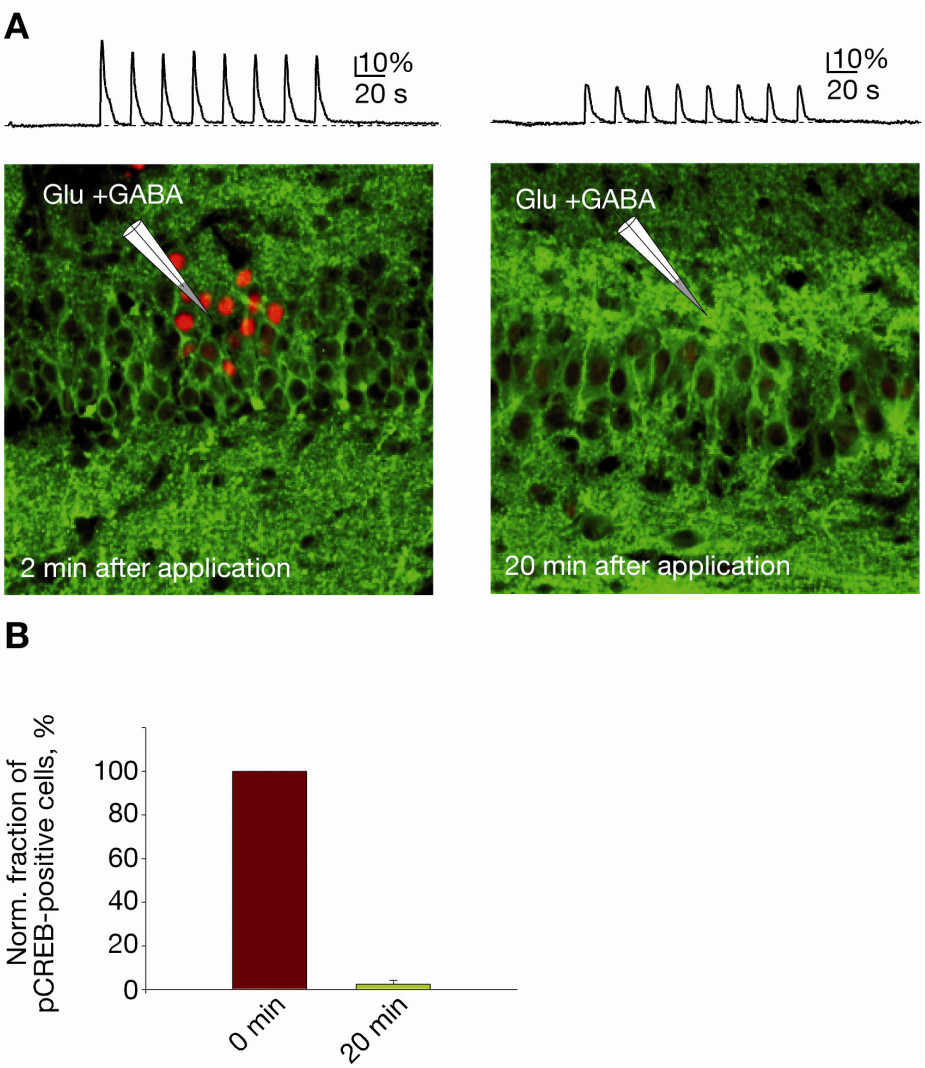

Figure 30: Mimicking of ENOs can induce a transient phosphorylation of CREB
A) To reduce background CREB phosphorylation slices were treated with 500nM TTX. Puff application of 1mM GABA and 1mM Glutamate for 50ms induced ENO like calcium transients (relative changes in fluorescence; ΔF/F), which are sufficient for CREB phosphorylation. 8 applications induced CREB phosphorylation, but 20 minutes after the mimicking of ENOs the CREB phosphorylation was not detectable anymore. B) Statistical analysis of the transient CREB phosphorylation (0min, n=11; 20min, n=11).

Mimicking of ENOs by the combined puff application of 1mM GABA and 1mM of glutamate for 50ms was carried out, to test whether artificial ENOs are sufficient to trigger the phosphorylation of CREB. Figure 30A shows that 8 evoked transients were sufficient to induce local CREB phosphorylation. This phosphorylation of CREB persisted not longer than 20 minutes (Figure 30A and B). Both applications were done in the same slice at different locations (1.puff CA1 and 2.puff CA4). To rule out any area specific effects, the experiment was also performed in the opposite order with similar results.

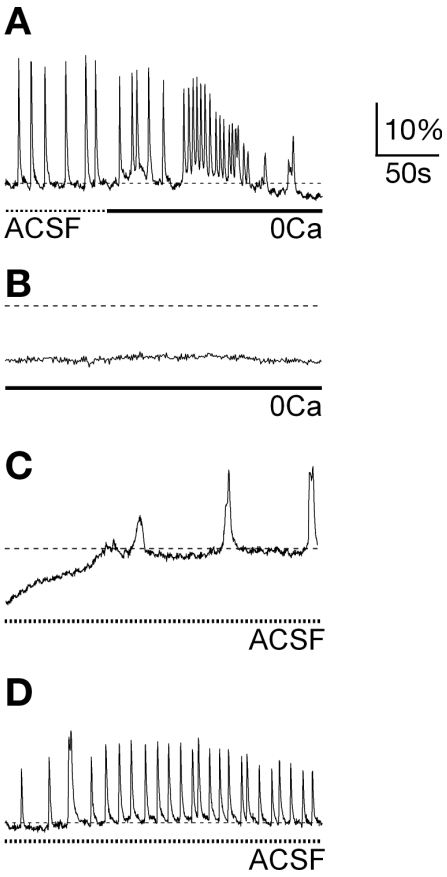

Figure 31: Blockage and reanimation of ENOs
A) ENO-induced calcium transients (relative changes in fluorescence; ΔF/F) before and during wash-in of 0Ca-ACSF. B) Prolonged perfusion with 0Ca blocked ENOs completely. Note the drop in intracellular resting calcium concentration during perfusion with 0Ca-ACSF (compared to the dashed line). C) 20minutes after wash-in of 0Ca the perfusion was switched to normal ACSF slowly increasing intracellular calcium concentrations and reestablishing ENOs. D) Recovered ENOs after prolonged wash-in of normal ACSF.

To test whether real ENOs could induce such a rephosphorylation in a slice, which was treated 20 minutes with 0Ca-ACSF, normal ACSF was perfused to reinitiate ENOs (Figure 31). First wash-in of 0Ca-ACSF (Figure 31A first panel) gradually decreased the number of pCREB positive cells from initially 74±2.8% to 1±0.4% of pCREB positive cells after 20 minutes (Figure 32B; ENO, 74±2.8%, n=13; 2min, 46.7±11.1%, n=6; 5min, 35.7±8.2%, n=7; 10min, 21±6.9%, n=11; 20min, 1±0.4%, n=4). After 20 minutes of 0Ca-ACSF (Figure 31B) ENOs were recovered by wash-in of normal ACSF (Figure 31C). After approximately 20 ENOs (Figure 31D) the slices were fixed and examined for pCREB positive cells. Indeed through the reinitiation of ENOs the phosphorylation of CREB could be rescued (Figure 32A and B; 75±6.6%, n=6).

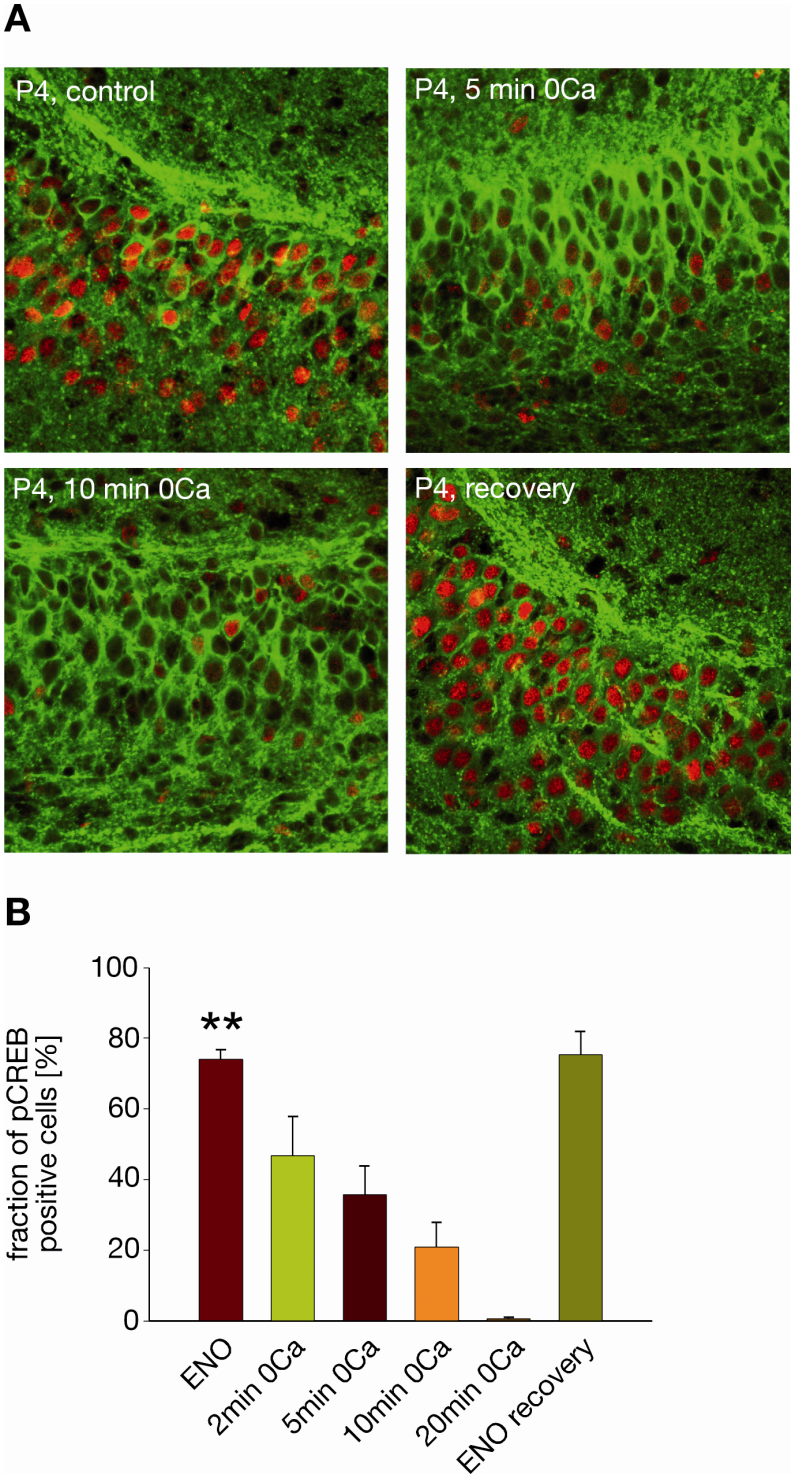

Figure 32: Time course of the dephosphorylation of CREB
A) Time course of the dephosphorylation of CREB after wash-in of 0Ca ACSF. Recovered ENOs (see Figure 31) lead to reestablishment of phosphorylation status of CREB. B) Statistical analysis of the decrease in pCREB immunoreactivity induced by wash-in of 0Ca-ACSF and its recovery (ENO, n=13; 2min, n=6; 5min, n=7; 10min, n=11; 20min, n=4; recovery, n=6).

4. Discussion

In this study the effects of mGluR-mediated calcium concentration changes on the phosphorylation status of CREB in hippocampal CA1 pyramidal neurons were examined. The three main findings are:

First, by using short puff applied pulses (500ms) of mGluR agonists (DHPG, t-ACPD) fast calcium changes in hippocampal neurons could be evoked. These calcium changes were sufficient to induce CREB phosphorylation at ser133 in a calcium release-dependent manner. Second, there is a correlation between the peak amplitude of the intracellular calcium concentration change (transient) and the relative amount of phosphorylated CREB in the nucleus of hippocampal pyramidal neurons. Third, the calcium-dependent mGluR-mediated CREB phosphorylation employs a signaling cascade via the Ras/MAPK pathway.

In the second part of this study it is shown that the persistent state of CREB phosphorylation observed in hippocampal slices in the first postnatal week, is strictly dependent on the presence of early network oscillations (ENOs). Inhibition of ENOs inevitably abolishes the presence of phosphorylated CREB.

4.1. Activity-dependent gene regulation in neurons

Synaptic activity in the brain regulates the expression of several genes responsible for neuronal survival, differentiation and complex behavior (Hevroni et al., 1998; Lonze and Ginty, 2002; Mayr and Montminy, 2001). Gene expression in turn changes the synaptic efficacy and therefore the excitability of the cell. CREB is an activity-induced transcription factor important for the accommodation of the cell to patterns of synaptic activity (Shaywitz and Greenberg, 1999; West et al., 2002).

A change in synaptic efficacy is best understood in the context of memory formation as a type of activity-dependent behavioral change. There are different cellular mechanisms of memory formation in the brain termed long-term potentiation (LTP) and long-term depression (LTD). Stability of LTP and LTD over time requires that synaptic activity initiates the synthesis of appropriate gene products (Huang et al., 1996), though protein degradation seems to play an important role as well (Fonseca et al., 2006).

CREB among others (Herdegen and Leah, 1998) has been discussed to be one of the transcription factors activated by synaptic activity (Impey et al., 1996; West et al., 2002) and implicated in the formation of LTP (Barco et al., 2002; Kandel, 2001; Leutgeb et al., 2005; Pittenger et al., 2002). However, Balschun and colleagues showed, that CREB conditional knockout mice exhibit almost no deficit in LTP induction and persistence (Balschun et al., 2003). LTP can be divided in an early phase (E-LTP, roughly the first 60 minutes), which is independent on protein synthesis and is mediated by incorporation of AMPAR into the postsynaptic membrane and a late phase (L-LTP) dependent on gene transcription and protein synthesis (Malenka and Bear, 2004). Hippocampal LTP at the Schaffer collateral synapse (see Figure 1) was shown to be dependent on NMDAR activation (Malenka and Bear, 2004) and CaMKII (Lisman et al., 2002). The exact signaling mechanisms involved in activation of gene transcription are still elusive, although studies suggest a role for PKA (Yasuda et al., 2003), PKC (Ling et al., 2002) CaMKIV (Bito et al., 1996) and MAPK (Thomas and Huganir, 2004). In addition, NMDARs, depending on their location can activate antagonistic signaling cascades modulating the phosphorylation of CREB. Whereas NMDARs located at the postsynaptic density promote CREB phosphorylation, extrasynaptic NMDARs in neuronal cell cultures of the hippocampus were shown to dephosphorylate CREB upon stimulation (Hardingham et al., 2002; Rao and Finkbeiner, 2007). These antagonistic effects are most likely due to the different composition of NMDAR subunits in these two locations. However, Figure 17B of this study shows that puff application of glutamate to the soma, which should open both extrasynaptic as well as synaptic NMDARs, exhibit a robust induction of pCREB immunoreactivity. These differences might be explained by the fact that in the study of Hardingham and colleagues the sustained application of glutamate to the bath (stimulation of synaptic and extrasynaptic NMDARs) is different from a short puff application and therefore does not antagonize the signal transduction to phospho-CREB.

There is accumulating evidence that the activation of mGluRs contribute to the induction of LTP (Malenka and Bear, 2004). For example, mGluRs were shown to be involved in NMDAR-mediated LTP in the hippocampus. Jia and colleagues showed in mGluR5 knockout mice that the NMDAR-mediated LTP is impaired and can be rescued by the application of a PKC agonist (Jia et al., 1998). Moreover there are several studies showing that MCPG a mGluR antagonist can block the induction of LTP and

LTD as well (Bashir et al., 1993a; Bashir et al., 1993b). A well established model of mGluR-mediated LTD is the parallel fiber to Purkinje cell synapse (Aiba et al., 1994) in the cerebellum. These studies suggest a role of mGluRs in LTP and LTD (Bortolotto et al., 1999; Malenka and Bear, 2004).

4.2. Calcium dependence of CREB phosphorylation

A common and important feature of virtually all pathways leading to activity-induced CREB phosphorylation is the employment of calcium as a second messenger or modulator of intracellular signaling cascades. NMDARs, which account for most of the glutamate-induced calcium influx (Yuste and Katz, 1991) and the increase in calcium concentration in the postsynaptic spine is an absolute requirement for the induction of LTP at least for the CA3-CA1 synapse of the hippocampus (Malenka and Bear, 2004). However, the phosphorylation of CREB as a readout for activity-induced gene regulation can be achieved via a diverse array of calcium-dependent and -independent stimuli (Johannessen et al., 2004).

One likely explanation for the ability to discriminate between calcium entry via different channels is the existence of proteins clustered at the intracellular domain of the receptors/channels. The clustering of signal transducing proteins including calcium binding proteins (e.g. calmodulin) with different types of channels has been proposed by several groups. In these signaling complexes calmodulin is thought to be activated when calcium enters the cell through a particular channel only (Rao and Finkbeiner, 2007). This was shown to be the case for calcium entry through L-VGCCs (Dolmetsch et al., 2001) and for LTP-inducing synaptic stimuli (NMDA-mediated) (Deisseroth et al., 1996). The extremely high calcium concentrations reached at the microdomain on the mouth of the channels (Naraghi and Neher, 1997) would initiate the propagation of the signal to the nucleus. Data provided in this study suggest that similar complexes are associated with mGluRs as well. Because the onset of the DHPG-evoked calcium transients was very fast and basically not distinguishable from glutamate-evoked transients (calcium influx through ionotropic channels, Figure 17) it can be hypothesized that the signaling from mGluR via the G-protein is accelerated by association with a signaling complex (Mao et al., 2005b). Other studies claim that for NMDA-mediated gene expression, instead of a calmodulin initiated signal entering the

nucleus, a critical parameter would be the elevation of nuclear calcium concentration (Hardingham et al., 2001). Additionally to that, it is hypothesized, that other proteins associated with the membrane receptor are implicated in the modulation of the signaling cascades (West et al., 2001). Especially mGluR-mediated CREB phosphorylation seems to be dependent on the interplay between calcium-independent receptor-associated proteins (e.g. Homer) and the stimulus-evoked calcium transients to convey signals towards the phosphorylation of CREB (Choe and Wang, 2002a; Gerber et al., 2007; Mao and Wang, 2002a; Mao et al., 2005b; West et al., 2001).

In this study, the establishment of the minimal requirement of mGluR-mediated CREB phosphorylation and the correlation between the measured mGluR-evoked intracellular calcium concentrations with the phosphorylation of CREB on ser133 was addressed on a single cell level. Therefore, a minimal stimulation procedure of 500ms puff application of DHPG was established, which proved to be sufficient to trigger the phosphorylation of CREB (Figure 11). In the vicinity of the application spot an increase in pCREB immunoreactivity could be observed. This was due to the agonist because a control application of ACSF was unable to initiate the phosphorylation of CREB (Figure 13).

Concurrent activation of mGluRs by bath application of agonists (DHPG) produces calcium transients with a very slow onset of several tens of seconds (Rae and Irving, 2004). Moreover the calcium dynamics are diverse ranging from single peak to multi peak oscillatory waves, most likely due to initiation of action potentials (Bianchi et al., 1999). In contrast, puff application of DHPG results in a slow depolarization of the cell, eventually leading to the initiation of action potential firing after application of DHPG (Figure 7) (Bianchi et al., 1999). The intracellular calcium concentration increased immediately after the application of DHPG and significantly before the initiation of action potentials and showed a wavelike spatial spread (Jaffe and Brown, 1994) into the stratum radiatum (dendritic region, see Figure 1) and stratum oriens (axonal region). Moreover, the initial calcium rise was surprisingly higher compared to the calcium transients triggered by the action potentials and the subsequent calcium influx through VGCCs.

Following the application of DHPG pCREB positive cells were sharply located within the stratum pyramidale at the site of application. This phosphorylation of CREB was

clearly attributable to the actions of mGluRs because the effects could be blocked using MCPG (Figure 14). To test whether there is calcium-dependent (Mao and Wang, 2002a) or -independent (Mao et al., 2005b) signaling from mGluR activation to the phosphorylation of CREB the involvement of calcium in the signaling cascade had to be characterized. Because mGluRs of the group I activate PLC, which in turn triggers the release of calcium from internal stores via IP_3 (Jaffe and Brown, 1994), it was expected that a treatment of the cells affecting calcium release would influence the DHPG-evoked calcium transients and DHPG-mediated CREB phosphorylation. The inhibition of the PLC by application of U73122 lead to a reduction of the calcium signal and had marked effects on DHPG-mediated CREB phosphorylation (Figure 24), which can be attributed not only to the reduced mobilization of IP_3 but also to the reduced induction of PKC via DAG (Choe and Wang, 2002b). These two mediators of PLC action may act in concert to induce mGluR-mediated CREB phosphorylation (Figure 2). DHPG puff application after depletion of internal stores with CPA showed a complete block of DHPG-mediated calcium transients (Figure 17), similar to results obtained from bath application of DHPG (Rae and Irving, 2004). In addition, there was a strong decrease in the number of pCREB positive cells. Topolnik and colleagues showed only a partial effect of CPA on DHPG-evoked calcium transients in hippocampal interneurons. In this case CPA depressed the amplitude of the calcium response of the fast component, but completely blocked the slow component in hippocampal interneurons. The authors claim that the slow component is triggered by calcium release through activation of mGluR5, whereas the fast component represents calcium influx through classical transient receptor potential channels (TRPC) triggered by mGluR1.

Therefore it can be concluded that the release of calcium from internal stores is required for mGluR-mediated CREB phosphorylation, though the calcium-dependent signal transduction is probably modulated by intracellular factors of other signaling pathways, for instance PKC (Choe and Wang, 2002b) or Homer (Mao et al., 2005b). It is likely that in hippocampal pyramidal neurons TRPC channels do not play a role in DHPG-evoked calcium transients, because they can be completely blocked by CPA. A possible explanation could be, that the mGluRs are associated with other G-proteins in different cell types and therefore employ other signaling cascades (Gerber et al., 2007; Hermans and Challiss, 2001). However, the involvement of TRPCs in DHPG-mediated

calcium transients cannot be totally ruled out, because in cerebellar Purkinje cells (Hartmann et al., in preparation; Kim et al., 2003) and CA3 hippocampal neurons (Gee et al., 2003) it was demonstrated that fast metabotropic calcium transients are linked to the activation of TRPCs.

In addition to calcium release from internal stores, extracellular calcium may play a role in mGluR-mediated CREB phosphorylation. Mao and colleagues demonstrated that bath application of DHPG in striatal neurons (Mao and Wang, 2002a) is not only dependent on PLC-mediated calcium release from internal stores. An additionally calcium-induced calcium influx through L-type VGCCs shapes the time course of the calcium signal and is required for triggering the phosphorylation of CREB. This is only partly true for the observations in this study, because in hippocampal slices, although having no effect on DHPG-induced calcium transients, the L-type channel blocker Nifedipine showed only a mild yet significant reduction in the number of pCREB positive cells (about 30%; Figure 23). Therefore L-type channels in the hippocampal preparation have some impact but cannot be considered as a prerequisite for DHPG-mediated CREB phosphorylation. Moreover, under conditions of 0Ca-ACSF for a short time (<7 minutes), leaving internal stores intact, DHPG-induced calcium changes showed little reduction in mean peak calcium concentration and the number of pCREB positive cells was only slightly reduced (Figure 15 and Figure 16). Whereas perfusion with 0Ca-ACSF for a time period long enough to deplete internal stores (>20minutes) completely abolished DHPG-evoked calcium transients and pCREB positive cells (Figure 19).

These results suggest that mGluR-mediated calcium transients and CREB phosphorylation is mainly dependent on calcium release from internal stores and that all pharmacological substances, shown to interfere with DHPG-induced changes of intracellular calcium concentration, had an effect on the DHPG-mediated CREB phosphorylation. The only exception to this was the application of the MEK1/2 inhibitor U0126, which had almost no effect on the calcium transients but completely blocked DHPG-mediated CREB phosphorylation (Figure 24). This can be explained by the fact that the MEK1/2 kinase is activated in the signaling pathway downstream of the calcium release (Figure 25).

To further verify the calcium dependence of mGluR-mediated CREB phosphorylation, the pCREB immunoreactivity was determined in the same cells as the

calcium concentration changes were measured (Figure 20). The plot of the peak calcium concentration against the relative pCREB fluorescence intensity showed a significant correlation between these two parameters. Cells with a peak calcium concentration of more than 300nM showed a significantly higher level of pCREB immunoreactivity compared to cells with smaller calcium concentration increases below 200nM (Figure 22).

It was reported, that for KCl-evoked influx of calcium through L-type VGCCs a threshold of about 400nM of intracellular calcium concentration has to be reached to efficiently trigger CREB-dependent gene expression (Dolmetsch et al., 2001). This is about twice as high as the suggested threshold for our model of CREB phosphorylation. But taking into consideration that Dolmetsch and colleagues examined a different route of entry and additionally were looking for CREB-dependent gene expression, which could require higher calcium concentrations, these results are in line with the correlation found in this study.

The phosphorylation of CREB evoked by DHPG puff application was very fast. Usually the slices were fixed for antibody treatment less than 3 minutes after the application was performed. Therefore it is surprising that the phosphorylation of CREB was strictly dependent on the Ras/MAPK pathway (blocked by U0126), which was described to exhibit slower kinetics of CREB phosphorylation (West et al., 2002; Wu et al., 2001). Wu and colleagues showed that the fast initiation of CREB phosphorylation by bath application of KCl was dependent on CaMKIV (Figure 2). They hypothesize that the differences in the kinetics can be explained by a model describing the detection of stimulus strength. Milder calcium mobilization lead to fast but short lived activation of the CaMK pathway, whereas stronger stimulation mobilizes enough calcium to activate the Ras/MAPK pathway. It is likely that the high concentration of DHPG in this study evoked calcium responses large enough to trigger the Ras/MAPK pathway more efficiently than the KCl bath application in the experiments performed by Wu and colleagues.

The phosphorylation of CREB at ser133 is necessary but not sufficient to trigger CREB-dependent gene expression. Activation of mGluRs via bath application of DHPG for several minutes was shown to be sufficient to trigger the expression of c-fos an immediate early gene (IEG) under the control of CREB (Mao and Wang, 2003). Whether the minimal stimulation procedure, applied in this study, is sufficient to trigger CREB-

dependent gene expression cannot be answered by the experiments carried out so far (see 5. Perspectives). However, the involvement of the Ras/MAPK pathway, which is thought to be a strong inducer of CREB-dependent gene expression (Wu et al., 2001), points towards a signal strong enough for the initiation of gene expression.

By combining the results of this study with the present literature, two alternative models for the implications of mGluRs in mediating glutamatergic synaptic activity-induced CREB phosphorylation can be thought of. First of all, the mGluRs could work in concert with the NMDA receptors (Mao and Wang, 2002b). Whereas NMDARs by itself are able to trigger only the CaMKIV pathway (Deisseroth et al., 1996), coactivation with mGluRs could lead to a further increase in the intracellular calcium concentration up to the level where the Ras/MAPK pathway is initiated. This in turn could lead to prolonged phosphorylation of CREB and possibly to a significant rise in CREB-dependent gene expression. This is supported by the fact that first, MCPG blocks NMDAR-mediated LTP (Bortolotto et al., 1999; Yang et al., 1998), which generally involves the phosphorylation of CREB and protein synthesis and second that mGluR5 knockout mice show impaired NMDAR-dependent LTP (Jia et al., 1998).

A second alternative model deals with the fact that IP_3-receptors are calcium sensitive (Simpson et al., 1995) and therefore the calcium influx through NMDARs can potentiate the IP_3-mediated response serving as a coincidence detector (Berridge, 1998). This could result in the generation of a calcium wave traveling to the nucleus via calcium-induced calcium release (CICR) (Berridge, 1998; Watanabe et al., 2006) , which in turn would activate CREB-dependent gene transcription by calcium sensitive nuclear factors (Hardingham et al., 2001). However, Figure 17 shows that glutamate-induced calcium transients and CREB phosphorylation were only mildly affected by the depletion of internal stores through application of CPA. This could be explained by the fact, that the puff application onto the somata of the cells increases the calcium concentration in the soma to a threshold capable to initiate the phosphorylation of CREB without additional calcium release. This is further supported by the study of Hardingham and colleagues, who demonstrated that synaptically evoked NMDA-mediated gene expression indeed is dependent on calcium release from internal stores (Hardingham et al., 2001) and on the hypothesized induced calcium wave.

Taken together, mGluR-mediated CREB phosphorylation in hippocampal pyramidal neurons is dependent on the release of calcium from internal stores and employs a

pathway involving MEK1/2, possibly coupling calcium release to the phosphorylation of CREB via the Ras/MAPK pathway (Figure 25). Furthermore, there is a positive correlation between the peak calcium concentration reached in the soma of the cell and the ability of the cell to phosphorylate CREB (Figure 22). A calcium concentration of 300nM in the soma is sufficient to trigger the phosphorylation of CREB.

4.3. CREB phosphorylation in the immature brain

In the first two weeks after birth massive changes in the organization of the cortex take place in the rodent brain (Uylings et al., 1990). Associated with the increase in size and synaptic connections formed, is the development of the dendritic arborization and the growth of axons. CREB-mediated control of gene expression is necessary for the survival and development of multiple neuronal cell types (Walton et al., 1999). A large number of genes important for development and differentiation of neuronal cells and networks are controlled by CREB (Mayr and Montminy, 2001; Wayman et al., 2006)(e.g. bcl2: apoptosis inhibitor; BDNF: neuronal growth factor). Apoptosis, a form of programmed cell death, plays a critical role in these processes and CREB was shown to shift the intracellular balance between pro-survival and death-promoting factors towards the ones which promote survival (Lonze et al., 2002; Mantamadiotis et al., 2002). During this early stage of development, sensory input to the cortical network is scarce. At this time, ENOs (Garaschuk et al., 2000) are a common form of intrinsic activity. ENOs are thought to guide several processes implicated in the development of single cells as well as neuronal networks (Moody and Bosma, 2005). ENOs are thought to drive the establishment of the wiring of neural networks (Garaschuk et al., 2000) and the differentiation of individual cells (Arumugam et al., 2005).

In this study for the first time a persistent CREB phosphorylation is described (Figure 26). This persistent pCREB could be detected in a restricted time window of the first two postnatal weeks (Figure 27). The phosphorylation of CREB at ser133 is dependent on ENO-like calcium transients, because it is blocked by all agents interfering with ENOs (Figure 29). These agents include TTX (blocking of action potentials), picrotoxin (inhibitor of GABAergic synaptic transmission, which is a major excitatory input in the immature brain (Ben-Ari et al., 2007)) and Ni^{2+} (blocker of VGCCs). In addition urethane, known to block ENOs *in vivo*, inhibited the ENO-driven

CREB phosphorylation. To conclude, the blockage of ENOs by inhibitors of synaptic transmission inevitably abolishes the persistent presence of phospho-CREB (Figure 29B).

The frequency of oscillations can vary between different brain regions. Therefore the frequency necessary for keeping CREB phosphorylated was investigated. The dephosphorylation process of pCREB took about 20 minutes (Figure 32). Because already 8 ENO-like puff applications are sufficient to phosphorylate CREB (Figure 30), the recorded frequencies of the ENOs are high enough to keep CREB phosphorylated. In other brain regions like the frontal cortex the frequency of network oscillations were shown to be much smaller (Garaschuk et al., 2000; Moody and Bosma, 2005). However, they still should be frequent enough to have similar pCREB-promoting effects on the neurons in that area. Therefore, a frequency of calcium oscillations in the range of one every 2-3 minutes would be sufficient to drive ENO-dependent CREB phosphorylation.

The observed correlation between the existence of ENOs and constitutive CREB phosphorylation could be summarized in a model explaining that neuronal cells which contribute to the generation and propagation of ENOs, receive pro-survival signals (Riccio et al., 1999) by the pCREB-dependent transcription of respective genes. This model is supported by the finding, that the maturation of synapses in the immature brain is accompanied by a switch from electrical (gap junctions) to chemical (synapse) communication and that this switch is dependent on NMDAR-mediated glutamatergic transmission followed by calcium-dependent CREB phosphorylation (Arumugam et al., 2005).

In conclusion, the persistence of CREB phosphorylation in the hippocampus during the first postnatal week is dependent on the presence of ENOs. The persistent CREB phosphorylation in turn may play a key role in modulating the development and maturation of the neuronal network.

5. Perspectives

The combination of fast calcium imaging, electrophysiological recordings and immunohistology applied to the same preparation made it possible to correlate intracellular calcium concentration changes and electrophysiological signals directly with an immunohistological readout.

Because the phosphorylation of CREB is necessary but not sufficient for CREB-dependent gene expression the next logical step would be to investigate mGluR-mediated CREB-dependent gene expression. There are basically two possible ways to do so. First, the simplest way would be to investigate the expression of newly synthesized protein. By using antibodies against CREB-controlled immediate early gene products, for instance BDNF, one could get a direct readout of CREB-dependent gene expression. Second, one step upstream of the protein synthesis the CREB-dependent transcription of new messenger-RNA (mRNA) could be investigated. To achieve this, the combination of the patch method with single cell quantitative PCR to detect increased levels of newly transcribed mRNA (Hartmann et al., in preparation) could be applied. After puff application of the agonist one would harvest cells, which show a large enough calcium response able to trigger the phosphorylation of CREB, with a pipette and do a PCR analysis to verify an increase in mRNA of a specific gene. These approaches of course are not limited to the application of mGluR agonists. Other important mediators involved in synaptic transmission can be applied alone or in concert to examine synergistic effects (NMDAR, AMPAR, GABA receptors and others), This could lead to new insights in synaptic potentiation and CREB-mediated transcription and further elucidate the controversial role of mGluRs in hippocampal LTP and LTD (Bortolotto et al., 1999).

The discovery that TRPC channels are associated with metabotropic signals in Purkinje cells (Hartmann et al., in preparation; Kim et al., 2003) and the postulated involvement in mGluR1 signaling in hippocampal interneurons (Topolnik et al., 2006) opens up a new aspect of the regulation of mGluR-mediated calcium signals. With the availability of specific TRPC knockouts (Hartmann et al., in preparation) it will be important to examine these new signaling pathways.

6. Summary and publications

Plasticity is a remarkable feature of the brain, allowing the nervous system to adapt its structure and function to patterns of intrinsic or extrinsic activity. One component of these long-term changes associated with learning and memory is the activity-driven induction of new gene expression, which is required for both late long-term potentiation (L-LTP) of synaptic transmission and the activity-dependent morphological changes that help to shape and wire the brain during development. The cAMP response element binding protein (CREB), an activity-induced transcription factor, is an important player in the regulation of these processes and therefore an ideal candidate to study activity-dependent gene regulation.

In this study it is shown for the first time that a single puff application (≤500ms) of a metabotropic glutamate receptor (mGluR) agonist (DHPG) triggers a somatic calcium transient in rat hippocampal CA1 neurons, which prove to be sufficient for the phosphorylation of CREB at the residue Ser133. The generation and the transduction of the stimulus to the phosphorylation of CREB occurred within less than 3 minutes after application of the agonist. A requirement for intracellular calcium release from the endoplasmic reticulum (ER) and the activation of MAPK/ERK-kinase 1/2 (MEK1/2) in the transduction of the signal to the phosphorylation of CREB was determined. Therefore, an involvement of the Ras/MAPK pathway can be assumed. Additionally, the combination of fast calcium imaging, electrophysiology and immunohistological techniques, made it possible to correlate the properties of the intracellular calcium transients to phospho-CREB (pCREB) immunoreactivity on a single cell level. A rise of the somatic calcium concentration to about 300nM was reliably potent to induce the phosphorylation of CREB. In conclusion, mGluR activation is sufficient to trigger the phosphorylation of CREB in a calcium release-dependent manner and may be important for glutamatergic synaptic activity-induced modulation of gene expression.

Moreover, the role of intrinsic network activity in driving CREB-dependent modulation of gene expression in the immature hippocampus (postnatal day 2-6) was investigated. A correlation between ENOs (early network oscillations), a form of intrinsic neuronal activity in the developing brain and pCREB could be identified, which is dependent on GABAergic synaptic transmission and calcium. After 20 minutes of blocking ENOs no pCREB positive cells could be detected. Nevertheless, the

persistence of pCREB could be rescued by re-induction or mimicking of ENOs. It is concluded, that ENOs are a prerequisite of the constitutive CREB phosphorylation in the immature hippocampus and are likely to modulate the expression of developmental relevant genes.

Publications resulting from experimental work in this study:

Hartmann, J., Abramowitz, J., Dragicevic, E., Adelsberger, H., Henning, H., Sumser, M., Blum, R., Dietrich, A., Freichel, M., Flockerzi, V., Birnbaumer, L., Konnerth, A. (submitted). TRPC3 is essential for slow synaptic transmission and motor coordination.

Sumser, M., Garaschuk, O., Konnerth, A. (in preparation). Calcium dependence of metabotropic glutamate receptor-mediated CREB phosphorylation in hippocampal neurons.

Yassin, L., Sumser, M., Garaschuk, O., Konnerth, A. (in preparation). Persistent state of CREB phosphorylation in the immature hippocampus is determined by ENOs.

7. References

Adelsberger, H., Garaschuk, O., and Konnerth, A. (2005). Cortical calcium waves in resting newborn mice. Nat Neurosci *8*, 988-990.

Aiba, A., Kano, M., Chen, C., Stanton, M. E., Fox, G. D., Herrup, K., Zwingman, T. A., and Tonegawa, S. (1994). Deficient cerebellar long-term depression and impaired motor learning in mGluR1 mutant mice. Cell *79*, 377-388.

Arumugam, H., Liu, X., Colombo, P. J., Corriveau, R. A., and Belousov, A. B. (2005). NMDA receptors regulate developmental gap junction uncoupling via CREB signaling. Nat Neurosci *8*, 1720-1726.

Balschun, D., Wolfer, D. P., Gass, P., Mantamadiotis, T., Welzl, H., Schutz, G., Frey, J. U., and Lipp, H. P. (2003). Does cAMP response element-binding protein have a pivotal role in hippocampal synaptic plasticity and hippocampus-dependent memory? J Neurosci *23*, 6304-6314.

Barco, A., Alarcon, J. M., and Kandel, E. R. (2002). Expression of constitutively active CREB protein facilitates the late phase of long-term potentiation by enhancing synaptic capture. Cell *108*, 689-703.

Bashir, Z. I., Bortolotto, Z. A., Davies, C. H., Berretta, N., Irving, A. J., Seal, A. J., Henley, J. M., Jane, D. E., Watkins, J. C., and Collingridge, G. L. (1993a). Induction of LTP in the hippocampus needs synaptic activation of glutamate metabotropic receptors. Nature *363*, 347-350.

Bashir, Z. I., Jane, D. E., Sunter, D. C., Watkins, J. C., and Collingridge, G. L. (1993b). Metabotropic glutamate receptors contribute to the induction of long-term depression in the CA1 region of the hippocampus. Eur J Pharmacol *239*, 265-266.

Ben-Ari, Y., Gaiarsa, J. L., Tyzio, R., and Khazipov, R. (2007). GABA: a pioneer transmitter that excites immature neurons and generates primitive oscillations. Physiol Rev *87*, 1215-1284.

Berridge, M. J. (1998). Neuronal calcium signaling. Neuron *21*, 13-26.

Bianchi, R., Young, S. R., and Wong, R. K. (1999). Group I mGluR activation causes voltage-dependent and -independent Ca2+ rises in hippocampal pyramidal cells. J Neurophysiol *81*, 2903-2913.

Bischofberger, J., Engel, D., Li, L., Geiger, J. R., and Jonas, P. (2006). Patch-clamp recording from mossy fiber terminals in hippocampal slices. Nat Protoc *1*, 2075-2081.

Bito, H., Deisseroth, K., and Tsien, R. W. (1996). CREB phosphorylation and dephosphorylation: a Ca(2+)- and stimulus duration-dependent switch for hippocampal gene expression. Cell *87*, 1203-1214.

Bonni, A., Brunet, A., West, A. E., Datta, S. R., Takasu, M. A., and Greenberg, M. E. (1999). Cell survival promoted by the Ras-MAPK signaling pathway by transcription-dependent and -independent mechanisms. Science *286*, 1358-1362.

Bortolotto, Z. A., Fitzjohn, S. M., and Collingridge, G. L. (1999). Roles of metabotropic glutamate receptors in LTP and LTD in the hippocampus. Curr Opin Neurobiol *9*, 299-304.

Bourtchuladze, R., Frenguelli, B., Blendy, J., Cioffi, D., Schutz, G., and Silva, A. J. (1994). Deficient long-term memory in mice with a targeted mutation of the cAMP-responsive element-binding protein. Cell *79*, 59-68.

Bradbury, M. J., Campbell, U., Giracello, D., Chapman, D., King, C., Tehrani, L., Cosford, N. D., Anderson, J., Varney, M. A., and Strack, A. M. (2005). Metabotropic glutamate receptor mGlu5 is a mediator of appetite and energy balance in rats and mice. J Pharmacol Exp Ther *313*, 395-402.

Brodkin, J., Bradbury, M., Busse, C., Warren, N., Bristow, L. J., and Varney, M. A. (2002). Reduced stress-induced hyperthermia in mGluR5 knockout mice. Eur J Neurosci *16*, 2241-2244.

Brody, S. A., Conquet, F., and Geyer, M. A. (2003). Disruption of prepulse inhibition in mice lacking mGluR1. Eur J Neurosci *18*, 3361-3366.

Carlezon, W. A., Jr., Duman, R. S., and Nestler, E. J. (2005). The many faces of CREB. Trends Neurosci *28*, 436-445.

Cha-Molstad, H., Keller, D. M., Yochum, G. S., Impey, S., and Goodman, R. H. (2004). Cell-type-specific binding of the transcription factor CREB to the cAMP-response element. Proc Natl Acad Sci U S A *101*, 13572-13577.

Chiamulera, C., Epping-Jordan, M. P., Zocchi, A., Marcon, C., Cottiny, C., Tacconi, S., Corsi, M., Orzi, F., and Conquet, F. (2001). Reinforcing and locomotor stimulant effects of cocaine are absent in mGluR5 null mutant mice. Nat Neurosci *4*, 873-874.

Choe, E. S., Parelkar, N. K., Kim, J. Y., Cho, H. W., Kang, H. S., Mao, L., and Wang, J. Q. (2004). The protein phosphatase 1/2A inhibitor okadaic acid increases CREB and Elk-1 phosphorylation and c-fos expression in the rat striatum in vivo. J Neurochem *89*, 383-390.

Choe, E. S., and Wang, J. Q. (2002a). CREB and Elk-1 phosphorylation by metabotropic glutamate receptors in striatal neurons (review). Int J Mol Med *9*, 3-10.

Choe, E. S., and Wang, J. Q. (2002b). Regulation of transcription factor phosphorylation by metabotropic glutamate receptor-associated signaling pathways in rat striatal neurons. Neuroscience *114*, 557-565.

Chrivia, J. C., Kwok, R. P., Lamb, N., Hagiwara, M., Montminy, M. R., and Goodman, R. H. (1993). Phosphorylated CREB binds specifically to the nuclear protein CBP. Nature *365*, 855-859.

Deisseroth, K., Bito, H., and Tsien, R. W. (1996). Signaling from synapse to nucleus: postsynaptic CREB phosphorylation during multiple forms of hippocampal synaptic plasticity. Neuron *16*, 89-101.

Deisseroth, K., and Tsien, R. W. (2002). Dynamic multiphosphorylation passwords for activity-dependent gene expression. Neuron *34*, 179-182.

Dingledine, R., Borges, K., Bowie, D., and Traynelis, S. F. (1999). The glutamate receptor ion channels. Pharmacol Rev *51*, 7-61.

Dolmetsch, R. E., Pajvani, U., Fife, K., Spotts, J. M., and Greenberg, M. E. (2001). Signaling to the nucleus by an L-type calcium channel-calmodulin complex through the MAP kinase pathway. Science *294*, 333-339.

Edwards, F. A., Konnerth, A., Sakmann, B., and Takahashi, T. (1989). A Thin Slice Preparation for Patch Clamp Recordings from Neurons of the Mammalian Central Nervous-System. Pflugers Archiv-European Journal of Physiology *414*, 600-612.

Ferraguti, F., and Shigemoto, R. (2006). Metabotropic glutamate receptors. Cell Tissue Res *326*, 483-504.

Finkbeiner, S., Tavazoie, S. F., Maloratsky, A., Jacobs, K. M., Harris, K. M., and Greenberg, M. E. (1997). CREB: a major mediator of neuronal neurotrophin responses. Neuron *19*, 1031-1047.

Fonseca, R., Vabulas, R. M., Hartl, F. U., Bonhoeffer, T., and Nagerl, U. V. (2006). A balance of protein synthesis and proteasome-dependent degradation determines the maintenance of LTP. Neuron *52*, 239-245.

Garaschuk, O., Hanse, E., and Konnerth, A. (1998). Developmental profile and synaptic origin of early network oscillations in the CA1 region of rat neonatal hippocampus. J Physiol *507 (Pt 1)*, 219-236.

Garaschuk, O., Linn, J., Eilers, J., and Konnerth, A. (2000). Large-scale oscillatory calcium waves in the immature cortex. Nat Neurosci *3*, 452-459.

Gee, C. E., Benquet, P., and Gerber, U. (2003). Group I metabotropic glutamate receptors activate a calcium-sensitive transient receptor potential-like conductance in rat hippocampus. J Physiol *546*, 655-664.

Gerber, U., Gee, C. E., and Benquet, P. (2007). Metabotropic glutamate receptors: intracellular signaling pathways. Curr Opin Pharmacol *7*, 56-61.

Gonzalez, G. A., and Montminy, M. R. (1989). Cyclic AMP stimulates somatostatin gene transcription by phosphorylation of CREB at serine 133. Cell *59*, 675-680.

Grynkiewicz, G., Poenie, M., and Tsien, R. Y. (1985). A new generation of Ca2+ indicators with greatly improved fluorescence properties. J Biol Chem *260*, 3440-3450.

Gutkind, J. S. (2000). Regulation of mitogen-activated protein kinase signaling networks by G protein-coupled receptors. Sci STKE *2000*, RE1.

Hardingham, G. E., Arnold, F. J., and Bading, H. (2001). Nuclear calcium signaling controls CREB-mediated gene expression triggered by synaptic activity. Nat Neurosci *4*, 261-267.

Hardingham, G. E., Fukunaga, Y., and Bading, H. (2002). Extrasynaptic NMDARs oppose synaptic NMDARs by triggering CREB shut-off and cell death pathways. Nat Neurosci *5*, 405-414.

Hartmann, J., Abramowitz, J., Dragicevic, E., Adelsberger, H., Henning, H., Sumser, M., Blum, R., Dietrich, A., Freichel, M., Flockerzi, V.*, et al.* (in preparation). TRPC3 is essential for slow synaptic transmission and motor coordination.

Helmchen, F., Yuste, R., Lanni, F., and Konnerth, A. (2000). Calibration of fluorescent calcium indicators. In: Imaging Neurons: A Laboratory Manual. Cold Spring Harbor Laboratory Press *Chapter 32*.

Herdegen, T., and Leah, J. D. (1998). Inducible and constitutive transcription factors in the mammalian nervous system: control of gene expression by Jun, Fos and Krox, and CREB/ATF proteins. Brain Res Brain Res Rev *28*, 370-490.

Hermans, E., and Challiss, R. A. (2001). Structural, signalling and regulatory properties of the group I metabotropic glutamate receptors: prototypic family C G-protein-coupled receptors. Biochem J *359*, 465-484.

Hevroni, D., Rattner, A., Bundman, M., Lederfein, D., Gabarah, A., Mangelus, M., Silverman, M. A., Kedar, H., Naor, C., Kornuc, M.*, et al.* (1998). Hippocampal plasticity involves extensive gene induction and multiple cellular mechanisms. J Mol Neurosci *10*, 75-98.

Hong, E. J., West, A. E., and Greenberg, M. E. (2005). Transcriptional control of cognitive development. Current Opinion in Neurobiology *15*, 21-28.

Huang, Y. Y., Nguyen, P. V., Abel, T., and Kandel, E. R. (1996). Long-lasting forms of synaptic potentiation in the mammalian hippocampus. Learn Mem *3*, 74-85.

Ichise, T., Kano, M., Hashimoto, K., Yanagihara, D., Nakao, K., Shigemoto, R., Katsuki, M., and Aiba, A. (2000). mGluR1 in cerebellar Purkinje cells essential for long-term depression, synapse elimination, and motor coordination. Science *288*, 1832-1835.

Impey, S., Mark, M., Villacres, E. C., Poser, S., Chavkin, C., and Storm, D. R. (1996). Induction of CRE-mediated gene expression by stimuli that generate long-lasting LTP in area CA1 of the hippocampus. Neuron *16*, 973-982.

Jaffe, D. B., and Brown, T. H. (1994). Metabotropic glutamate receptor activation induces calcium waves within hippocampal dendrites. J Neurophysiol *72*, 471-474.

Jia, Z., Lu, Y., Henderson, J., Taverna, F., Romano, C., Abramow-Newerly, W., Wojtowicz, J. M., and Roder, J. (1998). Selective abolition of the NMDA component of long-term potentiation in mice lacking mGluR5. Learn Mem *5*, 331-343.

Johannessen, M., Delghandi, M. P., and Moens, U. (2004). What turns CREB on? Cell Signal *16*, 1211-1227.

Kandel, E. R. (2001). The molecular biology of memory storage: a dialogue between genes and synapses. Science *294*, 1030-1038.

Kida, S., Josselyn, S. A., de Ortiz, S. P., Kogan, J. H., Chevere, I., Masushige, S., and Silva, A. J. (2002). CREB required for the stability of new and reactivated fear memories. Nat Neurosci *5*, 348-355.

Kim, S. J., Kim, Y. S., Yuan, J. P., Petralia, R. S., Worley, P. F., and Linden, D. J. (2003). Activation of the TRPC1 cation channel by metabotropic glutamate receptor mGluR1. Nature *426*, 285-291.

Kornhauser, J. M., Cowan, C. W., Shaywitz, A. J., Dolmetsch, R. E., Griffith, E. C., Hu, L. S., Haddad, C., Xia, Z., and Greenberg, M. E. (2002). CREB transcriptional activity in neurons is regulated by multiple, calcium-specific phosphorylation events. Neuron *34*, 221-233.

LeBeau, F. E., El Manira, A., and Griller, S. (2005). Tuning the network: modulation of neuronal microcircuits in the spinal cord and hippocampus. Trends Neurosci *28*, 552-561.

Lein, E. S., Hawrylycz, M. J., Ao, N., Ayres, M., Bensinger, A., Bernard, A., Boe, A. F., Boguski, M. S., Brockway, K. S., Byrnes, E. J.*, et al.* (2007). Genome-wide atlas of gene expression in the adult mouse brain. Nature *445*, 168-176.

Leutgeb, J. K., Frey, J. U., and Behnisch, T. (2005). Single cell analysis of activity-dependent cyclic AMP-responsive element-binding protein phosphorylation during long-lasting long-term potentiation in area CA1 of mature rat hippocampal-organotypic cultures. Neuroscience *131*, 601-610.

Ling, D. S., Benardo, L. S., Serrano, P. A., Blace, N., Kelly, M. T., Crary, J. F., and Sacktor, T. C. (2002). Protein kinase Mzeta is necessary and sufficient for LTP maintenance. Nat Neurosci *5*, 295-296.

Lisman, J., Schulman, H., and Cline, H. (2002). The molecular basis of CaMKII function in synaptic and behavioural memory. Nat Rev Neurosci *3*, 175-190.

Lonze, B. E., and Ginty, D. D. (2002). Function and regulation of CREB family transcription factors in the nervous system. Neuron *35*, 605-623.

Lonze, B. E., Riccio, A., Cohen, S., and Ginty, D. D. (2002). Apoptosis, axonal growth defects, and degeneration of peripheral neurons in mice lacking CREB. Neuron *34*, 371-385.

Lopes da Silva, F. H., and Arnolds, D. E. (1978). Physiology of the hippocampus and related structures. Annu Rev Physiol *40*, 185-216.

Lu, Y. M., Jia, Z., Janus, C., Henderson, J. T., Gerlai, R., Wojtowicz, J. M., and Roder, J. C. (1997). Mice lacking metabotropic glutamate receptor 5 show impaired learning and reduced CA1 long-term potentiation (LTP) but normal CA3 LTP. J Neurosci *17*, 5196-5205.

Macdonald, S. G., Crews, C. M., Wu, L., Driller, J., Clark, R., Erikson, R. L., and McCormick, F. (1993). Reconstitution of the Raf-1-MEK-ERK signal transduction pathway in vitro. Mol Cell Biol *13*, 6615-6620.

Malenka, R. C., and Bear, M. F. (2004). LTP and LTD: an embarrassment of riches. Neuron *44*, 5-21.

Mantamadiotis, T., Lemberger, T., Bleckmann, S. C., Kern, H., Kretz, O., Martin Villalba, A., Tronche, F., Kellendonk, C., Gau, D., Kapfhammer, J.*, et al.* (2002). Disruption of CREB function in brain leads to neurodegeneration. Nat Genet *31*, 47-54.

Mao, L., and Wang, J. Q. (2002a). Glutamate cascade to cAMP response element-binding protein phosphorylation in cultured striatal neurons through calcium-coupled group I metabotropic glutamate receptors. Mol Pharmacol *62*, 473-484.

Mao, L., and Wang, J. Q. (2002b). Interactions between ionotropic and metabotropic glutamate receptors regulate cAMP response element-binding protein phosphorylation in cultured striatal neurons. Neuroscience *115*, 395-402.

Mao, L., and Wang, J. Q. (2003). Group I metabotropic glutamate receptor-mediated calcium signalling and immediate early gene expression in cultured rat striatal neurons. Eur J Neurosci *17*, 741-750.

Mao, L., Yang, L., Arora, A., Choe, E. S., Zhang, G., Liu, Z., Fibuch, E. E., and Wang, J. Q. (2005a). Role of protein phosphatase 2A in mGluR5-regulated MEK/ERK phosphorylation in neurons. J Biol Chem *280*, 12602-12610.

Mao, L., Yang, L., Tang, Q., Samdani, S., Zhang, G., and Wang, J. Q. (2005b). The scaffold protein Homer1b/c links metabotropic glutamate receptor 5 to extracellular signal-regulated protein kinase cascades in neurons. J Neurosci *25*, 2741-2752.

Masu, M., Tanabe, Y., Tsuchida, K., Shigemoto, R., and Nakanishi, S. (1991). Sequence and expression of a metabotropic glutamate receptor. Nature *349*, 760-765.

Mayford, M. (2007). Protein kinase signaling in synaptic plasticity and memory. Curr Opin Neurobiol *17*, 313-317.

Mayr, B., and Montminy, M. (2001). Transcriptional regulation by the phosphorylation-dependent factor CREB. Nat Rev Mol Cell Biol *2*, 599-609.

McHugh, T. J., Blum, K. I., Tsien, J. Z., Tonegawa, S., and Wilson, M. A. (1996). Impaired hippocampal representation of space in CA1-specific NMDAR1 knockout mice. Cell *87*, 1339-1349.

Miura, M., Watanabe, M., Offermanns, S., Simon, M. I., and Kano, M. (2002). Group I metabotropic glutamate receptor signaling via Galpha q/Galpha 11 secures the induction of long-term potentiation in the hippocampal area CA1. J Neurosci *22*, 8379-8390.

Montminy, M. R., Sevarino, K. A., Wagner, J. A., Mandel, G., and Goodman, R. H. (1986). Identification of a cyclic-AMP-responsive element within the rat somatostatin gene. Proc Natl Acad Sci U S A *83*, 6682-6686.

Moody, W. J., and Bosma, M. M. (2005). Ion channel development, spontaneous activity, and activity-dependent development in nerve and muscle cells. Physiol Rev *85*, 883-941.

Morris, R. G. (2006). Elements of a neurobiological theory of hippocampal function: the role of synaptic plasticity, synaptic tagging and schemas. Eur J Neurosci *23*, 2829-2846.

Morris, R. G., Moser, E. I., Riedel, G., Martin, S. J., Sandin, J., Day, M., and O'Carroll, C. (2003). Elements of a neurobiological theory of the hippocampus: the role of activity-dependent synaptic plasticity in memory. Philos Trans R Soc Lond B Biol Sci *358*, 773-786.

Nakajima, T., Uchida, C., Anderson, S. F., Parvin, J. D., and Montminy, M. (1997). Analysis of a cAMP-responsive activator reveals a two-component mechanism for transcriptional induction via signal-dependent factors. Genes Dev *11*, 738-747.

Naraghi, M., and Neher, E. (1997). Linearized buffered Ca2+ diffusion in microdomains and its implications for calculation of [Ca2+] at the mouth of a calcium channel. J Neurosci *17*, 6961-6973.

Neher, E., Yuste, R., Lanni, F., and Konnerth, A. (2000). Calibration of fluorescent calcium indicators. In: Imaging Neurons: A Laboratory Manual. Cold Spring Harbor Laboratory Press *Chapter 31*.

Numberger, M., and Draguhn, A. (1996). Patch-Clamp Technik. Spektrum Akademischer Verlag Heidelberg.

Ogryzko, V. V., Schiltz, R. L., Russanova, V., Howard, B. H., and Nakatani, Y. (1996). The transcriptional coactivators p300 and CBP are histone acetyltransferases. Cell *87*, 953-959.

Pittenger, C., Huang, Y. Y., Paletzki, R. F., Bourtchouladze, R., Scanlin, H., Vronskaya, S., and Kandel, E. R. (2002). Reversible inhibition of CREB/ATF transcription factors in region CA1 of the dorsal hippocampus disrupts hippocampus-dependent spatial memory. Neuron *34*, 447-462.

Rae, M. G., and Irving, A. J. (2004). Both mGluR1 and mGluR5 mediate Ca2+ release and inward currents in hippocampal CA1 pyramidal neurons. Neuropharmacology *46*, 1057-1069.

Rampon, C., Tang, Y. P., Goodhouse, J., Shimizu, E., Kyin, M., and Tsien, J. Z. (2000). Enrichment induces structural changes and recovery from nonspatial memory deficits in CA1 NMDAR1-knockout mice. Nat Neurosci *3*, 238-244.

Rao, V. R., and Finkbeiner, S. (2007). NMDA and AMPA receptors: old channels, new tricks. Trends Neurosci *30*, 284-291.

Riccio, A., Ahn, S., Davenport, C. M., Blendy, J. A., and Ginty, D. D. (1999). Mediation by a CREB family transcription factor of NGF-dependent survival of sympathetic neurons. Science *286*, 2358-2361.

Shaywitz, A. J., and Greenberg, M. E. (1999). CREB: a stimulus-induced transcription factor activated by a diverse array of extracellular signals. Annu Rev Biochem *68*, 821-861.

Simpson, P. B., Challiss, R. A., and Nahorski, S. R. (1995). Neuronal Ca2+ stores: activation and function. Trends Neurosci *18*, 299-306.

Squire, L. R. (1992). Memory and the hippocampus: a synthesis from findings with rats, monkeys, and humans. Psychol Rev *99*, 195-231.

Stoop, R., Conquet, F., and Pralong, E. (2003). Determination of group I metabotropic glutamate receptor subtypes involved in the frequency of epileptiform activity in vitro using mGluR1 and mGluR5 mutant mice. Neuropharmacology *44*, 157-162.

Sugiyama, H., Ito, I., and Hirono, C. (1987). A new type of glutamate receptor linked to inositol phospholipid metabolism. Nature *325*, 531-533.

Thomas, G. M., and Huganir, R. L. (2004). MAPK cascade signalling and synaptic plasticity. Nat Rev Neurosci *5*, 173-183.

Topolnik, L., Azzi, M., Morin, F., Kougioumoutzakis, A., and Lacaille, J. C. (2006). mGluR1/5 subtype-specific calcium signalling and induction of long-term potentiation in rat hippocampal oriens/alveus interneurones. J Physiol *575*, 115-131.

Tsien, R., and Pozzan, T. (1989). Measurement of cytosolic free Ca2+ with quin2. Methods Enzymol *172*, 230-262.

Uylings, H. B. M., Van Eden, C. G., Parnavelas, J. G., and Kalsbeek, A. (1990). The Prenatal and Postnatal Development of Rat Cerebral Cortex. The Cerebral Cortex of the Rat; MIT Press, Cambridge, Massachusetts *Eds. Kolb, B. & Tees, R.C.*, 36-76.

Vargha-Khadem, F., Gadian, D. G., Watkins, K. E., Connelly, A., Van Paesschen, W., and Mishkin, M. (1997). Differential effects of early hippocampal pathology on episodic and semantic memory. Science *277*, 376-380.

Walton, M., Woodgate, A. M., Muravlev, A., Xu, R., During, M. J., and Dragunow, M. (1999). CREB phosphorylation promotes nerve cell survival. J Neurochem *73*, 1836-1842.

Watanabe, S., Hong, M., Lasser-Ross, N., and Ross, W. N. (2006). Modulation of calcium wave propagation in the dendrites and to the soma of rat hippocampal pyramidal neurons. J Physiol *575*, 455-468.

Wayman, G. A., Impey, S., Marks, D., Saneyoshi, T., Grant, W. F., Derkach, V., and Soderling, T. R. (2006). Activity-dependent dendritic arborization mediated by CaM-kinase I activation and enhanced CREB-dependent transcription of Wnt-2. Neuron *50*, 897-909.

West, A. E., Chen, W. G., Dalva, M. B., Dolmetsch, R. E., Kornhauser, J. M., Shaywitz, A. J., Takasu, M. A., Tao, X., and Greenberg, M. E. (2001). Calcium regulation of neuronal gene expression. Proc Natl Acad Sci U S A *98*, 11024-11031.

West, A. E., Griffith, E. C., and Greenberg, M. E. (2002). Regulation of transcription factors by neuronal activity. Nat Rev Neurosci *3*, 921-931.

Wu, G. Y., Deisseroth, K., and Tsien, R. W. (2001). Activity-dependent CREB phosphorylation: convergence of a fast, sensitive calmodulin kinase pathway and a slow, less sensitive mitogen-activated protein kinase pathway. Proc Natl Acad Sci U S A *98*, 2808-2813.

Wu, X., Spiro, C., Owen, W. G., and McMurray, C. T. (1998). cAMP response element-binding protein monomers cooperatively assemble to form dimers on DNA. J Biol Chem *273*, 20820-20827.

Yang, S. N., Wu, J. N., Liu, D., and Tung, C. S. (1998). Metabotropic glutamate receptors are involved in calcium-induced LTP of AMPA and NMDA receptor-mediated responses in the rat hippocampus. Brain Res Bull *46*, 505-512.

Yasuda, H., Barth, A. L., Stellwagen, D., and Malenka, R. C. (2003). A developmental switch in the signaling cascades for LTP induction. Nat Neurosci *6*, 15-16.

Yuste, R., and Katz, L. C. (1991). Control of postsynaptic Ca2+ influx in developing neocortex by excitatory and inhibitory neurotransmitters. Neuron *6*, 333-344.

Zhang, X., Odom, D. T., Koo, S. H., Conkright, M. D., Canettieri, G., Best, J., Chen, H., Jenner, R., Herbolsheimer, E., Jacobsen, E*., et al.* (2005). Genome-wide analysis of cAMP-response element binding protein occupancy, phosphorylation, and target gene activation in human tissues. Proc Natl Acad Sci U S A *102*, 4459-4464.

8. Supplemental materials

Following reagents were purchased from:

Chemicals	Supplier
(1S,3R)-ACPD	Tocris, Ellisville (USA)
ATP	Sigma Aldrich, Taufkirchen (Germany)
BAPTA-AM	Dojindo Laboratories, Kumamoto (Japan)
CaCl2	Sigma Aldrich, Taufkirchen (Germany)
CPA	Merck Biosciences, Darmstadt (Germany)
(S)-DHPG	Ascent Scientific, Weston-Super-Mare (UK)
DMSO	Sigma Aldrich, Taufkirchen (Germany)
Dulbecco PBS	Sigma Aldrich, Taufkirchen (Germany)
EGTA	Sigma Aldrich, Taufkirchen (Germany)
Fura-2-5K	MoBiTec, Göttingen (Germany)
Fura-2-AM	MoBiTec, Göttingen (Germany)
Glucose	Merck Biosciences, Darmstadt (Germany)
Glutamate	Sigma Aldrich, Taufkirchen (Germany)
GTP	Sigma Aldrich, Taufkirchen (Germany)
HEPES	Sigma Aldrich, Taufkirchen (Germany)
Ionomycin	Invitrogen, Carlsbad (USA)
KCl	Merck Biosciences, Darmstadt (Germany)
(±)-MCPG	Sigma Aldrich, Taufkirchen (Germany)
MgCl2	Merck Biosciences, Darmstadt (Germany)
Mowiol 4-88	Sigma Aldrich, Taufkirchen (Germany)
NaCl	Merck Biosciences, Darmstadt (Germany)
NaH2PO4	Sigma Aldrich, Taufkirchen (Germany)
NaHCO3	Merck Biosciences, Darmstadt (Germany)
Neurobiotin	Vector Laboratories, Burlingame (USA)
Nifedipine	Tocris, Ellisville (USA)
Normal goat serum	Millipore, Billerica (USA)
Oregon Green BAPTA-1-AM	Invitrogen, Carlsbad (USA)
PFA	Sigma Aldrich, Taufkirchen (Germany)
Pluronic acid F-127	Invitrogen, Carlsbad (USA)
Tetrodotoxin	Ascent Scientific, Weston-Super-Mare (UK)
Triton X-100	Carl Roth, Karlsruhe (Germany)
U0126	Cell signaling Technologies, Danvers (USA)
U73122	Tocris, Ellisville (USA)

Antibodies	
anti-phospho CREB (ser133), polyclonal rabbit	Cell signaling Technologies, Danvers (USA)
anti-MAP5/MAP1B, monoclonal mouse	Millipore, Billerica (USA)
Goat anti mouse Alexa488	Invitrogen, Carlsbad (USA)
Goat anti rabbit cy3	Invitrogen, Carlsbad (USA)
Streptavidin Alexa 647	Invitrogen, Carlsbad (USA)

9. Danksagungen

Die vorliegende Arbeit wurde am Friedrich Schiedel Institut für Neurowissenschaften der Technischen Universität München, unter Anleitung von Prof. Arthur Konnerth und im Rahmen des DIP Projektes G3.2 (Deutsch-Israelische Projektkoordination) angefertigt.

Danken möchte ich,

Prof. Arthur Konnerth für die wissenschaftliche Betreuung und Unterstützung in diesem Projekt. Dafür, dass ich mich nicht nur auf wissenschaftlicher Ebene weiterentwickeln, sondern mir auch das Skifahren aneignen konnte. Beides möchte ich nicht missen.

Prof. Michael Schemann für die unkomplizierte Betreuung der Dissertation als Mitglied des Wissenschaftszentrums Weihenstephan.

PD Dr. Knut Holthoff und Prof. Olga Garaschuk, die mir beim Schreiben der Dissertation mit ihrer konstruktiven Kritik zur Seite standen.

Dr. Lina Yassin für die manchmal anstrengende aber immer spannende Zusammenarbeit.

Allen Kollegen am Institut für Neurowissenschaften die meinen Weg begleitet haben.

Zu besonderem Dank bin ich verpflichtet,

Kathrin, ohne die ich wahrscheinlich noch in 10 Jahren schreiben würde und die mir immer zur Seite stand in guten wie in schlechten Tagen…

Meiner Familie für ihre Geduld, die Liebe und Unterstützung, die ich immer spüren durfte und insbesondere meinen Eltern, denen ich im Grunde alles zu verdanken habe und die immer an mich geglaubt haben.